OBSERVATIONS OF THE SOLAR-WIND TURBULENCE NEAR THE SUN

Thesis by

Philip Sidney Callahan

In Partial Fulfillment of the Requirements

for the Degree of

Doctor of Philosophy

California Institute of Technology

Pasadena, California

1974

(Submitted February 1, 1974)

Acknowledgements

I have more than the usual number of people to thank for their assistance during my stay at Caltech -and for my staying here at all. We all remember the War, the Draft, and the Great Draft Lottery of 1969: I lost the lottery, but (as most of the white, educated middle class did) avoided the War. Prof. M. Cohen, my first mentor, assisted me in getting a job at JPL. Prof. Ward Whaling has spent the last four years bending rules in my favor so I could keep the job. To both I am grateful.

Many people at JPL have helped me in the course of this work. I would especially like to thank Don Trask and Pete MacDoran for their assistance and encouragement. The data for this thesis would not have existed without the hard work of Warren Martin and Art Zygielbaum. I also thank Jack Lorell of the Mariner Mars 1971 Celestial Mechanics Experiment for assisting me in obtaining the data from that mission.

I am indebted to Dorothe Horttor of JPL who has worked beyond the call of duty typing the thesis for me.

I have benefitted greatly from my association with my advisor Prof. J. R. Jokipii. His comments on this manuscript were extremely valuable in making it coherent and readable. I also thank Prof. D. O. Muhleman for his comments. Profs. James Gunn and Peter Goldreich have done much to stimulate my learning about astrophysics; I thank them for their patience.

Many friends have made my stay at Caltech more pleasant. I especially thank Paul Schechter for his companionship and for taking a date to the party where I met my wife, Judy. She deserves special

credit for keeping me sane and happy enough to finish this endeavor.

During the course of my graduate study I have been supported by an NSF Fellowship, tuition fellowships from Cal Tech, and my job at JPL. Computer funds were supplied by JPL. The Jet Propulsion Laboratory, California Institute of Technology is operated under NASA contract, number NAS 7-100. I also acknowledge partial support from NASA Grant NGR 05-002-160.

ABSTRACT

The solar-wind turbulence near the sun is investigated with data obtained near the superior conjunctions of Mariners 6, 7, and 9. The data are time histories of the change in the electron columnar content between the earth and spacecraft. The data were obtained with a group-phase technique which is sensitive only to the change in the columnar content. The measurement technique is discussed. The theory of power spectra is outlined. The relationship between the temporal power spectrum of the columnar content data and the comoving wave-number spectrum of the solar wind is derived. It is found that comoving spectrum is well represented by a power-law ($P(\nu) \alpha \nu^{-\beta}$) of index $\beta = 3.9 \pm 0.2$. Comparison of the overall average spectral amplitude near the sun ($r \cong 0.15$ a.u.) to that near 1 a.u. shows that the turbulence declines with heliocentric distance as $\Delta n(r) \alpha r^{-2.38 \pm 0.11}$, ignoring time variations. In the region near the sun ($0.07 \lesssim r \lesssim 0.22$ a. u.) $\Delta n(r)$ declines more slowly. It is suggested that there is a region of enhanced turbulence near the sun. The Mariner 9 spectral amplitudes correlate with Zurich sunspot number. The data are used to investigate the relationship between McMath calcium plage regions and density enhancements intersecting the line of sight. The relationship of the present observations to theories of solar wind heating and to interplanetary scintillation observations is discussed.

TABLE OF CONTENTS

I: INTRODUCTION TO THE SOLAR WIND AND SUMMARY OF THE PRESENT INVESTIGATION

Ever since Biermann (1951, 1957) suggested from his study of ionic comet tails that there was a continuous emission of particles from the sun, the solar wind has been the object of increasing study. Many new techniques, including the one used in this investigation, have come into use, but Brandt (1970) points out that studies of comets can still provide valuable information about the solar wind, particularly at large heliographic distances or high latitudes. Brandt (1970) provides an interesting history and exposition of current ideas about the solar wind. Much recent work and references to earlier work can be found in Solar Wind (Sonnet, et al., eds., 1972).

The description of the solar wind (as well as the term) was first given by Parker in the late 1950's. His work is well summarized in Parker (1963). The key feature of the solar wind, as opposed to other theories of the solar corona current in the late 1950's, is its continuous, supersonic expansion to zero pressure at infinity. Parker reasoned that such a model was necessary since the pressure at infinity of static models is much larger than that expected in interstellar space.

Parker's analysis of the solar wind may be briefly summarized as follows. The solar atmosphere is treated as a single, inviscous, spherically symmetric fluid which must obey the equation of continuity,

$$n(r)\, v(r)\, r^2 = \text{constant}, \tag{1.1}$$

and the momentum equation,

$$nm_p\, v \frac{dv}{dr} + 2k \frac{d}{dr} nT + \frac{GM_\odot nm_p}{r^2} = F(r) \tag{1.2}$$

where m_p is the proton mass, T is the temperature, G is the gravitational constant, and F is the sum of other forces (if any). Note that there is no energy equation so T(r) must be specified. When these equations are solved together, with F = 0, a temperature distribution which falls off less rapidly than r^{-1} (the solar wind is roughly isothermal), and the requirement of zero pressure at $r = \infty$, a solution with a "critical point" is found. At this point ($r = r_c$) the fluid velocity, assumed to be less than the speed of sound originally, exceeds the local sound speed; the wind then expands to $r = \infty$ with supersonic speed. The behavior is like that of a Laval nozzle in which the fluid reaches the sound speed at the point of minimum area and then expands outward supersonically. The solar gravitational field provides the "throat" for the subsonic to supersonic transition of the solar wind. The critical radius for the solar wind is $r_c \cong 3\ R_\odot$. Barnes (1973) notes that if the external force F is large enough, or if the coronal temperature is high enough (Parker, 1963), the supersonic flow may be shut off.

Parker's analysis of the solar wind is important for several reasons. First, it explains many observations made by interplanetary spacecraft and radio astronomy techniques. Second, it shows the importance of critical points for understanding physical phenomena. Such analysis may prove very useful in other gas dynamics problems in astrophysics such as "galactic winds" and the nuclei of active galaxies. Third, stellar winds may have a significant effect on the evolution of the sun and other stars, and the effect can be estimated by the use of solar-wind models. The effect on solar rotation could be particularly important (Brandt, 1970). Thus, the solar wind provides a useful astrophysical laboratory in which to test our theoretical tools.

While many observations have confirmed the broad outlines of Parker's model, they have turned up new and intriguing problems as well. Generally, the state of observations is only good enough to raise questions, not conclusively resolve them. Solar wind observations typically yield the values of various quantities shown in Table 1.1. However, as the variations of these values show, the solar-wind flow is not smooth but fluctuates. The amplitudes of the changes may be of the order of the mean.

The fluctuations are particularly interesting because they are probably related to the energy source which maintains the corona at its observed temperature of 1-2 x 10^6 K. Brandt (1970) presents a

Table 1.1

Observed Properties of the Solar Wind Near 1 a.u.

Density	$n \sim 5\text{-}8^{+50}_{-4}$ cm^{-3}
Velocity	$v \sim 300\text{-}400^{+250}_{-50}$ km s^{-1}
Electron Temperature	$T_e \sim 1.5 \times 10^5$ K
Proton Temperature	$T_p \sim 4 \times 10^4 \; ^{+1\times10^5}_{-\sim 0}$ K
Magnetic Field	$\langle \lvert B \rvert \rangle \sim 5\text{-}7$ γ
Magnetic Field Fluctuations	$\langle \delta B_i \rangle \sim 1\text{-}3$ γ

schematic picture of $\sim$ 5 minute (the time scale of the granulation seen in the photosphere) oscillations generated in the sun's convection zone propagating into the lower corona where they are dissipated and turned into thermal energy. A number of other authors (see the review by Barnes, 1973) have used waves as a direct energy source for the solar wind. The exact mechanisms for generating and dissipating the waves have not yet been made clear. It is likely that the fluctuations observed in the solar wind are the remnants of this turbulence which have escaped dissipation because of their long wavelengths or particular wave mode (Belcher and Davis, 1971).

Unfortunately, it is very difficult to observe fluctuations nearer to the sun than a few solar radii. Newkirk (1967) reviews the structure of the corona and the methods used to measure it. New techniques have been introduced but little progress has been made.

The inner corona and the region out to $r \sim 5\ R_\odot$ can be investigated with eclipse and coronagraph photographs. The former are of much higher quality but are, of course, somewhat hard to obtain. Also, eclipses do not last long enough to see significant temporal changes. Coronagraph pictures can be obtained daily but contain information only out to $r \sim 2\ R_\odot$. Altschuler and Perry (1972), and Perry and Altschuler (1973) have developed a technique for obtaining the three-dimensional coronal electron density for $r \leq 2\ R_\odot$ from coronagraph observations, if the structure is assumed to be static for 14 days.

Radio observations--scintillations, two-frequency interferometry, spacecraft tracking, Faraday rotation, pulsar timing--are limited by the large phase changes introduced by fluctuations in the electron density near the sun. The very turbulence which one wishes to observe proves to be an obstacle. Observations near $r = 1.4\ R_\odot$ have been made by James (1970) using radar backscatter, but the data are difficult to interpret. Useful radio data generally exist only for $r \gtrsim 5\ R_\odot$. Sufficient phase stability to measure the turbulence well occurs for $r \gtrsim 10\ R_\odot$. The data presented here have the point of the ray path's closest approach to the sun in the range $14\ R_\odot \lesssim r \lesssim 46\ R_\odot$.

Theoretical studies have shown that waves are probably an important source of energy for the solar wind and corona. In order to have a complete understanding of the solar wind we must learn more about the temporal and spatial distribution of wave energy. Since one cannot probe the convection zone and it is difficult to observe the inner corona, one would like to understand the fluctuations in the solar wind: What is their relationship to the underlying average solar wind? How are they related to the sun or features in the lower corona? What is their amplitude and frequency distribution with heliocentric distance? In this study new information which will help in answering these questions is presented, and its relationship to these questions is discussed.

The data consist of records of the change in the integrated electron columnar content, $\Delta I = \int \Delta n(s)\, ds$, where $\Delta n(s)$ is the change in the electron density at point s, along the line of sight to Mariners 6, 7, and 9. The data from Mariners 6 and 7, the Mariner Mars 1969 (hereafter, MM69) spacecraft, were obtained in 1970 May through July. The data from Mariner 9, the Mariner Mars 1971 (MM71) spacecraft, were obtained in 1972 August through October. The data were obtained when the ray paths went near the sun. This geometry probed regions of the solar wind which are usually accessible only to less direct methods of observation (radio source scintillations).

Here we present a brief summary of the observational findings of this study. The observations are presented in detail in Chapter V. A preliminary analysis of the MM69 data was published in Callahan et al. (1972). The present work revises and extends that analysis.

The data give the scale size of the density fluctuations rather directly. It is found that the typical size for a large change in density is $L \sim 1.5\text{-}3.0 \times 10^6$ km, in agreement with previous spacecraft observations (Intriligator and Wolfe, 1970). The density fluctuations were also investigated with power spectral analysis. The power spectrum gives the mean squared amplitude per unit frequency at a given frequency. Since density fluctuations are approximately frozen into the solar wind (the convection velocity is much larger than the propagation speeds of any waves), frequency and size are related by $L \sim v_{SW}/\nu$. Power spectra are than a convenient way of characterizing the amplitudes of the fluctuations that occur

on various scales. It has been found that a power law ($P(\nu) \propto \nu^{-\beta}$) is a good representation of the low frequency ($10^{-5} \lesssim \nu \lesssim 10^{-2}$ Hz) power spectrum of the solar-wind density, velocity, and magnetic field. A power law fits the observations presented here if $\beta = 3.9 \pm 0.2$, a value consistent with both spacecraft and radio scintillation observations.

The data provide important information about the radial dependence of the amplitude of the low frequency density fluctuations. Information is obtained both by comparing the overall average of the observations near the sun to spacecraft data near 1 a.u. and by comparing the amplitudes of small groups of the observations. By comparing the observations near the sun to the results of Intriligator and Wolfe (1970) it is found that the density fluctuations decrease as $r^{-2.38\pm0.11}$ between r = 0.15 and r = 1 a.u., if long-term time variations are unimportant. If the overall fluctuation amplitudes are approximately proportional to sunspot number (see below), which changed about of factor of 4 between the Intriligator and Wolfe measurements and the MM69 and MM71 measurements, then the radial decrease of the fluctuations is about r^{-2}. Anderson et al. (1972) using MM69 data and Anderson and Lau (1973) using MM71 data found that the large-scale variation of the solar wind density is $r^{-2.0\pm0.2}$.

The radial variation of the fluctuations near the sun is different for the MM69 and the MM71 observations. The radial decline for the MM69 data is not well determined, but it is approximately r^{-2} to $r^{-2.5}$. For the MM71 data the decline is $r^{-1.5\pm0.2}$, for $0.07 \leq r \leq 0.22$ a.u., considerably slower than the large-scale radial dependence of the density fluctuations. The MM69 observations are also consistent with the near-sun radial fall-off being less steep than the large-scale radial decline. These observations suggest a region of enhanced turbulence near the sun.

It is found that the amplitude of the spectra varies on a time scale of weeks in the MM71 data. However, the amplitudes of the MM69 and MM71 data taken 2 years apart agree fairly well. The short-term variations are correlated with Zurich sunspot number and 2.8 GHz radio flux. The variation in the sunspot number between the MM69 and MM71 observations is only about 30%. The spectral amplitudes change by roughly the same amount, but no firm conclusion on the fluctuation amplitude-sunspot relationship can be drawn from these data. The spectral amplitudes do not depend on heliographic latitude. Also, no correlation with solar-wind velocity measurements or solar x-ray flux is found.

Chapter VII discusses the relationship of these findings to previous observations of the solar wind and to current ideas about the heating and acceleration of the solar wind. The picture of the turbulence suggested in Chapter VII is represented schematically in Figure 1.1. Short wavelength waves heat the lower corona, help to accelerate the solar wind, and feed the longer wavelength turbulence very near the sun, $0.01 \lesssim r \lesssim 0.2$ a.u. (1 a.u. = 216 $R_\odot$). A highly turbulent region is formed out to about $r \sim 45\ R_\odot$. Since most of the remaining energy is in the longer wavelength waves, the turbulence is only slowly dissipated and reduced by expansion (r^{-2}) as it propagates to 1 a.u. The detailed mechanisms of this plausible picture are difficult to fill in. More observations like those reported here and others nearer the sun would be a great help in understanding the processes at work.

In Chapter VI another attempt is made to relate the observations to the sun. Because the measurements of the columnar content change are made by a signal propagating to and from the spacecraft, it is possible to locate density enhancements along the ray path. The suspected density enhancements detected are mapped to the sun along Archimedian spirals (the apparent trajectory of the radially moving plasma as seen from the rotating sun). The points on the sun are compared to the locations of McMath calcium plage regions to see if dense streams originate in solar active regions. The conclusion of the investigation is that the original data records are not long enough to give reliable detection of streams.

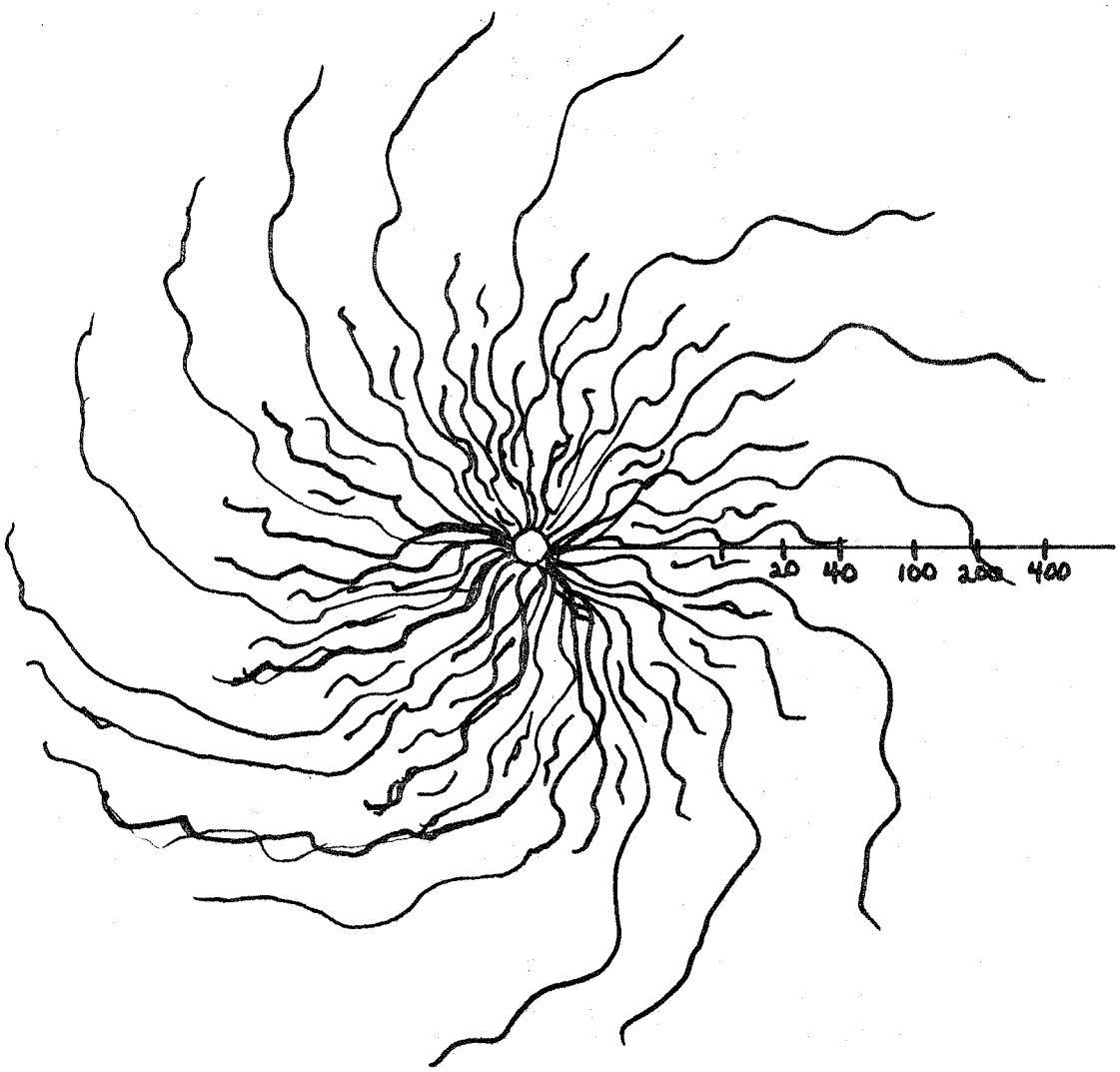

Figure 1.1. Schematic picture of solar-wind turbulence. Turbulence is enhanced in the region $r \lesssim 45 R_\odot$. Spiralling of magnetic field lines because of solar rotation is also shown (not to scale). Radial scale is logarithmic in units of solar radii (1 a.u. = 216 $R_\odot$).

The organization of this work is as follows. Chapter II deals with the data acquisition equipment and procedures. Chapter III describes the data reduction used. The theory of power spectra is presented. The computer programs used are described. Chapter IV is a formal development of the relationship between the three-dimensional wavenumber power spectrum of the solar wind and the temporal power spectrum of the spacecraft data. Chapter V gives the results of the data analysis. The radial and temporal variations of the spectra are discussed. The results are summarized at the end of Chapter V. Chapter VI discusses the finding of density enhancements and mapping to the sun's surface. Chapter VII discusses previous observations, theoretical findings, and the information provided by the present work about the solar-wind turbulence.

II. DRVID DATA: PHYSICS, IMPLEMENTATION, AND COLLECTION

Differenced Range Versus Integrated Doppler (DRVID) is a group-phase technique developed at JPL to measure changes in the electron columnar content between the earth and a distant spacecraft. The original purpose of the technique was to correct Doppler radio-tracking data for columnar content changes. The first section of this chapter discusses the physics of the group-phase technique. The advantages and disadvantages of this method of columnar content measurement are pointed out. In the second section the hardware used to implement the DRVID technique is described. In the final section the operational constraints on obtaining DRVID data near the superior conjunction of MM71 are discussed.

A. PHYSICS OF THE DRVID TECHNIQUE

DRVID is a group-phase technique for measuring the change in electron columnar content. The technique was first discussed by Muhleman and Johnston (1966). The discussion here follows MacDoran (1970).

It can easily be shown from Maxwell's equations that the dispersion relation for a tenuous plasma is given by

$$k^2 = \frac{\omega^2}{c^2}\left(1 - \frac{\omega_p^2}{\omega^2}\right) \qquad (2.1)$$

where ω_p is the plasma frequency, $\omega_p^2 = 4\pi n_e e^2/m_e$, and n_e is the number density of electrons.

The phase velocity of an electromagnetic wave is $v_p = \omega/k$, or from equation (2.1)

$$v_p = c\left(1 - \frac{\omega_p^2}{\omega^2}\right)^{-1/2} \cong c\left(1 + \frac{1}{2}\frac{\omega_p^2}{\omega^2}\right). \tag{2.2}$$

The latter expression holds if $\omega \gg \omega_p$, as is the case for spacecraft communications in the solar wind. The group velocity, $v_g = d\omega/dk$, is given by

$$v_g = c\left(1 - \frac{\omega_p^2}{\omega^2}\right)^{1/2} \cong c\left(1 - \frac{1}{2}\frac{\omega_p^2}{\omega^2}\right). \tag{2.3}$$

In tracking spacecraft two types of data are obtained--"range" and "Doppler". Range data are measurements of the time-of-flight for a radio signal from the earth to the spacecraft and back. The distance (range) to the spacecraft is deduced by multiplying the measured time by the speed of light.

Doppler data consist of measurements of the spacecraft's line-of-sight velocity taken at frequent intervals. The data are obtained by transmitting a known frequency from the earth to a phase-locked transponder aboard the spacecraft. When the signal is received back at the earth another phase-locked receiver counts the zero crossings of the difference between the received and transmitted

frequencies. The count is accumulated over some interval; the Doppler frequency for that interval is the cycle count divided by the time span.

It is clear from the above explanation that range data are associated with the group velocity, Doppler, with the phase velocity. Since the difference in the velocities is proportional to the electron density, comparison of range and Doppler data should given information about the electron density distribution.

The apparent one-way range to the spacecraft is

$$\rho_g = \frac{c}{2} \int_{\text{ray path}} \frac{ds}{v_g} = \frac{1}{2} \int ds + \frac{1}{4\omega^2} \int \omega_p^2(s) ds \tag{2.4}$$

where again it is assumed that $\omega_\rho^2/\omega^2 \ll 1$. This may be written as

$$\rho_g(t) = R(t) + \frac{A}{f^2} \int_0^R \left[n\left(s,\ t - \frac{2R-s}{c}\right) + n\left(s,\ t - \frac{s}{c}\right) \right] ds = R(t) + \frac{A}{f^2} I(t), \tag{2.5}$$

where R is the true distance to the spacecraft,

t is reception time at the earth,

n(s,t) is the electron density at position s along the raypath,

$\omega = 2\pi f$, f being the radio frequency, and

$A = e^2/4\pi m_e = 2.02 \times 10^7$ in cgs units.

I(t) is the electron columnar content. Since the plasma effect is quite small, the integral in equation (2.5) is carried out along the straight line path from the earth to the spacecraft.

The velocity inferred from a Doppler measurement in the presence of a changing columnar content is easily shown to be

$$\dot{\rho}_f(t) = \dot{R}(t) - \frac{A}{f^2}\dot{I}(t), \tag{2.6}$$

where a dot denotes time differentiation. If the range difference between times t_0 and t is computed by integrating the velocity of equation (2.6), the result is

$$\Delta\rho_f(t, t_0) = R(t) - R(t_0) - \frac{A}{f^2}\left[I(t) - I(t_0)\right]. \tag{2.7}$$

The range difference between these times can also be obtained from equation (2.4):

$$\Delta\rho_g(t, t_0) = R(t) - R(t_0) + \frac{A}{f^2}\left[I(t) - I(t_0)\right]. \tag{2.8}$$

Eqs. (2.7) and (2.8) have opposite signs on the terms involving the columnar content. From Eqs. (2.7) and (2.8) one can form Differenced Range minus (Versus) Integrated Doppler to explicitly exhibit the columnar content effect

$$\begin{aligned} \mathrm{DRVID}(t) &= \Delta\rho_g(t, t_0) - \Delta\rho_f(t, t_0) = \frac{2A}{f^2}\left[I(t) - I(t_0)\right] \\ &= \frac{2A}{f^2}\,\Delta I(t) \quad . \end{aligned} \tag{2.9}$$

This expression relates one-way DRVID data to round trip columnar content changes. Thus, DRVID data give the columnar content at time t offset by the unknown content at t_o.

In practice the expression for DRVID is somewhat more complicated than equation (2.9) indicates because of a frequency multiplication in the spacecraft transponder. In order to fully separate transmission to and from the spacecraft, the transponder coherently multiplies the received frequency by $b \equiv 240/221$ before rebroadcasting it. A similar scaling is done to the reference frequency at the earth-based receiver so that the correct Doppler cycle count is obtained. Because the effect of the plasma on the signal propagation is proportional to f^{-2}, the expression for DRVID is modified to be (MacDoran, 1970)

$$\mathrm{DRVID}(t) = \frac{2A}{f^2}\left[I_u(t) - I_u(t_0) + \frac{1}{b^2}\left(I_d(t) - I_d(t_0) \right) \right] , \tag{2.10}$$

where the subscripts refer to the transmission to ("u") and from ("d") the spacecraft. If it is assumed that $\Delta I_u = \Delta I_d = \Delta I(t)/2$, one obtains

$$\mathrm{DRVID}(t) = \frac{2A}{f^2}\,\Delta I(t)\left[\frac{b^2 + 1}{2b^2} \right] . \tag{2.11}$$

The validity of the assumption $\Delta I_u = \Delta I_d$ is somewhat questionable for long ray paths that pass near the sun. However, the data contain no way to separate ΔI_u from ΔI_d, so the approximation will be used. The resulting error should always be less than 8% since the bracketed quantity is equation (2.11) is nearly 1.

As equation (2.11) stands it relates the round trip columnar content change $\Delta I(t)$ in units of cm^{-2} to the value of DRVID(t) (one-way) in cm. Actually, DRVID(t) is measured in round trip time units (usually microseconds). Equation (2.11) gives for the columnar content change

$$\Delta I(t)\left[cm^{-2} \right] = \frac{f^2 b^2 c \left[cm\ \mu sec^{-1} \right] \mathrm{DRVID}(t)\left[\mu sec \right]}{2A(b^2 + 1)} , \tag{2.12}$$

where the units of quantities are in square brackets, c is the speed of light, and DRVID(t) is the value output by the equipment described

in the next section. Finally, the quantity of primary interest is the one-way columnar content change, $\Delta I(t)/2 \equiv \Delta I_{1W}(t)$. The numerical result relating DRVID(t) to $\Delta I_{1W}(t)$ is

$$\Delta I_{1W}(t)\left[\text{cm}^{-2}\right] = 8.99 \times 10^{14} \left[\text{cm}^{-2}\ \mu\text{sec}^{-1}\right] \times \text{DRVID}(t)\ [\text{observed, } \mu\text{sec}] \ . \tag{2.13}$$

While the DRVID method does not give the total column content, it has some advantages over other charged-particle measuring techniques which do not involve differencing (MacDoran, 1970) or a round trip measurement. First, any real motion of the spacecraft is cancelled. The method is not sensitive to orbit determination errors or spacecraft attitude control motions as range or Doppler residuals are. Second, any propagation effect which affects both phase and group velocities in the same way, e.g., the earth's troposphere or general relativistic delay, will not enter the measurement of $\Delta I(t)$. Third, any equipment delays which are common to both the range and Doppler systems will be removed by differencing. Finally, it will be shown in Chapter VI that the round trip nature of the DRVID measurements presents the possibility of detecting where localized electron density disturbances are along the ray path.

Equation (2.9) and its derivation make clear the two principal theoretical limitations of DRVID data. First, DRVID data record only the changes in the columnar content from the initial, unknown value. DRVID data cannot reveal the average properties of the medium through which the radio signal propagates. Second, a continuous count of Doppler cycles is necessary so that $\dot{R}(t')$ is known at every instant, and the integral in equation (2.7) can be carried out. If the Doppler count is lost, the DRVID data will have some additional (and unknown) offset besides $I(t_0)$. In practice this limitation is not quite so severe as it seems because the slope of $\Delta I(t)$ is preserved across a Doppler discontinuity, and the data on either side can be adjusted to match the slopes. However, there are practical limitations to the accuracy of such adjustments, and one would hope to make as few of them as possible.

In addition to these theoretical limitations there is one major practical limitation to the DRVID method--the difficulty in measuring distances of the order of 1.5×10^{13} cm with accuracy and stability. Equation (2.8) makes no allowances for drifts in the equipment or for errors of measurement. Drifts show up as spurious additions to $\Delta I(t)$. Errors of measurement in $R(t)$ mask any real variations of $\Delta I(t)$. These limitations will be discussed further in the next section.

B. IMPLEMENTATION OF THE DRVID TECHNIQUE

The implementation of the DRVID technique requires a sophisticated range measuring system which has the stability and accuracy needed to make meaningful columnar content measurements. Such a system was developed by W. L. Martin of JPL (Martin, 1969a, 1969b, 1970). It is the Binary-Coded Sequential Acquisition Ranging System, more commonly known as the "Mu system" or "Mu machine". The device was first installed on the 64 m antenna (DSS 14) at Goldstone, California in 1969, September. It was used on a research and development basis during the MM69 Extended Mission and throughout the MM71 mission.

A block diagram of the Mu-system taken from MacDoran and Martin (1970) is shown in Figure 2.1. Only the barest essentials of the system are discussed here; details may be found in MacDoran and Martin (1970), and Martin (1969a, b).

The key to the system is "Doppler rate aiding", a scheme whereby the received Doppler frequency is used in generating a model of the received range code. The rate-aiding allows the ranging code components to be sent sequentially. (The rest of the Mu system's name comes from the fact that the period of the nth component is $P_n = 2^n \times 64/f_s$, where f_s is a reference frequency in the radio tracking system.) However, it has another property with respect to DRVID measurements: Since the range code model is generated using

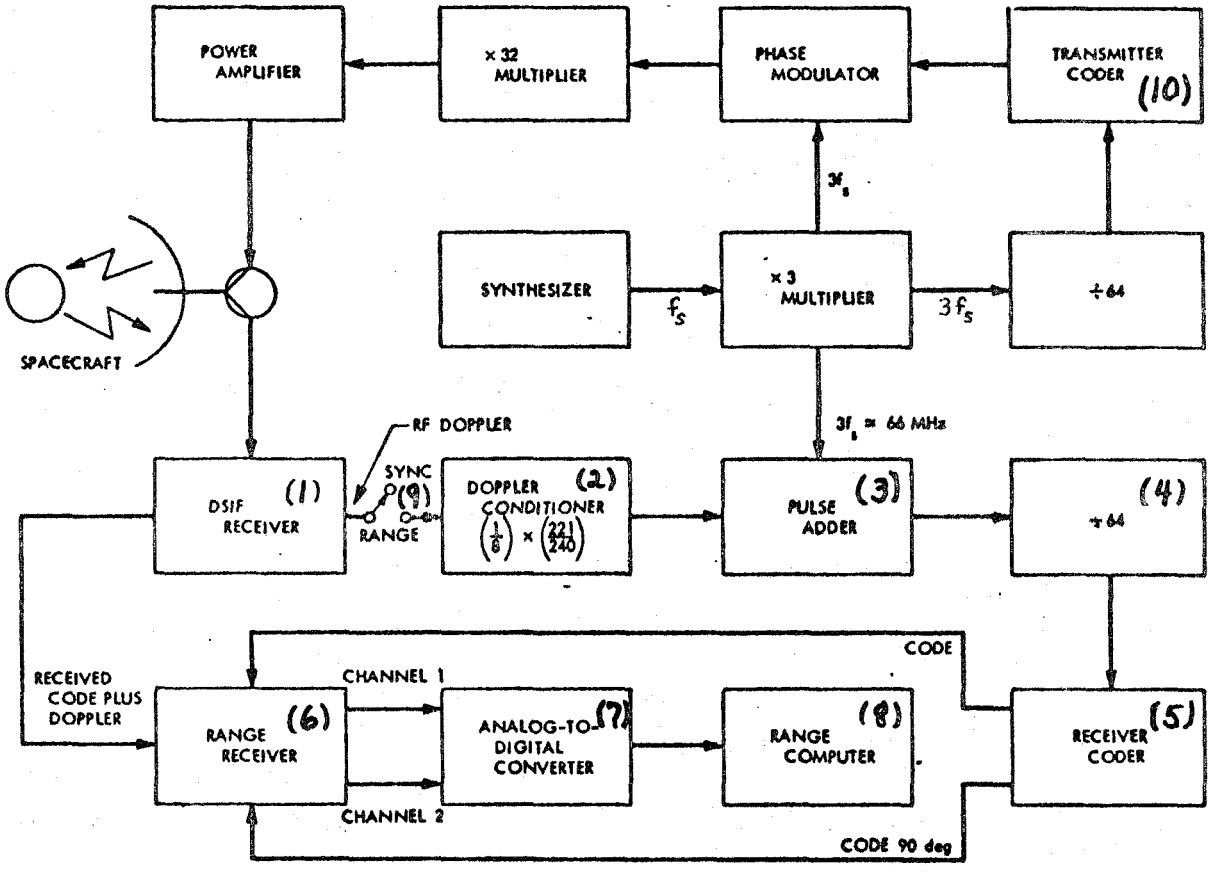

Figure 2.1. Block diagram of the Binary-Coded Sequential Acquisition (Mu) Ranging System. Block numbers are referred to in the text. (From MacDoran and Martin, 1970.)

the received Doppler frequency (blocks (1-5) of Figure 2.1), the repeated measurement of a single range code component shows only the effects of a changing columnar content.

The range measurement is made by comparing the phase (block (6)) of a received range code component to the phase of the code model. Just before the measurement is begun (t_0) the model code is synchronized (switch (9)) with the transmitted code (block (10)). The initial phase difference between the received code and the model is a measure of the range to the spacecraft. In the absence of columnar content changes the rate-aiding system (blocks (2-4)) will cause the same phase to be measured at any future time. Phase offsets are a measure of changes in the columnar content. Suppose the columnar content is increasing. Equation (2.6) shows that the received Doppler frequency will decrease; the model code will have its phase retarded as time goes on. The received range code will be delayed by the increased columnar content and its phase advanced. Thus a phase measurement at some later time will show a positive offset relative to the initial determination, indicating an increasing columnar content.

During a range measurement ("acquisition") the Mu machine sends a series of code components (typically 6-10, up to a maximum of 18) beginning with the highest frequency one. When it has completed the transmission of the lower frequency components, it returns to the high frequency one and reestimates its phase at

intervals determined by the operator. These reestimations are the DRVID data.

The Mu system automatically provides DRVID observations. To see if they are meaningful measurements of $\Delta I(t)$ the stability and accuracy of the system must be investigated. Such tests were performed by Martin (1970) during the early part of the MM69 Extended Mission, 1969 September through 1970 January.

In a bench test of the Mu system itself the stability was measured to be better than 10 psec hr^{-1}. After the Mu system was installed at DSS 14, tests were made of the total ground radio system delay, and its short- and long-term stability. From 1969 November 22 to 1970 January 24 Martin (1970) found an average total system delay of 3.34 μsec with a standard deviation of 26 nsec. A linear fit showed a slope of -15 nsec $month^{-1}$.

Short term stability tests were done on 1969 November 4 for 8 hr and 1969 December 6 for 3.5 hr. Peak drift rates of 2.9 nsec hr^{-1} and 3.7 nsec hr^{-1} were found. Peak variations were 7.6 nsec and 9.2 nsec, respectively. The total system delay was found not to vary significantly with received ranging power. (Delay in the spacecraft transponder does depend on the received signal level, but no significant power variations should occur in one day.)

Finally, a test of the reacquisition accuracy of the ground system was made on 1969 November 12 for one hour; the received signal

level was also varied. A systematic drift with peak to peak amplitude of 3 nsec was found. No completely satisfactory explanation for the drift was found, but it should be noted that it is not inconsistent with other measurements reported above. Thus the short term system stability and reacquisition accuracy would allow one-way columnar content changes $\Delta I_{1W} \gtrsim 9 \times 10^{12}$ cm^{-2} to be measured over periods of a few hours. Unfortunately this is not the only limit on the accuracy of DRVID data.

The chief constraint on the accuracy of DRVID data is fluctuations of the measured phase caused by noise on the received ranging signal. Figure 2.2 is a plot of the calculated (Martin, 1971) standard deviation (σ) of the range observations as a function of received signal level and integration (averaging) time on each reestimation of the high frequency code. Near the superior conjunctions of MM69 and MM71 the received ranging power was in the range -185 to -200 dbm. To obtain a useful number of DRVID points during a tracking pass an integration time near 100 sec (typically 60 or 120 sec) was used. Thus the expected standard deviation of the data is in the range 50 to 100 nsec, far greater than the measured equipment drifts. In fact observations near superior conjunction showed the noise to be worse, often by a factor of 2, than calculated. Part of this effect may be due to the increasing system temperature as the antenna is pointed toward the sun. How-

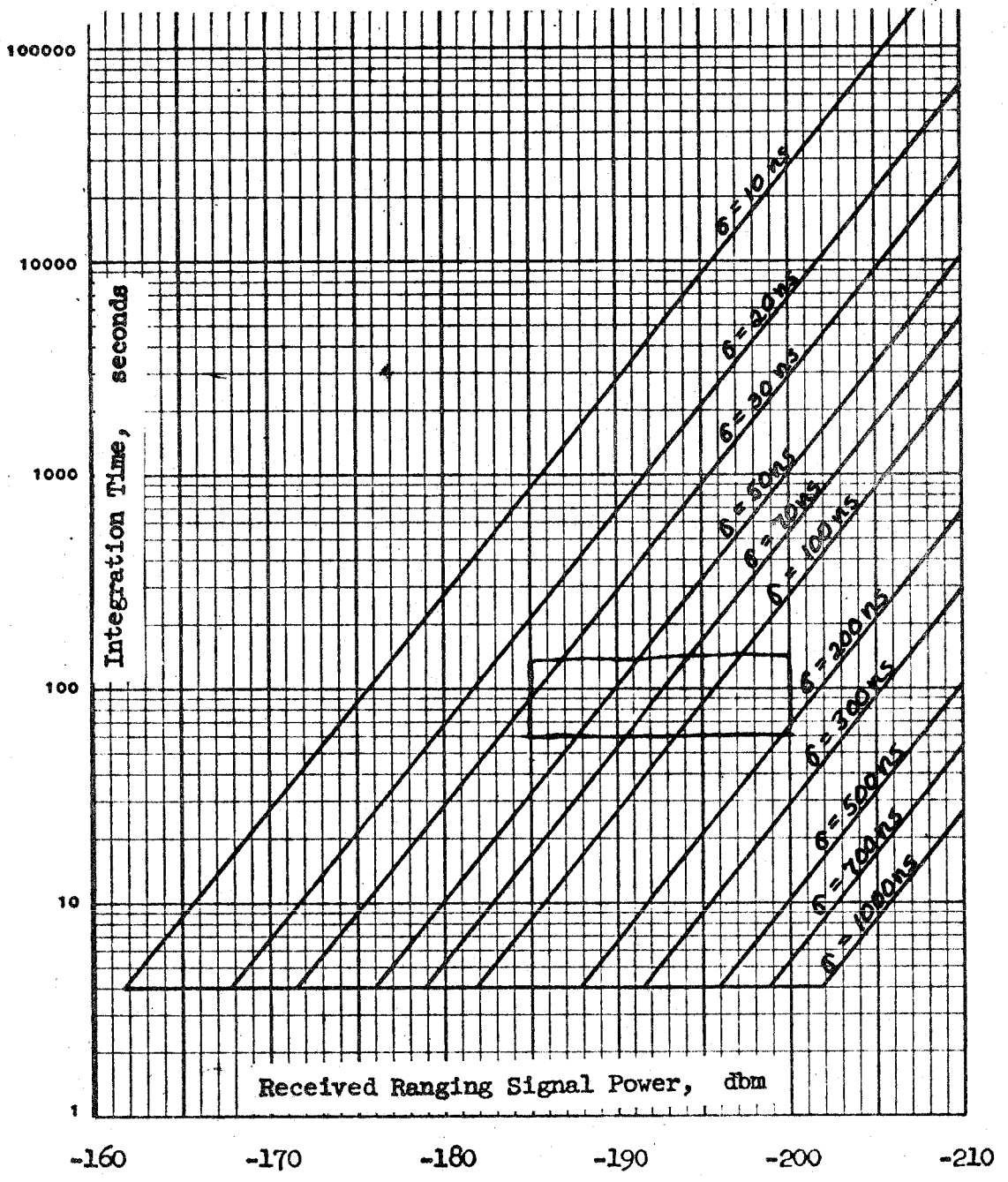

Figure 2.2. Mu ranging system phase jitter (RMS of points from their average) as a function of received signal power and integration time for an assumed system noise temperature of 30 K. Values of parameters that obtained during DRVID observations are in the boxed region. Jitter near the Sun was generally found to be larger than these predictions.

ever, even looking in the antisolar direction the curves of Figure 2.2 proved to be optimistic. The Doppler observations introduce essentially no noise into the DRVID data.

C. COLLECTION OF DRVID DATA

The DRVID data used in this study were obtained during the MM69 and MM71 Extended Missions. The MM69 data were obtained by P. F. MacDoran. As a member of the Celestial Mechanics Experiment Team, I assisted with the collection of data during the MM71 mission. Near the superior conjunction of MM71 33 days of usuable DRVID data were obtained. Seventeen days of data were collected during the MM69 mission. Table 2.1 lists all the data used in this study. The columns of the table give (1) the GMT date on which the pass began; (2) the GMT hour in which the pass began; (3) the length of the DRVID record; (4) the number of reacquisitions during the pass; (5) the length of the longest segment; (6) the total number of data points obtained during the pass; (7) the standard deviation of the data about its mean; and (8) the distance of closest approach of the ray path to the sun (q).

Near the superior conjunction of MM71 there were two competitors for the use of the Mu system: a group attempting to differentiate among relativistic theories of gravity on the basis of the time delay of the radio signal as it passed near the sun and my experiment investigating the solar wind near the sun. The relativity experiment had priority. The team's strategy for collecting data

was the opposite of mine: They wished to make many independent range measurements during a day and to make as few reestimations of each value as possible. I desired a single acquisition with as many reestimations as possible. In addition to this conflict there were other constraints: Commands had to be sent to the spacecraft. DSS 14, the only station with a Mu system, was wanted for other tasks. The high power transmitter (20-400 kW) malfunctioned. During certain periods the spacecraft was occulted by Mars. Other experimenters desired that no ranging signal be sent. For ray paths very near the sun the phase-locked receiver on the ground could not maintain phase-lock.

In spite of these problems both the relativity and DRVID experiments have produced worthwhile results. Much of the credit belongs to A. I. Zygielbaum of JPL who wrote a special program for the Mu system which allowed it to produce a maximum of data in the time available. Because of the large amount of data produced the DRVID experiment was given approximately three long (4-6 hr) uninterrupted segments of reestimation per week; on those days about 12 independent range values were acquired altogether. On other tracking days the data were taken as the relativity team wished but with the stipulation that at least two and, if possible four or more reestimations of each value be made. On these days from 12 to as many as 60 range values were obtained.

TABLE 2.1

Summary of all DRVID Data Used in Study

	(1) Date (GMT)	(2) Hour (GMT)	(3) Length (Hours)	(4) # Reacqui-sitions	(5) Longest Segment	(6) Total Points	(7) Std. Dev. (μ sec)	(8) q (a.u.)
	1970							
1	05/21	23	4.6	1	-	137	0.073	0.130
2	05/23	15	3.4	1	-	102	0.102	0.073
3	05/29	17	4.2	1	-	126	0.088	0.174
4	05/29	23	5.2	1	-	156	0.192	0.102
5	06/02	16	4.0	1	-	119	0.151	0.195
6	06/04	16	4.9	1	-	147	0.066	0.205
7	06/06	18	4.2	1	-	127	0.078	0.216
8	06/06	23	3.8	1	-	115	0.099	0.139
9	06/08	22	5.4	1	-	163	0.086	0.148
10	06/14	16	4.8	1	-	145	0.098	0.257
11	06/14	23	5.3	1	-	157	0.105	0.174
12	06/16	18	5.9	1	-	176	0.136	0.183
13	06/17	17	6.9	1	-	205	0.045	0.186
14	06/20	16	5.4	1	-	160	0.071	0.286
15	06/20	22	3.7	1	-	112	0.046	0.199
16	06/28	23	4.8	1	-	143	0.039	0.231

TABLE 2.1 (cont.)

17	07/02 1972	21	5.2	1	-	157	0.057	0.246
18	08/10	17	9.0	16	-	167	0.162	0.161
19	08/11	17	9.0	14	2.7	313	0.206	0.156
20	08/14	19	7.3	16	-	113	0.136	0.138
21	08/16	16	10.3	16	1.8	311	0.179	0.127
22	08/17	16	9.8	21	-	187	0.147	0.122
23	08/18	16	10.0	15	4.9	373	0.234	0.116
24	08/20	16	9.7	14	-	151	0.293	0.104
25	08/21	15	9.7	13	4.9	361	0.553	0.099
26	08/23	15	9.5	19	-	190	0.539	0.088
27	08/24	15	10.1	14	5.8	388	0.195	0.083
28	08/25	16	9.1	17	-	178	0.325	0.077
29	08/26	17	7.9	7	4.8	200	0.411	0.071
30	08/27	18	5.3	2	4.9	154	0.210	0.065
31	09/16	17	8.2	28	-	52	0.710	0.057
32	09/17	15	9.5	22	4.4	297	0.208	0.062
33	09/18	15	9.3	55	-	140	0.214	0.067
34	09/20	15	9.3	46	-	86	0.267	0.079
35	09/21	15	9.5	22	5.0	357	0.173	0.084
36	09/22	15	9.5	28	1.0	123	0.178	0.090
37	09/23	15	9.7	31	-	123	0.315	0.095

TABLE 2.1 (cont.)

38	09/24	15	9.3	23	4.8	331	0.144	0.101
39	09/25	15	9.6	25	1.4	153	0.127	0.107
40	10/01	15	9.0	23	4.0	284	0.128	0.141
41	10/05	15	9.3	18	3.9	168	0.165	0.165
42	10/06	15	9.3	23	3.0	256	0.131	0.170
43	10/08	15	9.0	31	-	89	1.115	0.182
44	10/09	15	9.0	17	3.6	158	0.147	0.187
45	10/11	15	9.1	15	2.5	197	0.227	0.198
56	10/12	15	9.0	25	-	71	0.083	0.204
47	10/14	15	6.7	15	-	55	0.192	0.216
48	10/15	15	5.8	15	-	70	0.106	0.222
49	10/16	15	8.5	16	-	62	0.248	0.227
50	10/25	15	8.3	11	2.0	198	0.233	0.279

III. DRVID DATA REDUCTION

To make a quantitative investigation of the solar wind using DRVID data extensive data processing was necessary. Figure 3.1 is a block diagram of the overall data reduction scheme. The elements of that scheme will be discussed in this chapter. First, a computer program was needed to use Doppler cycle counts to make the range reacquisitions from a pass into a continuous DRVID record. Second, the autocorrelation function and power spectrum of each record of $\Delta I(t)$ were computed. Third, a program added together individual power spectra to produce spectra with increased statistical reliability. The program also computed the earth-Sun-spacecraft geometry so that variations of the averaged spectra with heliocentric distance and other parameters could be investigated quantitatively. Finally, a program to map points along the earth-spacecraft ray path to the Sun's surface was used to investigate the relationship between features on the Sun's surface and disturbances located along the ray path. (See Chapter VI for discussion of the technique used to locate the disturbances.)

These programs were coded in FORTRAN V for the Univac 1108 computer at JPL. Computer funds were supplied by the Deep Space Network and the Celestial Mechanics Experiment of the MM71 mission.

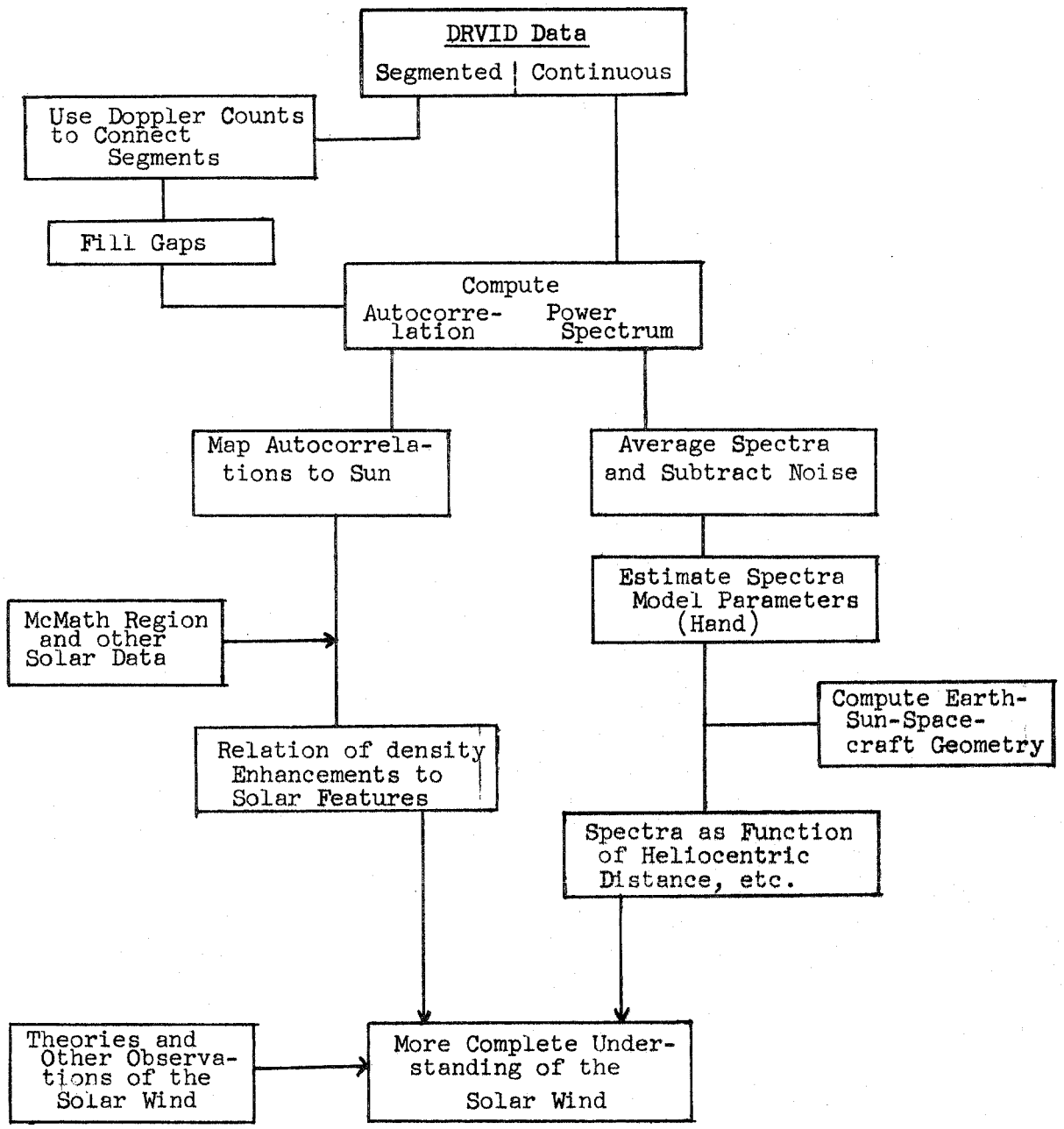

Figure 3.1. Block diagram of data reduction scheme.

None of the data used in this study were corrected for the columnar content of the earth's ionosphere. The total change in the ionospheric columnar content from zenith to near the horizon is about $7 \times 10^{13} cm^{-2}$, less than the noise on most DRVID records. Furthermore, when the spacecraft is near superior conjunction, the pattern of tracking tends to reduce the ionospheric columnar content change during a day. Thus, it did not seem necessary to remove this effect from the data.

A. DRVID DATA RECORDS FROM MULTIPLE RANGE ACQUISITIONS

Much of the DRVID data from the MM71 mission was obtained in very short segments (see Table 2.1.). In order to make a continuous record of $\Delta I(t)$ it was necessary to use Doppler cycle counts to relate the segments. The technique is simply a mechanization of the definition of DRVID.

The Doppler cycle count at the beginning of each range acquisition was used to find the range change that had occurred since the first acquisition:

$$\Delta R_{Di} = (DC(T_i) - DC(T_0)) * \lambda \qquad (3.1)$$

where $DC(T_i)$ is the Doppler count at T_i and λ is the radio wavelength, $\cong$ 13 cm. ΔR_{Di} was then reduced by the largest integral number of range ambiguity units possible. The range ambiguity is

due to the finite length of the range code. The ambiguity interval is far larger than any conceivable columnar content change. The reduced value of ΔR_{Di} is the effective integrated Doppler range change from the beginning of the DRVID record to time T_i.

The range difference for T_i was computed by subtracting the initial value of the first range acquisition from the initial value of the acquisition at time T_i. Finally, the difference of the range difference and the reduced value of ΔR_{Di} give the DRVID value at the beginning of the segment. Other points in the segment are computed by subtracting the initial range value for the segment from the value in question and then adding the DRVID value for the beginning of the segment. Of course, at the beginning of the first segment the DRVID value is zero. Figure 3.2a. shows a sample output of the computer program which carried out the prescription just described.

Occasionally the Doppler cycle count was reset during the day. This introduced an offset between the DRVID data on either side of the reset. Offsets were easily detectable and usually fairly easy to repair to within the data noise. A best estimate of the jump, based on both the values and the slope at the break, was applied to all data past the break. Data with many resets or for which a reconstruction was very difficult or ambiguous were discarded. If the reconstruction was somewhat difficult, several reasonable ones were made; it was found that the final power spectrum did not depend significantly on which of them was used.

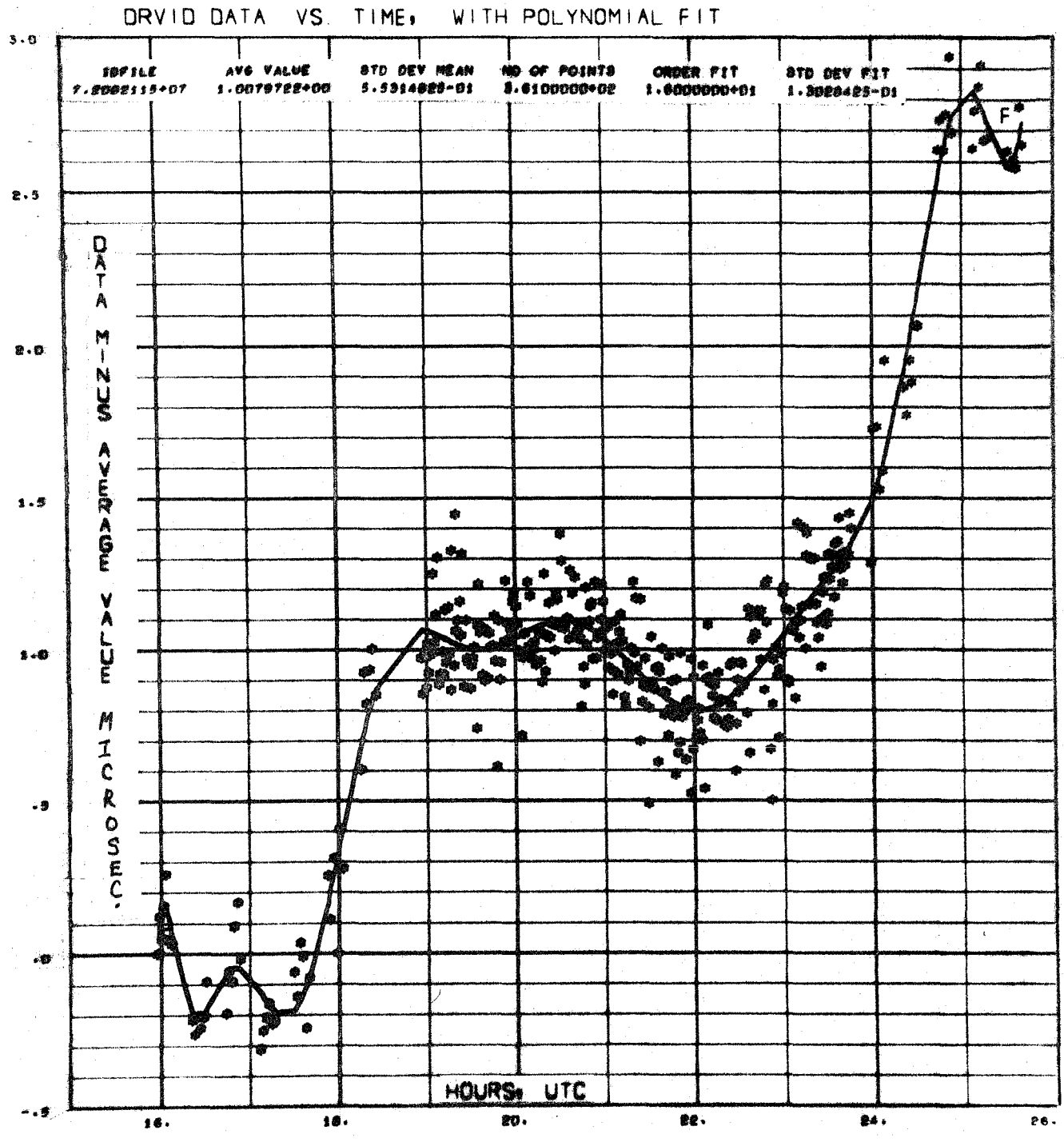

Figure 3.2a. An example of segmented DRVID data without the gaps filled. The values are in microseconds and are twice the round trip range change. The solid line is a least-squares polynomial fit to the data points. At the top of the frame is information output by the plotting routine.

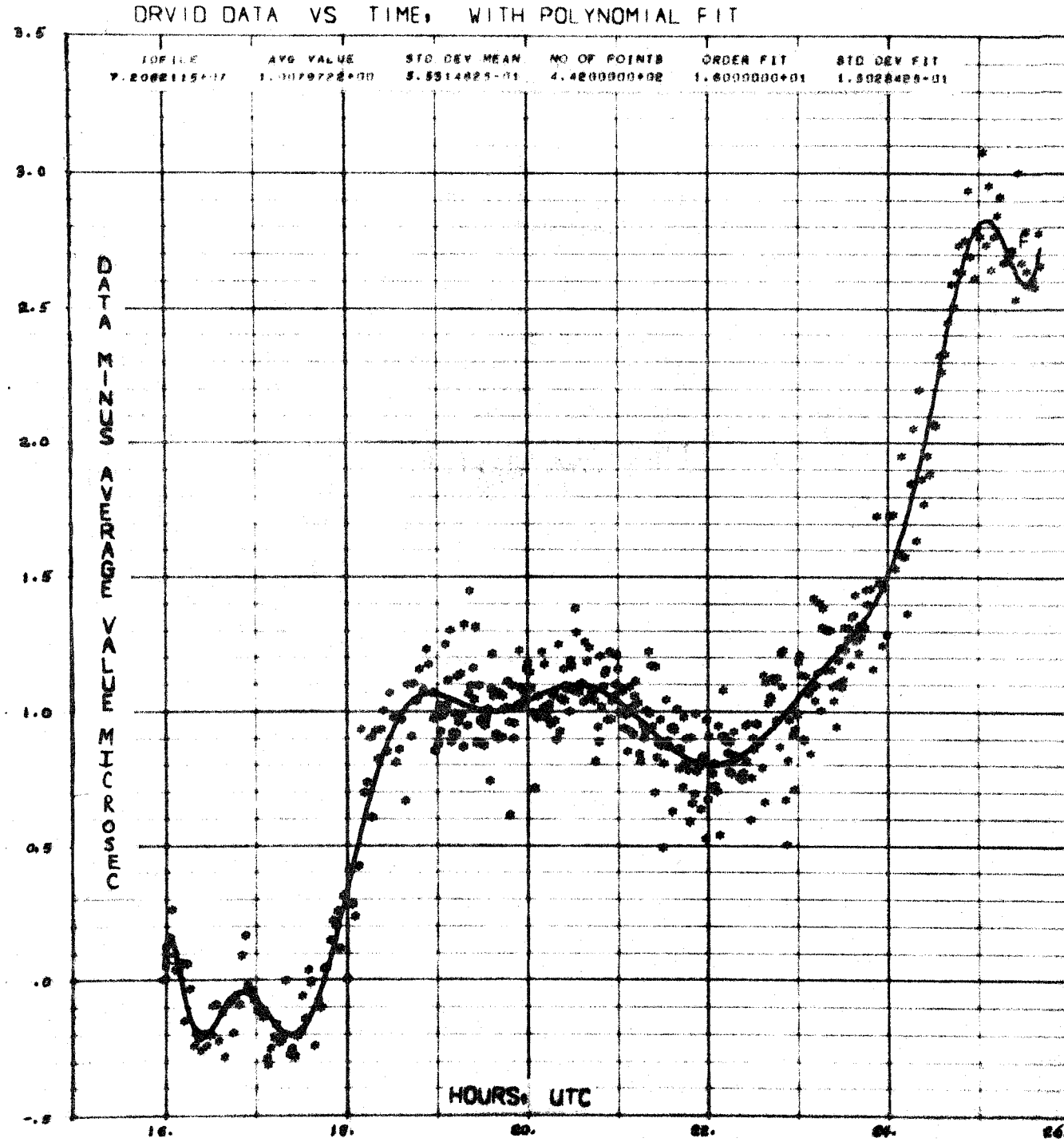

Figure 3.2b. The same DRVID data as in Figure 3.2a but with the gaps filled. Note that there are now 442 points as opposed to the original 361. The statistics of the points are not recomputed after filling the gaps.

Several of the DRVID records show extremely large rates of columnar content change. During such high rates of change it is likely that the Doppler counter will lose phase lock and give an incorrect cycle count. However, all the reconstructions used in this study are believed to be essentially correct: They do not contain errors due to loss of phase lock in the Doppler counter or to resets of the counter. All have been checked against range residuals and have the correct sense of variation and amplitude.

The program normally used to perform the autocorrelation and spectrum analysis requires equally spaced (in time) data points. It was therefore necessary to fill the gaps between the segments. This was done by passing a low order polynomial through the segments. The polynomial was then evaluated at equally spaced intervals in the gaps. The standard deviation of the real data from the fit was multiplied by a Gaussianly distributed pseudorandom number and added to each point to simulate data noise. Figure 3.2b. shows the results of filling the gaps in the data of Figure 3.2a.

A check was made to be sure that the gap-filling procedure did not affect the spectra of the DRVID records. The power spectrum program was modified to accept data with gaps. (Only those points which matched with other real points were counted in computing the autocorrelation function.) The resulting spectra of all the data listed in Table 2.1 were essentially the same as the spectra of the equally spaced data in the frequency range 1×10^{-4} to 1×10^{-3} Hz.

The chief difference between the two sets of spectra was that some of the spectra of the unequally spaced data had peaks in the frequency range 1 to 3 x 10^{-3} Hz. These peaks resulted from the periodic way in which the range segments were acquired.

In the discussion of the spectra in Chapter V the spectra of the equally spaced data will be used. They are used because the peaks in the spectra of the unequally spaced data interfere with the adding together of spectra. This averaging of the spectra was used to remove the high frequency noise and to investigate the variation of the spectra with distance from the sun.

B. POWER SPECTRA OF INDIVIDUAL RECORDS

DRVID data record the change in the electron columnar content as a function of time. This quantity does not change in any deterministic way and so may be classified as a random variable. The DRVID record shown in Figure 3.2b is a textbook example of a sample of a random variable.

A random variable, x(t), may be specified by its moments R_N given by (Bendat and Piersol, 1966)

$$\begin{aligned} R_N(t_0, \tau_1, \tau_2 \ldots \tau_{N-1}) &= \langle x(t_0)x(t_0 + \tau_1) \\ &\times x(t_0 + \tau_2)\ldots x(t + \tau_{N-1})\rangle \\ &= \lim_{M \to \infty} \left\{\frac{1}{M}\sum_{k=1}^{M} x_k(t_0)x_k(t_0 + \tau_1)\right. \\ &\left.\times x_k(t_0 + \tau_2)\ldots x_k(t_0 + \tau_{N-1})\right\} \end{aligned} \tag{3.2}$$

where the angular brackets denote an ensemble average. An ensemble average is taken over M identical systems, measured at the specified arguments as M tends to infinity. If the random variable is ergodic, the ensemble average may be replaced by an average over the independent argument of any sample of the random variable; i.e., the quantities

$$R_k(t_0, \tau_1, \tau_2 \cdots \tau_{N-1}) = \lim_{T \to \infty} \frac{1}{T} \int_0^T dt \{x_k(t_0 + t) \; x_k(t_0 + \tau_1 + t) \cdots x_k(t_0 + \tau_{N-1} + t)\} \tag{3.3}$$

are all equal (Bendat and Piersol, 1966), and we may take $R_N = R_k$. If R_N defined in equation (3.2) does not depend on the initial value of the independent argument, the random variable is said to be stationary. Since in practice one deals almost exclusively with ergodic processes, a more useful concept is self-stationarity (Bendat and Piersol, 1966): The moments R_k of equation (3.3) do not depend on t_0 when T is reasonably large.

It is assumed that the DRVID records are samples from an ergodic, self-stationary process. These assumptions are usually true of real, physically interesting processes.

The two most important moments for characterizing data are R_1 and R_2--the average value and the autocorrelation function. For

DRVID data the average value has little physical significance since DRVID data only record changes in the columnar content. However, the autocorrelation function, and its close relative the power spectrum, are very important. The autocorrelation function,

$$R_2(\tau) = \lim_{T \to \infty} \left\{ \frac{1}{T} \int_0^T x(t)x(t + \tau)dt \right\}, \qquad (3.4)$$

provides an estimate of the coherence time of the process--the time over which it "remembers". $R_2(\tau)$ is an even function of τ for ergodic, self-stationary processess. As will be discussed in Chapter VI the autocorrelation function of DRVID data also can provide the position of localized disturbances of $\Delta I(t)$.

Often, one deals with the power spectral density function, or power spectrum, rather than the autocorrelation function. The power spectrum tells the mean square value of the random variable within a frequency interval, i.e.,

$$P_x(\nu) \equiv \lim_{\Delta f \to 0} \lim_{T \to \infty} \frac{1}{\Delta f \cdot T} \int_0^T x^2(t, \nu, \Delta f)dt \qquad (3.5)$$

where ν is frequency and Δf is the frequency interval (Bendat and Piersol, 1966). $P_x(\nu)$ is real and non-negative. It can be shown that (the Wiener-Khinchen Theorem) the function $P_x(\nu)$ in equation (3.5) can also be obtained from

$$P(\nu) = 2\int_{-\infty}^{\infty} R_2(\tau)\,\exp(-i2\pi\nu\tau)\,d\tau \qquad (3.6)$$

The DRVID data present two practical problems to the analysis presented so far: The data records are of finite length. The data are discretely sampled, not continuous.

The finite length of the records limits the lowest frequencies at which reliable estimates of the power spectrum may be obtained. The lowest frequency which can be used is limited by the variance in the spectral estimates which can be tolerated. The relative variance of an estimate (discrete data) is given approximately by (Bendat and Piersol, 1966)

$$\epsilon \cong \sqrt{\frac{m}{N}} \qquad \left(m < \frac{N}{5}\right) \qquad (3.7)$$

where m is the maximum number of correlation lags and N is the number of data points. Typically, m/N is in the range 0.1-0.2 so that $\epsilon \cong$ 30-45%, and the lowest frequency reached is $\gtrsim 5/T$. Another estimate of the variance may be obtained by assuming that spectral estimates have a chi-squared distribution with 2N/m degrees of freedom. For m/N in the range 0.1-0.2 the errors found by this method are $\epsilon \sim$ 40-55% (Blackman and Tukey, 1959). The variance of the autocorrelation function is discussed in Chapter VI. The relative variance of $R(\tau)$ is $\lesssim \sqrt{m/2N}$.

The discrete sampling of the data results in an upper limit to the observable frequency range called the Nyquist frequency or aliasing frequency. The Nyquist frequency is given by $\nu_N = 1/2*\Delta t$ where Δt is the sampling interval. Processes occurring at rates greater than ν_N cannot be unambiguously reconstructed from data sampled only every Δt seconds. Frequencies higher than ν_N are aliased with frequencies ν given by

$$\nu = \nu + 2n\nu_N, \qquad n = 1, 2, 3..., \tag{3.8}$$

(Bendat and Piersol, 1966). For fairly rapidly decreasing spectra aliasing is a problem only near ν_N. The Nyquist frequencies of the DRVID data records are in the range $4\text{-}8 \times 10^{-3}$ Hz. However, the data noise flattens the DRVID spectra before aliasing becomes a problem.

To estimate the autocorrelation function and power spectrum of discrete data the integrals of equations (3.4) and (3.6) go into sums. Formulae from Bendat and Piersol (1966) were programmed into a subroutine to produce the autocorrelation functions and power spectra of DRVID data records. The "Hanning" window was used for smoothing the spectra. The autocorrelation functions and power spectra were output onto magnetic tape for further processing.

The DRVID data records were fit with low order polynomials, even if there were no gaps in the data. The differences between a data record and its fit were autocorrelated and spectrum analyzed. These autocorrelations were used to detect localized density enhancements along the ray path since it was necessary to remove the low frequency variations in order to obtain usable information from the data. The spectra of the residuals were used to check that the high frequency data noise had a flat spectrum and to investigate its level.

C. ADDITION AND AVERAGING OF DRVID POWER SPECTRA

The power spectra of individual DRVID data records showed rather large variability in amplitude, shape (spectral index), and relative noise level. Part of these variations was real and represented the differences in the columnar content change from day to day. However, part of the variations was statistical and could be removed by averaging spectra together. The program which did the averaging also calculated individual and average values of the earth-sun-spacecraft geometry.

The spectra were grouped in many different ways for averaging. Groupings were done to check the stability of the averaged spectra as different individual spectra were added. Spectra were grouped by distance from the sun to study the variation of spectral parameters with distance from the sun. The MM71 data were grouped by time to check for differences between the preconjunction and postconjunction periods. The spectral results are reported in Chapter V.

As was pointed out in Chapter II the DRVID data were noisier than predicted. The noise limited the frequency range of the spectra by overwhelming the signal at the higher ($\gtrsim 1 \times 10^3$ Hz) frequencies. Power spectra of the data minus a low order polynomial fit showed that the noise had a flat spectrum. When a large number of spectra were averaged, the noise region was quite flat, and a good estimate of the noise level could be made. By averaging N data sets together one expects an improvement in the signal to noise ratio of $\sim \sqrt{N}$. Such an improvement in the case of the DRVID data results in an extension of the useful frequency range by up to a factor of 2.

The improved signal to noise ratio was obtained by subtracting the minimum spectral estimate of the averaged spectrum from each estimate. The value in the minimum cell was replaced by the smaller of the two adjacent points. The resulting spectra had the same shape as before and the expected increase in frequency range. Hereafter the term averaged spectra will refer to spectra with the noise subtracted.

The averaged spectra were characterized by a three parameter model of the form

$$P_F(\nu) = S + D\nu^{(\beta-1)} \quad . \tag{3.9}$$

An attempt was made to fit this model to the averaged spectra by least-squares techniques. However, as is almost always the case with such models, a strong correlation ($\gtrsim 0.999$) exists between D and β. The equations are singular or near singular, and the solutions are very unstable. After a number of attempts at scaling the equations and introducing recoveries from singular solutions failed, the least-squares technique was abandoned. Fits of the form (3.9) were done by eye and plotted over the data for inspection and iteration, if necessary. In some cases two rather different sets of parameters could be selected to characterize a single spectrum. These variations were always within the range found for different data groupings and were taken as estimates of the errors in the spectral parameters.

D. MAPPING OF AUTOCORRELATION LAGS TO THE SOLAR SURFACE

It will be shown in Chapter VI that is is possible to find where localized solar-wind density enhancements intersect the ray path from the autocorrelation function. To investigate the relationship between these enhancements and features on the solar surface a program was written to map points along the ray path to longitudes and latitudes on the Sun.

The mapping used ideal Archimedian spirals corresponding to velocities of 400 and 700 km sec^{-1}. Intermediate velocities could easily be interpolated from these results. A point corresponding to each correlation lag was mapped assuming constant radial velocity.

The coordinate system on the Sun consisted of Carrington longitudes and heliographic latitudes. The program used a mean synodic equatorial rotation rate to output the times at which the foot of the spiral was at the sub-Earth point and 60° east or west of that point as viewed from the Earth. Contours of Carrington longitude, and the day of the year the spiral foot was sub-Earth, 60° east, and 60° west were plotted versus position along the ray path for ease of interpolation.

Data on solar active regions as defined by the McMath calcium plage observations were obtained from the World Data for Solar-Terrestial Physics, Boulder, Colorado, on magnetic tape. The data were sorted by region number. The Carrington longitude and the day of the year the region was sub-Earth, 60° east and west were obtained for each region which was reported on four or more days. The data on the McMath regions were compared to the output of the mapping program by hand for all correlation lags indicating localized density enhancements. The results of this analysis are in Chapter VI.

IV: THE RELATIONSHIP OF DRVID OBSERVATIONS TO THE SOLAR-WIND TURBULENCE

DRVID measurements are of interest only insofar as they can be related to the physical state of the solar wind. As was discussed in Chapter I its fluctuations are particularly interesting because they are probably related to the waves which heat the corona and drive the solar wind. One is interested in the location and extent of the region where the heating occurs. One also wishes to characterize the fluctuations or waves which cause the heating by wavelength or frequency. These goals are both met by studying the power spectrum (contribution to the rms density fluctuation by waves of a given frequency) of the solar-wind fluctuations as a function of distance from the sun.

In the first section of this chapter, the relationship between the comoving wavenumber spectrum of the solar-wind density fluctuations and the temporal power spectrum of DRVID data is deduced. A slightly different version of this section has been published in Callahan (1974). The development here is formal. The first section of Chapter V contains a qualitative (i.e., without power spectra) discussion of the scale sizes and amplitudes of solar-wind density changes.

The effects on the power spectrum of DRVID data of different density and velocity distributions as functions of heliocentric distance are discussed in the second section. It is found that the DRVID spectra are quite sensitive to the velocity and density near the sun. This makes DRVID data a very useful probe of this region where it is likely that much of the heating of the solar wind occurs. The DRVID results for the radial distribution of the solar-wind fluctuations are given in Chapter V. Their implications for theories of the solar wind are discussed in Chapter VII.

The relationship between the spectrum of DRVID data and the spectrum measured by a stationary spacecraft is derived in the third section. In Chapter V this relationship is used to compare DRVID spectra to data taken near 1 a.u. and thus find the overall radial dependence of the solar-wind fluctuations.

For the reader more interested in the observational findings of this study than in formal mathematical development, the two key results of this chapter will be summarized here. This summary will also make clear the goals of this chapter for the reader who pursues it in detail.

First, if the wave number spectrum in the rest-frame of the solar wind ("comoving") is a power-law ($g(\underset{\sim}{k}) \propto |\underset{\sim}{k}|^{-\beta}$), and if the amplitude of the density fluctuations depends on heliocentric distance as $\Delta n(r) \propto r^{-2+\gamma}$, then the temporal power spectrum of DRVID

data, denoted $c_{nt}(\nu)$, is [see Eqs. (4.19) and (4.21)]

$$c_{nt}(\nu) \propto \frac{[1 + e^{-\alpha\nu} \cos \lambda\nu]}{q^{3+2\gamma} \nu^{\beta-1}} \quad ,$$

where q is the distance to the ray path's point of closest approach to the sun, and α and λ are constants which depend on the exact geometry. The cosine term in the numerator causes sharp minima in the spectra at frequencies which are odd-integral multiples of 3×10^{-4} Hz for the geometry that obtained during the observations reported here. Different velocity and density distributions along the line-of-sight reduce, but do not eliminate, the minima. The minima occur because of the round trip manner in which the DRVID measurements are made. From observations one wishes to determine β and γ. The observed spectra will also be checked carefully for the predicted minima.

The second important result relates the power spectrum of DRVID data to the power spectrum deduced from density measurements made aboard a spacecraft at rest (approximately) with respect to the sun. If the functions above are used for the wave number spectrum and the radial fall-off of the density fluctuations the relationship is found to be [see Eq. (4.28)]

$$c_{nt}(\nu) \cong \left[\frac{F_{nt}(\nu)}{\nu}\right] 1.59 \times 10^{24+2\gamma} \frac{\Gamma\left(\frac{\beta-1}{2}\right)}{\Gamma\left(\frac{\beta-2}{2}\right)} \left(\frac{R_0}{\text{a.u.}}\right)$$

$$\cdot \left[\frac{\frac{R_0}{\text{a.u.}}}{\frac{q}{0.1\ \text{a.u.}}}\right]^{3+2\gamma} \left(\frac{v_0}{400\ \text{km s}^{-1}}\right) \left[\frac{1 + e^{-\alpha\nu} \cos \lambda\nu}{2}\right]$$

where the spacecraft observed spectrum, denoted $F_{nt}(\nu)$, is measured at R_0 (a.u.) from the sun, and v_0 is the solar-wind velocity. This result will be used to determine the large-scale, i. e., between approximately 0.15 and 1 a.u., radial fall-off of the density fluctuations. The fall-off will be characterized by the value of γ which gives the best agreement between the observed values of $c_{nt}(\nu)$, q and $F_{nt}(\nu)$, R_0.

A. INTERPRETATION OF DRVID MEASUREMENTS OF THE SOLAR-WIND TURBULENCE

Direct spacecraft measurements near the earth have shown that the solar wind is turbulent. Radio scintillation observations of regions nearer the sun also show that the solar wind is turbulent. Many discussions of the relationship of the scintillation spectra to the solar-wind turbulence spectrum have appeared in the literature. (See, for example, Salpeter (1967), Young (1971), Jokipii and Lee (1972).) Here the relationship between the spectra of DRVID measurements of the columnar content change and the solar-wind turbulence spectrum is derived.

After data reduction (see Chapters II and III) a time series of DRVID measurements gives

$$\Delta I(t) = \int_{\text{ray path}} \Delta n(\underset{\sim}{r},\ t - \frac{s}{c})ds \qquad (4.1)$$

where $\Delta n(\underset{\sim}{r})$ is the fluctuation in the electron content at r, s measures distance along the ray path, and $\Delta I(t)$ is the change in the electron columnar content. Observations of $\Delta I(t)$ near a spacecraft's superior conjunction can give estimates of both the solar-wind turbulence spectrum near the sun and the radial dependence of $\Delta n(\underset{\sim}{r})$.

We wish to investigate the relationship between the three-dimensional wave number spectrum of $\Delta n(\underset{\sim}{r})$ that would be observed moving with the solar wind ("comoving") and the frequency spectrum of $\Delta I(t)$ defined in Eq. (4.1). Let the frame of the solar wind s' move with velocity $\underset{\sim}{v}$ with respect to our frame s. In s', $\Delta n(\underset{\sim}{r}')$ has an autocorrelation function given by

$$b(\underset{\sim}{r}')\, G_{nr}(\underset{\sim}{R}) = \langle \Delta n(\underset{\sim}{r}') \cdot \Delta n(\underset{\sim}{r}' + \underset{\sim}{R}) \rangle, \tag{4.2}$$

where the angular brackets denote a spatial average.

We explicitly show the nonstationary nature of $\Delta n(\underset{\sim}{r}')$ caused by the variation of the solar-wind density with heliocentric radius. Such variation is assumed to be on a scale far larger than the turbulence. It is assumed that the density autocorrelation function is separable into a function depending only on the separation of the points involved multiplied by an amplitude function depending only on heliocentric radius.

For this nonstationary case, we will define the Fourier transform of $G_{nr}(\underset{\sim}{R})$, $g_{nr}(\underset{\sim}{k})$, to be the power spectrum of $\Delta n(\underset{\sim}{r}')$. Thus the power spectrum of $\Delta n(\underset{\sim}{r}')$ is given by

$$\text{(a)} \quad g_{nr}(\underset{\sim}{k}) = \int_{-\infty}^{\infty} G_{nr}(\underset{\sim}{R}) \exp\,(-i\underset{\sim}{k}\cdot\underset{\sim}{R})\, d^3R$$

or (4.3)

$$\text{(b)} \quad G_{nr}(\underset{\sim}{R}) = \frac{1}{(2\pi)^3} \int_{-\infty}^{\infty} g_{nr}(\underset{\sim}{k}) \exp(i\underset{\sim}{k}\cdot\underset{\sim}{R}) d^3k.$$

The coordinate system s is shown in Fig. 4.1. The z-axis is along the earth-spacecraft ray path. The projection of $\underset{\sim}{v}$ into the x-z plane is shown. If s and s' coincide at t = 0,

$$\underset{\sim}{r}' = \underset{\sim}{r} - \underset{\sim}{v}t \tag{4.4}$$

gives the coordinate transformation between the two frames.

Eq. (4.1) may be written explicitly in frame s as

$$\Delta I(t) = \int_0^L \Delta n(\underset{\sim}{r}, t - \frac{2L - z}{c})dz + \int_0^L \Delta n(\underset{\sim}{r}, t - \frac{z}{c})dz, \tag{4.5}$$

where t is measured at the earth-based receiver.

It is assumed that the spacecraft is at a fixed distance L during the observation. Propagation to and from the spacecraft is included. It is also assumed that the signal propagates along a single, straight ray path. The effects of multipathing or scintillation must be small for the DRVID technique to work. The curvature introduced by the varying refractive index can be shown to be negligible in the solar wind.

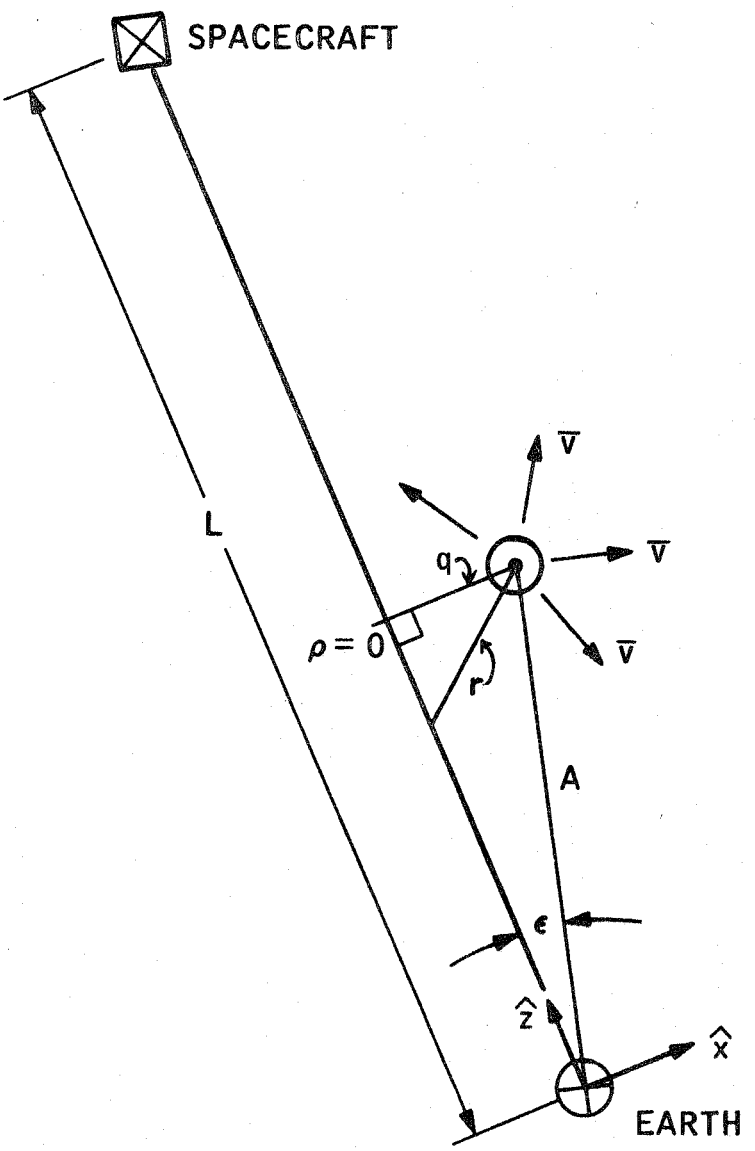

Figure 4.1. Earth-Sun-Spacecraft geometry.

By using Eq. (4.4) one can rewrite Eq. (4.5) in the rest frame of the solar wind as

$$\Delta I(t) = \int_0^L \Delta n \left[\underset{\sim}{r} - \underset{\sim}{v}\left(t - \frac{2L - z}{c}\right) \right] dz + \int_0^L \Delta n \left[\underset{\sim}{r} - \underset{\sim}{v}\left(t - \frac{z}{c}\right) \right] dz. \tag{4.6}$$

It is straightforward to write the autocorrelation of $\Delta I(t)$ in terms of $G_{nr}(\underset{\sim}{R})$. The result is

$$C_{nt}(\tau) = \left\langle \Delta I(t)\Delta I(t+\tau) \right\rangle_t = \int_0^L b(\underset{\sim}{r})\, ds \int_{-s}^{L-s} d\ell \cdot \left\{ G_{nr}\left[\underset{\sim}{R} - \underset{\sim}{v}\left(\tau + \frac{\ell}{c}\right)\right] + G_{nr}\left[\underset{\sim}{R} - \underset{\sim}{v}\left(\tau + \frac{\ell + 2(s - L)}{c}\right)\right] + G_{nr}\left[\underset{\sim}{R} - \underset{\sim}{v}\left(\tau - \frac{\ell + 2(s - L)}{c}\right)\right] + G_{nr}\left[\underset{\sim}{R} - \underset{\sim}{v}\left(\tau - \frac{\ell}{c}\right)\right] \right\}, \tag{4.7}$$

where $\underset{\sim}{R} = (0, 0, \ell)$, and the angular brackets sub-t denote a time average.

It is assumed that $\underset{\sim}{v}$ does not change in a correlation scale, i. e., $\underset{\sim}{v}$ is independent of ℓ. Since $\underset{\sim}{v}$ is the bulk velocity of the solar wind, the approximation should be very good. For the complex Fourier transforms which follow only the third and fourth terms of Eq. (4.7) will be used because $C_{nt}(\tau)$ is a real, symmetric function. One may recover correct results by taking twice the real part of any expression.

To reduce Eq. (4.7) to the desired relationship between the observed and the comoving power spectrum, one takes the Fourier transform of Eq. (4.7) and writes $G_{nr}(\underset{\sim}{\xi})$ using Eq. (4.3b)

$$c_{nt}(\nu) = \int_{-\infty}^{\infty} d\tau \exp(-i2\pi\nu\tau) \int_{0}^{L} b(\underset{\sim}{r})ds \int_{-s}^{L-s} d\ell \int_{-\infty}^{\infty} g_{nr}(\underset{\sim}{k}) \left[\exp(i\underset{\sim}{k}\cdot\underset{\sim}{\xi}_a) + \exp(i\underset{\sim}{k}\cdot\underset{\sim}{\xi}_b) \right] \frac{d^3k}{(2\pi)^3} \tag{4.8}$$

where $\underset{\sim}{\xi}_a = \underset{\sim}{R} - \underset{\sim}{v}\left[\tau - (\ell/c)\right]$, $\underset{\sim}{\xi}_b = \underset{\sim}{R} - \underset{\sim}{v}\left[\tau - (\ell + 2(s - L)/c)\right]$.

Rearrangement of (4.8) makes the important features of the result clearer

$$c_{nt}(\nu) = \int_{0}^{L} b(\underset{\sim}{r})ds \int_{-\infty}^{\infty} \frac{d^3k}{(2\pi)^3} \left\{ g_{nr}(\underset{\sim}{k}) \left\{ 1 + \exp\left[\frac{i2\underset{\sim}{k}\cdot\underset{\sim}{v}(s - L)}{c} \right] \right\} \right.$$

$$\left. \int_{-s}^{L-S} d\ell \exp\left[i\ell\left(k_z + \underset{\sim}{k}\cdot\frac{\underset{\sim}{v}}{c}\right) \right] \int_{-\infty}^{\infty} d\tau \exp\left[-i\tau(\underset{\sim}{k}\cdot\underset{\sim}{v} + 2\pi\nu) \right] \right\} . \tag{4.9}$$

The last two integrals express the convection of the solar wind. The sum in the braces enters because of the round trip nature of DRVID data. The change from the time to the frequency domains requires the k-integral. Finally, the s-integral sums up the contributions to the observed spectrum along the ray path.

A great simplification occurs in Eq. (4.9) if one assumes that the correlation scale is much smaller than the other scales in the problem. For the solar wind more than a few degrees from the sun such an approximation is reasonable since the correlation scale is $\sim 10^6$ km while the distance scale is $\gtrsim 10^7$ km. This assumption allows the limits on the ℓ-integral to be moved to infinity. Each of the last two integrals then results in a δ-function so that one obtains

$$c_{nt}(\nu) = \int_0^L b(\underset{\sim}{r})ds \int_{-\infty}^{\infty} \frac{d^3k}{2\pi} g_{nr}(\underset{\sim}{k}) \left[1 + e^{i2\underset{\sim}{k}\cdot\underset{\sim}{v}(s-L)/c}\right] \times \left\{\delta(2\pi\nu + \underset{\sim}{k}\cdot\underset{\sim}{v})\ \delta(k_z + \underset{\sim}{k}\cdot\underset{\sim}{v}/c)\right\}. \tag{4.10}$$

The δ-functions allow two of the k-integrals to be done at once. The result is the most transparent if one does the k_x and k_z integrals to get

$$c_{nt}(\nu) = \int_0^L \frac{b(\underset{\sim}{r})ds}{v_x} \int_{-\infty}^{\infty} \frac{dk_y}{2\pi} \left[1 + e^{-i4\pi\nu(s-L)/c}\right] \cdot \tag{4.11}$$

$$g_{nr}\left(\frac{\frac{-2\pi\nu(v_z + c)}{c} - k_y v_y}{v_x}, k_y, \frac{2\pi\nu}{c}\right).$$

Under the assumptions that $\underset{\sim}{v}$ does not change in a correlation scale and that the correlation scale is much less than the distance scale, Eq. (4.11) is the general relation between the three-dimensional wave number spectrum of the solar wind and the temporal spectrum observed in DRVID data. Eliminating the second term in square brackets gives the result for one-way spacecraft data. The assumptions used in this analysis remove the solar-wind velocity from the terms in Eq. (4.11) which directly involve ν. Thus, only the bulk properties of the velocity are important to the predicted spectrum.

To evaluate Eq. (4.11) it is necessary to assume specific forms for $g_{nr}(\underset{\sim}{k})$, $b(\underset{\sim}{r})$, and v_x. Many spacecraft observations have shown that solar-wind magnetic field fluctuations can be represented by a power-law spectrum, $f(\nu) \propto \nu^{-\beta}$, over a large range of frequencies, $10^{-5} \underset{\sim}{<} \nu \underset{\sim}{<} 10^{-2}$Hz. The suggestion that the charged particle fluctuations would have the same spectra was confirmed by Intriligator and Wolfe (1970). Using <u>in situ</u> spacecraft measurements they found a power law index of 1.3 ± 0.3. Cronyn (1970) has shown that an index derived from <u>in situ</u> observations is related to the comoving index by

$$\beta_{IS} = \beta_{CM} - 2 \quad . \tag{4.12}$$

The schematic solar wind spectrum of Jokipii and Coleman (1968) suggests a long wavelength flattening to the spectrum. A flattening must occur in a power-law spectrum if the total power is to be finite. Thus for a model spectrum we choose

$$g_{nr}(\underset{\sim}{k}) = (k_0^2 + a_x^2 k_x^2 + a_y^2 k_y^2 + a_z^2 k_z^2)^{-\beta/2} \tag{4.13}$$

where the a's allow for an anisotropic spectrum. One expects β to be between 3 and 4.

If Eq. (4.13) is used in Eq. (4.11) the k_y-integral can be done simply only if $\beta = 4$. However, observations show that the solar wind velocity is essentially radial so $\underset{\sim}{v}$ may be taken to be in the x-z plane. Since the solar wind velocity is always much less than that of light, v_z may be neglected in the expression for k_x. With these approximations Eq. (4.11) reduces to

$$c_{nt}(\nu) = \frac{\Gamma\left(\frac{\beta - 1}{2}\right)}{2\sqrt{\pi}\,\Gamma(\beta/2)} \cdot \int_0^L \frac{b(\underset{\sim}{r})\left[1 + e^{-i4\pi\nu(s-L)/c}\right] ds}{a_y v_x \left[k_0^2 + \left(\frac{2\pi\nu a_x}{v_x}\right)^2 + \left(\frac{2\pi\nu a_z}{c}\right)^2\right]^{(\beta-1)/2}} . \tag{4.14}$$

To finish the evaluation one must specify the functions $b(\underset{\sim}{r})$, v_x, a_x, a_y, a_z, and k_0 along the ray path. Of course, observations are not nearly complete enough to determine so many functions, so let us set a_x, a_y, a_z, and k_0 to constants. For $b(\underset{\sim}{r})$ the obvious choice is a power-law of heliocentric distance; from observation one can attempt to determine the exponent. The solar wind velocity is taken to be constant and radial so that $v_x(s)$ is just the projection of $\underset{\sim}{v}$ onto the x-axis. Except very near the sun ($\underset{\sim}{<} 10R_\odot$) this should be a good approximation for $\underset{\sim}{v}$ (Ekers and Little, 1971. See the next section.).

The integral is more easily written in terms of (see Fig. 4.1)

$$\begin{aligned} b(\rho) &= D(\rho^2 + q^2)^{-(2+\gamma)} \\ v_x(\rho) &= v_0 q(\rho^2 + q^2)^{-1/2} \end{aligned} \tag{4.15}$$

where D is a scale factor for the solar-wind density.

Substitution of Eqs. (4.15) into Eq. (4.14) and some algebraic manipulations yield

$$c_{nt}(\nu) = \frac{D\,\Gamma\left(\frac{\beta-1}{2}\right) v_0^{\beta-2}}{2\sqrt{\pi}\, a_y \Gamma\left(\frac{\beta}{2}\right)\left(2\pi\nu a_x\right)^{\beta-1} q^{3+2\gamma}} \cdot$$

$$\int_{-\mu_1}^{\mu_2} \frac{d\mu\left[1 + e^{-i4\pi\nu\mu q/c_e} + i\phi\right]}{\left(1+\mu^2\right)^{3/2+\gamma}\left[\left(\frac{v_0 k_0}{2\pi\nu a_x}\right)^2 + \left(\frac{a_z v_0}{a_x c}\right)^2 + 1 + \mu^2\right]^{(\beta-1)/2}} \qquad (4.16)$$

where

$$\mu = \frac{\rho}{q},\ \mu_1 = \frac{A\cos\epsilon}{q},\ \mu_2 = \frac{L - A\cos\epsilon}{q} \quad ,$$

and

$$\phi = 4\pi\nu q\mu_2/c.$$

In Eq. (4.16) we can see the form of $c_{nt}(\nu)$ since the integral is of the order of 1 except for certain frequencies where the numerator vanishes. Except for this factor the observed spectrum is one power less steep than the comoving spectrum, and its amplitude depends on the distance of closest approach q to the $(3+2\gamma)$ power. From Counselman and Rankin (1972) we expect that $0 \lesssim \gamma \lesssim 1/2$.

As Eq. (4.16) stands it must be integrated numerically. The parameter of principal interest is k_0. Integrations have been carried out as functions of ϵ, β, γ, and k_0 with $a_x = a_y = a_z = 1$, L = 2.6 a.u., and $[(v_0)/c]^2$ neglected. Fig. 4.2 shows the results of the integrations for three values of ϵ and two values of k_0 with $\beta = 3.5$, $\gamma = 0.25$. For frequencies $\nu > 2 \times 10^{-4}$ Hz the effect of changing k_0 is seen to be negligible. Integrations with smaller values of k_0 (i.e., $\ell_0 = 2\pi/k_0 > 8 \times 10^6$ km) show that little additional change occurs as $\ell \to \infty$ for $\nu \gtrsim 2.0 \times 10^{-4}$ Hz. In this frequency range the envelope of the spectra is $\nu^{\beta-1}$.

The deep minima in the spectra occur at odd-integral multiples of the frequency corresponding to twice the round trip light travel time from the ray path's point of closest approach to the sun to the spacecraft. The minima occur because the round trip nature of the measurement insures that fluctuations at these frequencies ($\nu = kv_x/2\pi$) will be observed by the up and down legs with a phase difference of π. The variation of velocity along the ray path is slow enough so that the rather steep spectrum ($\beta \sim 3$-4) and density fall-off ($\propto \mu^{4+2\gamma}$) give a sharp resonance. The numerical integrations show the expected results as parameters are changed: The minima are deeper for larger values of β and γ, and are less deep for larger values of ϵ. In the first two cases the range of k and μ, respectively, which contribute significantly to the integral are reduced; thus

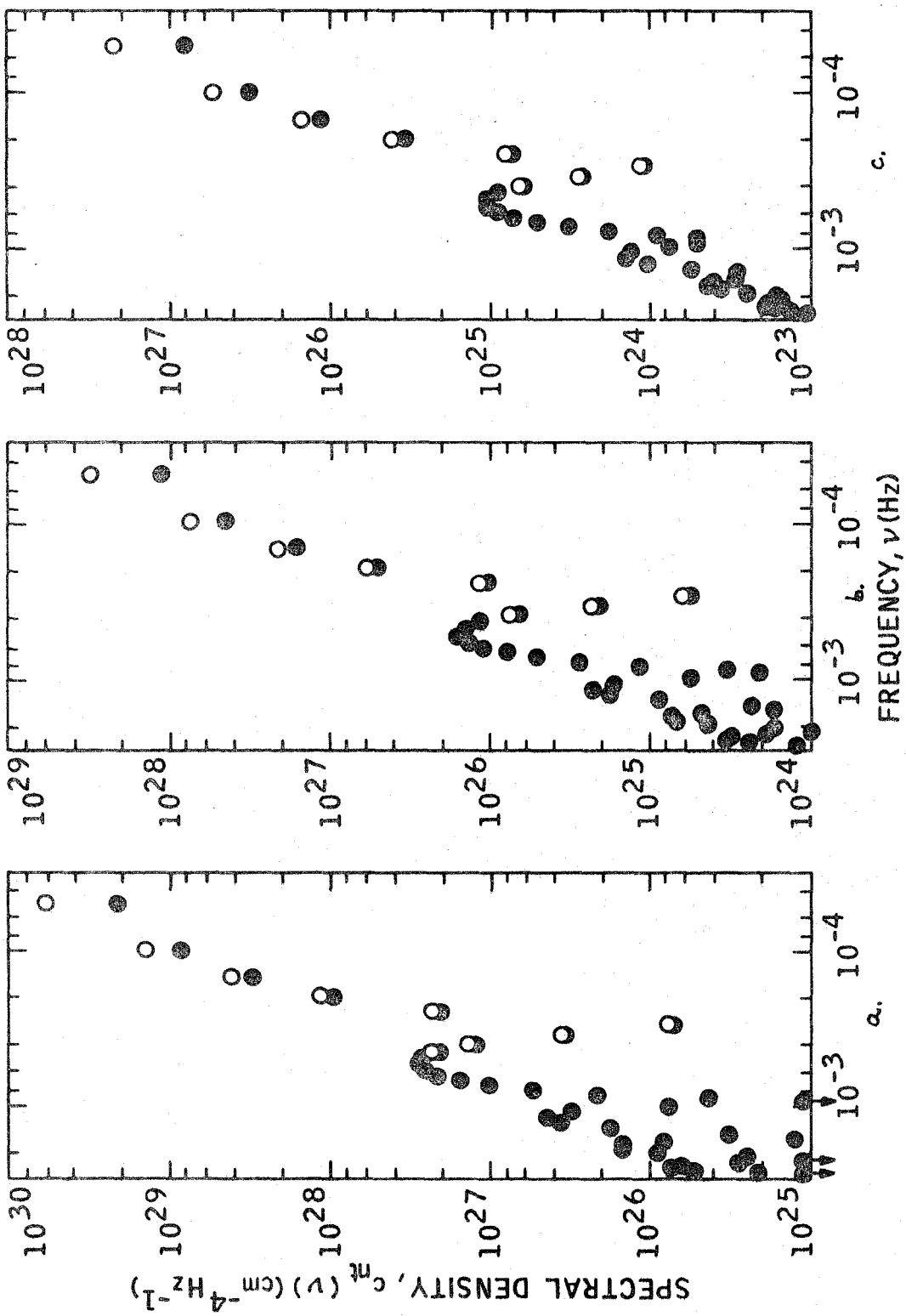

Figure 4.2. Predicted power spectra from numerical integration, normalized to an RMS fluctuation of 0.5 cm^{-3} at 1 a.u. Note the deep minima at multiples of $3x10^{-4}$ Hz. Parameters: β = 3.5, γ= 0.25; ●, ℓ_o= $4x10^6$ km; ○, ℓ_o =$8x10^6$ km. Part a, ϵ =3°; b, ϵ =7°; c, ϵ =15°. The minima are deeper nearer the sun. The low frequency amplitudes increase as ℓ_o increases.

the resonance is sharpened. As ϵ is increased, the ray path no longer goes near the sun so that no particular value of μ dominates the integral.

Examination of Eqs. (4.8) and (4.9) show that the deep minima in the theoretical power spectra occur because of the assumption that the solar wind velocity does not change in a density correlation length. Except very near the sun ($\lesssim 10R_\odot$) or when the solar wind is very active this should be a valid assumption, and Eq. (4.16) should represent the observed spectrum fairly well. DRVID data taken near the sun ($15R_\odot \lesssim q \lesssim 50R_\odot$) will be carefully examined for the deep minima found in Eq. (4.16).

The numerical integrations of Eq. (4.16) suggest that for realistic values of k_0 and $\nu \gtrsim 1 \times 10^{-4}$ Hz the term $[(v_0 k_0)/(2\pi\nu)]^2$ (< 0.2) can be ignored without disastrous consequences. If that term is ignored (as well as $(v_0/c)^2$), Eq. (4.16) reduces to the relatively simple form

$$c_{nt}(\nu) = \frac{D\,\Gamma\left(\frac{\beta-1}{2}\right) v_0^{\beta-2} q^{-3-2\gamma}}{2\sqrt{\pi}\, a_y\, \Gamma(\beta/2)\, (2\pi\nu a_x)^{\beta-1}} \times \int_{-\mu_1}^{\mu_2} \frac{d\mu\left[1 + e^{-i4\pi\nu\mu q/c_e + i\phi}\right]}{\left[1+\mu^2\right]^{1+\gamma+\beta/2}} \,. \tag{4.17}$$

For several plausible pairs of values of β and γ the integral reduces to a single case. If one chooses

$$\begin{aligned} &\text{(a)} \quad \beta = 3.0, \ \gamma = 0.5, \text{ or} \\ &\text{(b)} \quad \beta = 3.5, \ \gamma = 0.25, \text{ or} \\ &\text{(c)} \quad \beta = 4.0, \ \gamma = 0 \end{aligned} \tag{4.18}$$

the power in the denominator is 3. These values of the exponents span the expected range, so we will evaluate this case in more detail. Of course, any combination of γ and β that gives $1 + \gamma + \beta/2 > 0$ allows the integral in Eq. (4.17) to be done by the method given in Appendix A.

Using the result of Appendix A with $\gamma + \beta/2 = 2$ the observed spectrum is

$$\begin{aligned} c_{nt}(\nu) = \frac{3D}{8/\pi\, a_y} \frac{\Gamma\left(\frac{\beta-1}{2}\right)}{\Gamma(\beta/2)} \frac{v_0^{\beta-2}}{(2\pi\nu a_x)^{\beta-1}\, q^{3+2\gamma}} \Bigg\{ \Bigg[\tan^{-1}\mu_2 + \tan^{-1}\mu_1 \\ + \frac{\mu_2}{1+\mu_2^2} + \frac{\mu_1}{1+\mu_1^2} + \frac{2}{3}\left[\frac{\mu_2}{\left(1+\mu_2^2\right)^2} + \frac{\mu_1}{\left(1+\mu_1^2\right)^2} \right] \Bigg] \\ + \pi \cos\phi\, e^{-4\pi\nu q/c} \left[\frac{1}{3}\left(\frac{4\pi\nu q}{c}\right)^2 + \left(\frac{4\pi\nu q}{c}\right) + 1 \right] \Bigg\} \end{aligned} \tag{4.19}$$

where $\mu_1 = (A \cos \epsilon)/q$, $\mu_2 = (L - A \cos \epsilon)/q$, $q = A \sin \epsilon$, and $\phi = (4\pi\nu q\mu_2)/c$. The constant in Eq. (4.19) is appropriate for interpreting DRVID data as one-way columnar content measurements when the power spectrum is defined as in Eq. (4.3a). The spectral amplitudes obtained from Eq. (4.19) will be one-half as large as those output by the computer routines described in Chapter III.

Eq. (4.19) has been evaluated as a function of frequency for several values of ϵ in the three cases of Eq. (4.18). The results of the evaluation for $\beta = 3.5$, $\gamma = 0.25$ and three values of ϵ are shown in Figure 4.3. Comparison of Figures 4.2 and 4.3 shows excellent agreement except at the lowest frequencies. The deep minima still occur in the spectra at the same frequencies. The correction terms (Eq. A-5) were negligible, even at the minima. Thus Eq. (4.19) is a good representation of the temporal spectrum of two-way spacecraft observations for frequencies $\nu \gtrsim 1.5 \times 10^{-4}$ Hz.

In Chapter V DRVID measurements made near the superior conjunctions of Mariners 6, 7, and 9 will be presented and analyzed within the framework developed here. The observations will allow the determination of the solar-wind-density spectral index β near the sun. A search for sharp minima in the spectra will shed light on the velocity and density distributions near the sun. As can be seen from Eq. (4.16) measurements of the spectrum at different values of ϵ will allow the determination of γ which

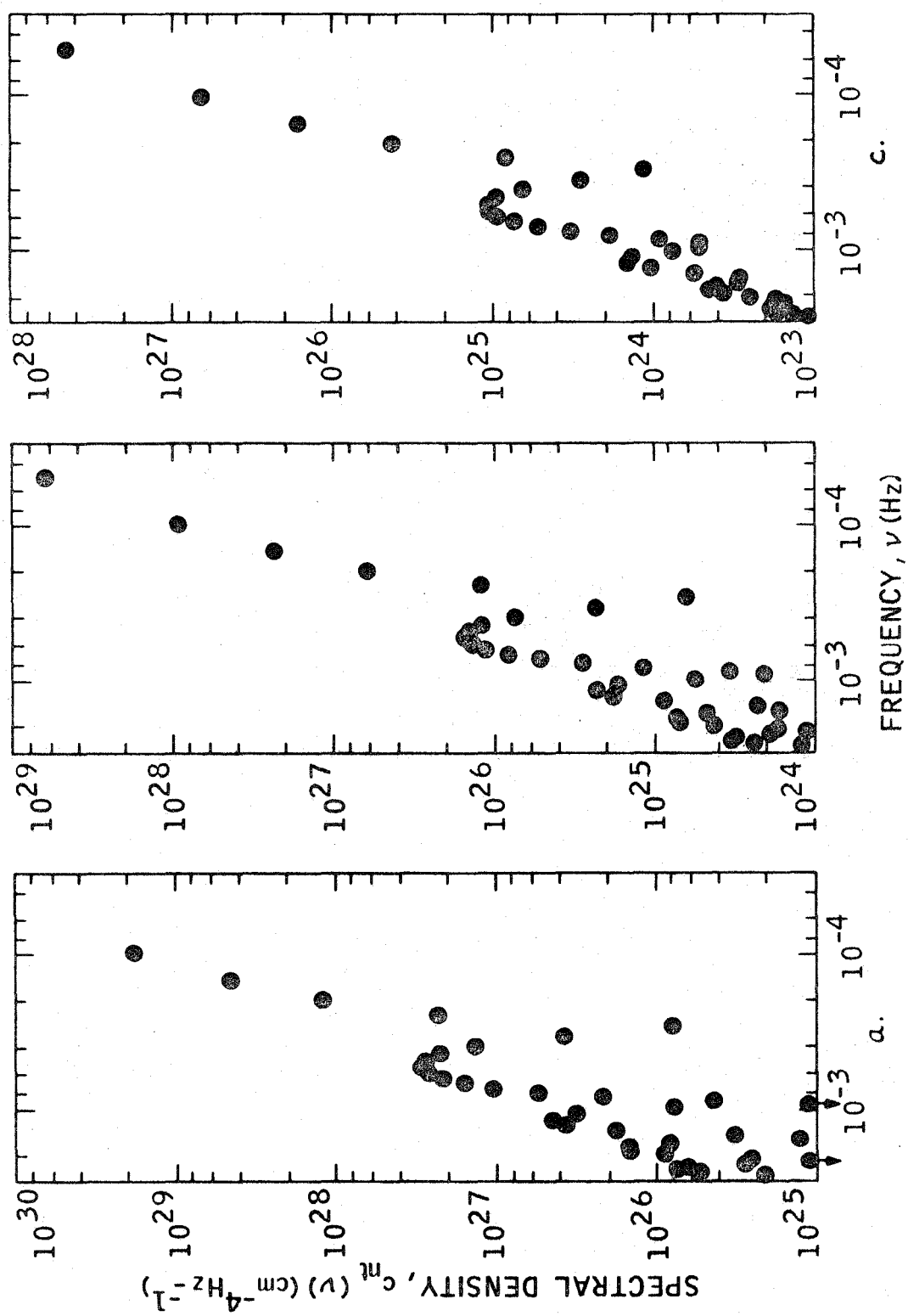

Figure 4.3. Theoretical power spectra from evaluation of equation (4.19), normalized as in Figure 4.2. The deep minima occur at the same frequencies and decrease away from the sun. The spectral amplitudes differ from those of Figure 4.2 only at the lowest frequencies. Parameters: $\beta = 3.5$, $\gamma = 0.25$, $\ell_o = \infty$. Part a, $\epsilon = 3°$; b, $\epsilon = 7°$; c, $\epsilon = 15°$.

measures the fall-off of density fluctuations with heliocentric distance. Comparison of measurements near the sun with those at 1 a.u. will give a very sensitive determination of the value of γ which characterizes the large scale behavior of the solar wind.

B. PREDICTED SPECTRA FOR DIFFERENT VELOCITY AND DENSITY MODELS

The results of the first section are for the simplest velocity and density models that might describe the solar wind. The functions are smooth functions of r and s, and thus do not allow for observed structures such as high speed streams (Neugebauer and Snyder, 1966) or density enhancements associated with magnetic sectors (Wilcox and Ness, 1965). It is also of interest to find out what sort of variations of $b(\underset{\sim}{r})$ and v_x will remove the deep minima in the spectra predicted by Eq. (4.19). The analysis here will deal only with large scale disturbances and will not attempt to modify the assumption that the velocity does not change significantly in a correlation scale or that the distance scale is much larger than the correlation scale.

To facilitate the investigation of velocity and density models Eq. (4.14) is recast in terms of μ and simplified. The terms involving k_0^2 and v_x^2/c^2, which were shown to be negligible, are discarded. The a's are set to 1. After these simplifications Eq. (4.14) becomes

$$c_{nt}(\nu) = \frac{\Gamma\left(\frac{\beta - 1}{2}\right) q^{-3-2\gamma}}{2\sqrt{\pi}\,\Gamma(\beta/2)(2\pi\nu)^{\beta-1}} \cdot$$

$$\int_{-\mu_1}^{\mu_2} b(\mu)\, v_x^{\beta-2}(\mu) \left[1 + e^{-i4\pi\nu q(\mu-\mu_2)/c} \right] d\mu \qquad (4.20)$$

where $b(\mu)$ and $v_x(\mu)$ are to be specified.

Before examining specific functions for $b(\mu)$ and $v_x(\mu)$ let us recall the results of the first section. The spectral minima were deeper for larger values of β and γ, and for ray paths nearer the sun. The region near the sun is critical for the resonance effect which produces the minima. Since in any sensible model $b(\mu)$ and $v_x(\mu)$ must vary inversely with μ, Eq. (4.20) shows that this region will be less important if $b(\mu)$ and $v_x(\mu)$ vary slowly with μ. Physically, this detunes the resonance by making a whole region near the sun equivalent. Mathematically, it changes the phase of the second term in Eq. (4.20). However, the large scale variation of $b(\mu)$ and $v_x(\mu)$ is fixed by solar wind observations near the earth. Thus, any changes in $v_x(\mu)$ and $b(\mu)$ must occur in fairly small ($\sim 10^7$ km) structures or in a region near the sun. The latter case is particularly interesting because of the observations by Ekers and Little (1971) of large turbulent (i. e., non-radial) velocities in the region from 6 to 30 $R_\odot$ ($\sim$ 0.03 to 0.14 a.u.).

The effect of several kinds of velocity and density distributions on the observed spectra of DRVID data will be discussed. Three cases are easily analyzed using Eq. (4.20):

A localized density enhancement ("stream") of variable width.

A high velocity stream.

A velocity everywhere perpendicular to the ray path.

In addition a number of cases simulating a region of turbulent velocity or a slow density fall-off near the sun were investigated with the computer program used to numerically integrate Eq. (4.16). The results obtained for these perturbed cases may be compared to a slightly simplified form of Eq. (4.19), viz.

$$c_{nt}(\nu) \cong \frac{3}{8\sqrt{\pi}} \frac{\Gamma\left(\frac{\beta - 1}{2}\right) v_0^{\beta-2} q^{-3-2\gamma}}{\Gamma\left(\frac{\beta}{2}\right)(2\pi\nu)^{\beta-1}} \left[\pi D(1 + e^{-d} \cos d\mu_2)\right] , \quad (4.21)$$

where $d = 4\pi\nu q/c$, and $\gamma + \beta/2 = 2$.

A high density stream of variable width can be represented by a delta function as

$$b_{SL}(\mu) = \frac{I_S \ell_0 (1 + \mu_0^2)^{-1} \delta(\mu - \mu_S)}{q^{4+2\gamma}(1 + \mu^2)^{1+\gamma}} , \quad (4.22)$$

where ℓ_0 is the dimensionless width of the stream, $\ell_0 = L_{stream}/q$, measured at μ_0, I_S is the square of the overdensity of the stream, and μ_S is the position at which the stream crosses the ray path. Such a stream adds a constant columnar content at all heliocentric distances. If Eq. (4.22) is used in Eq. (4.20)

along with a radial velocity, one finds for the addition to the spectrum of DRVID data

$$c_{nt}(\nu)_{stream} = \frac{3}{8\sqrt{\pi}} \frac{\Gamma\left(\frac{\beta-1}{2}\right) v_0^{\beta-2} q^{-3-2\gamma}}{\Gamma\left(\frac{\beta}{2}\right)(2\pi\nu)^{\beta-1}} \times \left\{ \frac{4}{3} \frac{I_S \ell_0 \left[1 + \cos\left[d(\mu_2 - \mu_S)\right]\right]}{(1+\mu_S^2)^{\gamma+\beta/2} (1+\mu_0^2)} \right\} . \quad (4.23)$$

For reasonable values of $I_S \ell_0$, of the same order as D, the perturbation is only important for $\mu_S \cong 0$. (The range of μ is $0 \lesssim \mu \lesssim 30$, for ray paths near the sun.) The stream must intersect the ray path near the sun in order to have a significant spectral amplitude. The cosine term is then in phase with that in Eq. (4.21) and no cancellation of the minima occurs. Note that the spectrum of the stream has the same q dependence as the unperturbed spectrum.

A high velocity stream represented by $v_1 \delta(\mu - \mu_S)$ coupled with the normal density distribution will clearly give a result very similar in form and interpretation to Eq. (4.23). To study a velocity everywhere normal to the ray path, i.e., $v_x(\mu) = v_0$, the integral in Eq.(4.20) must be carried out by contour integration. The result is (to within the approximations used) is exactly the same as Eq. (4.21).

From these three cases it is clear that neither streams nor large scale velocity and density distributions that primarily affect regions far from the sun ($\mu \gtrsim 2$) will affect the spectral minima predicted by Eq. (4.21). However, the analysis suggests that events occurring near the sun may be very important in determining the shape of the DRVID spectra.

Many numerical integrations of Eq. (4.16) were made in which the velocity and/or density in the region within 0.2 a.u. of the ray path's closest approach to the sun were modified. The sense of the modifications was to reduce or eliminate the radial dependence (i.e., dependence on μ) of Δn and v_x in this region. Reducing the μ-dependence of v_x introduces a non-radial velocity component. Fig. 4.4 is an example of the results. In this case both the velocity and the density were independent of μ in the region near the sun. For all the modified densities and velocities the depth of the minima was reduced, particularly at the higher frequencies. However, no reasonable distribution of velocity and density could be found which removed the minima completely. Furthermore, none of the modified distributions affected the large scale radial (q) dependence of the spectra.

This analysis has not considered the problem of the velocity having a correlation scale similar to that of the density. No doubt this will also tend to reduce the spectral minima by smearing the resonance effect. However, when the solar wind is

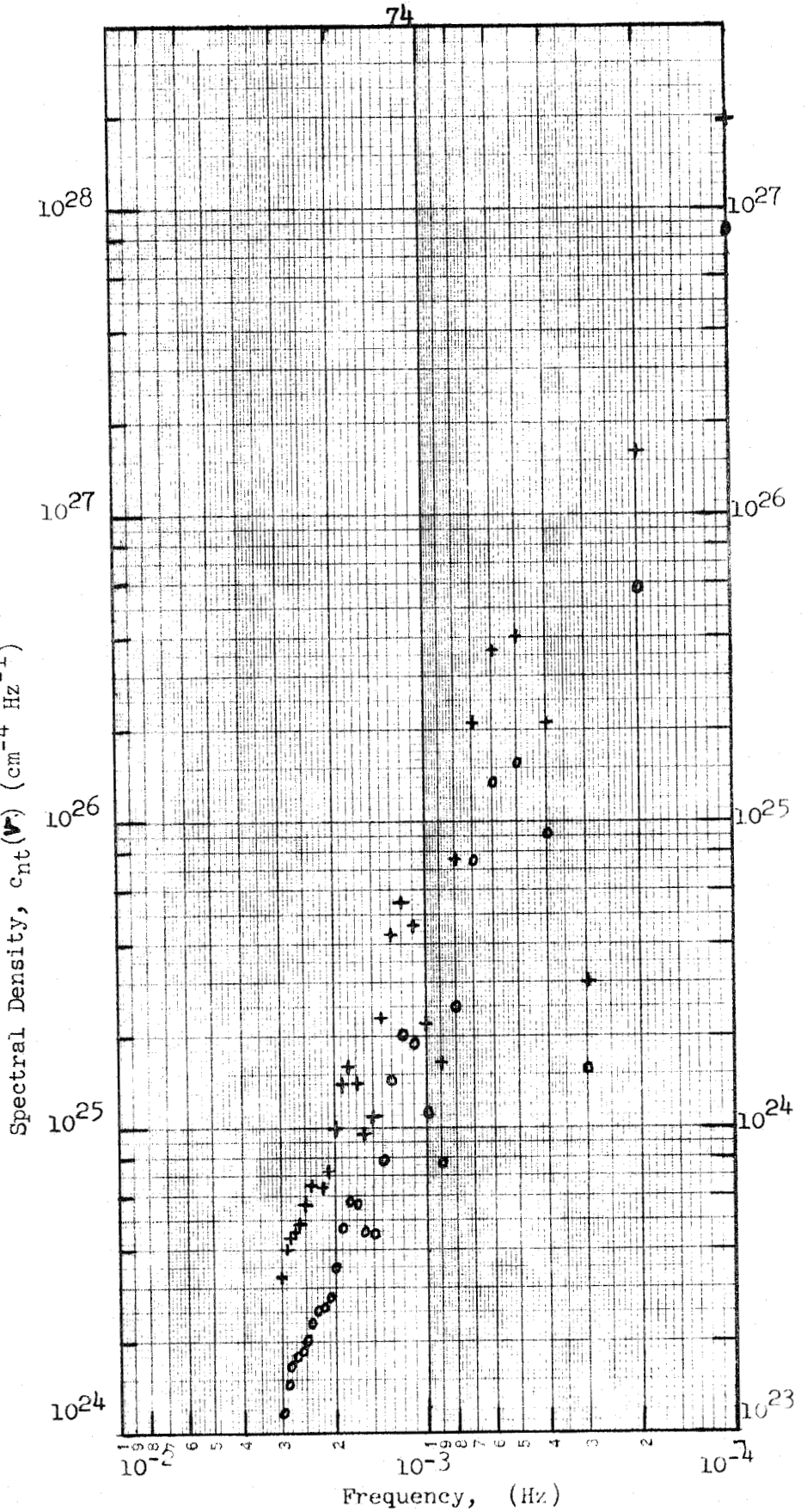

Figure 4.4. Predicted power spectra from numerical integration in which the velocity and density were kept constant within 0.2 a.u. of the sun. Parameters are the same as those used in Figures 4.2 and 4.3. The minima are not so deep, particularly at the higher frequencies. The +'s are for $\epsilon=7^{\circ}$, use left scale; O's, $\epsilon=15^{\circ}$, right scale.

quiet, one might hope that the velocity would be fairly steady, and this smearing would be minimized. The minima will also be reduced because near the sun the distance scale is only a few times the correlation scale. This results in some broadening of the delta function from the ℓ-integral in Eq. (4.10). The broadened delta function will fill up the minima from nearby regions of the spectrum. However, analysis shows that the delta function approximation should be adequate in the regime probed by the DRVID measurements. The spectra will be examined for the predicted minima at moderate distances from the sun when the solar wind is quiet to shed light on the velocity and density distributions near the sun.

C. THE RELATION OF DRVID SPECTRA TO IN SITU SPACECRAFT MEASUREMENTS

Most observations of the low-frequency spectrum of the solar-wind turbulence reported to date have been made by spacecraft at rest ($v \ll v_{SW}$) with respect to the sun. The spectrum found from such observations, $F_{nt}(\nu)$, can easily be related to the comoving wavenumber spectrum of the solar wind (Cronyn, 1970). In the notation of Section A the result is

$$F_{nt}(\nu) = \frac{b(R_0)}{(2\pi)^2 v_0} \int_{-\infty}^{\infty} dk_y \, dk_z \, g_{nr}\left(\frac{2\pi\nu}{v_0}, k_y, k_z\right), \qquad (4.25)$$

where R_0 is the spacecraft's distance from the sun. If a power-law spectrum of the form (4.13) is used the integrals may be carried out to give

$$F_{nt}(\nu) = \frac{\Gamma\left(\frac{\beta - 2}{2}\right) D\, v_0^{\beta-3}}{4\pi\Gamma(\beta/2)\, R_0^{4+2\gamma}\, (2\pi\nu)^{\beta-2}} \tag{4.26}$$

where Eq. (4.15) has been used for $b(R_0)$. As pointed out by Cronyn (1970) the spectrum is two powers less steep in frequency than the comoving spectrum. Comparison with the DRVID spectrum, Eq. (4.21), shows that $F_{nt}(\nu)$ is one power less steep in frequency, but one power more steep in heliocentric distance.

In order to facilitate the comparison of DRVID spectra to those of other investigators it is useful to write the DRVID spectrum $c_{nt}(\nu)$ in terms of $F_{nt}(\nu)$. The comoving amplitude D can be eliminated between Eqs. (4.21) and (4.26) to give

$$c_{nt}(\nu) \cong \left[\frac{F_{nt}(\nu)}{\nu}\right] 1.59 \times 10^{24+2\gamma} \frac{\Gamma\left(\frac{\beta - 1}{2}\right)}{\Gamma\left(\frac{\beta - 2}{2}\right)} \left(\frac{R_0}{a.u.}\right) \cdot \left(\frac{\frac{R_0}{a.u.}}{\frac{q}{0.1\ a.u.}}\right)^{3+2\gamma} \left(\frac{v_0}{400\ \text{km s}^{-1}}\right) \left\{\frac{(1 + e^{-d} \cos d\mu_2)}{2}\right\} . \tag{4.28}$$

Eq. (4.28) strictly holds only for $\gamma+\beta/2$. However, the only change caused by a violation of this restriction is to slightly modify the term in braces, which in any case is of the order of 1. Eq. (4.28) will be used in Chapter V to find the index γ which characterizes the fall-off of the density fluctuations with heliocentric distance.

V: DRVID MEASUREMENTS OF THE SOLAR-WIND TURBULENCE

The physics, implementation, and gathering of DRVID data have been discussed in Chapter II. Data reduction procedures were outlined in Chapter III. Chapter IV derived the relationship between the spectrum of DRVID data and the comoving wavenumber spectrum of the solar wind. In this chapter the spectra of the DRVID data obtained during the MM69 and MM71 missions are presented.

In the first section the DRVID data records are discussed in terms of their columnar content change and the size of the density fluctuations which contribute to the change. The data show that the dominant scale size for density changes is $\sim 1.5\text{-}3.0 \times 10^{6}$ km, in agreement with the suggestion of Jokipii and Hollweg (1970). Local density changes exceeding 100% are inferred.

The average spectra of the DRVID data for the MM69 and MM71 missions are presented. The spectra may be well represented by a power-law whose slope implies a comoving spectral index of $\beta = 3.9 \pm 0.2$ for $1.0 \times 10^{-4} \lesssim \nu \lesssim 1 \times 10^{-3}$ Hz. The slope and amplitude of these spectra are compared to the spectrum of proton density fluctuations of Intriligator and Wolfe (1970) (hereafter called IW). The DRVID spectra are somewhat steeper than that of IW whose data gave a comoving spectral index of $\beta = 3.3 \pm 0.3$. In order for the

amplitudes of the DRVID spectra to agree with that of IW the rms solar-wind density fluctuations must (1) decline as $r^{-2.38\pm0.11}$ between $r \cong 0.15$ and $r = 1$ a.u., assuming no long-term time variations; or (2) decline approximately as r^{-2}, if the turbulence amplitude is proportional to sunspot number throughout the solar cycle.

The temporal behavior of the MM71 data was investigated. The post-conjunction spectra have systematically lower amplitudes than the pre-conjunction spectra. This variation correlates with large scale indices of solar activity, viz. Zurich sunspot number and 2.8 GHz radio flux. No correlation with heliographic latitude and longitude, or with McMath plage regions is found.

To investigate the variation with radius near the sun the DRVID spectra were grouped by the distance of the ray path's closest approach to the sun (q) and averaged. For the MM71 data $\Delta n(r)$ is proportional to $r^{-1.5\pm0.2}$ in the region $0.07 \leq r \leq 0.22$ a.u. The slope for the MM69 data is not well determined but is approximately -2.0 to -2.5.

The average spectra contain only marginal evidence for the existence of the minima found in the analysis of Chapter IV.

The observational results on the spectrum of the solar-wind turbulence are summarized at the end of this chapter. The implications of these results for theories of the solar wind are discussed in Chapter VII.

A. QUALITATIVE DESCRIPTION OF DRVID DATA

Plots of the DRVID data records reveal much information about the scale of fluctuations in the solar-wind density. Callahan (1973) discusses some of the MM71 DRVID data qualitatively. The data may be characterized by the change in the columnar content during a day, the rate of the columnar content change, and the overall shape of the change.

The DRVID records show that the columnar content change in a record (6-10 hours) is highly variable from day to day. Values of ΔI are rather uniformly spread in the interval 1.8 to 20 x 10^{14} cm^{-2}, with two examples approaching 30 x 10^{14} cm^{-2}. The day to day variations in ΔI mask any changes caused by the varying distance of the ray path from the sun. Figure 5.1 shows the standard deviation of each DRVID record about its mean plotted against q. There is some indication that the value increases near the sun, but the scatter is nearly as large as the effect.

The rate of change of ΔI can be found from the plots of the DRVID data. Typical rates are $\sim 4 \times 10^{10}$ cm^{-2} sec^{-1}. The maximum rate found was 2.5 x 10^{11} cm^{-2} sec^{-1}. When ΔI reverses its sense of variation, the change requires less than one hour. Thus, the second derivative of ΔI is of the order of 2 x 10^{7} cm^{-2} sec^{-2}.

Two general types of DRVID records are found. First, there are "slopes" in which the columnar content changes at a rather uniform rate for several hours and then slowly takes on a new rate. The data have little small scale structure that exceeds

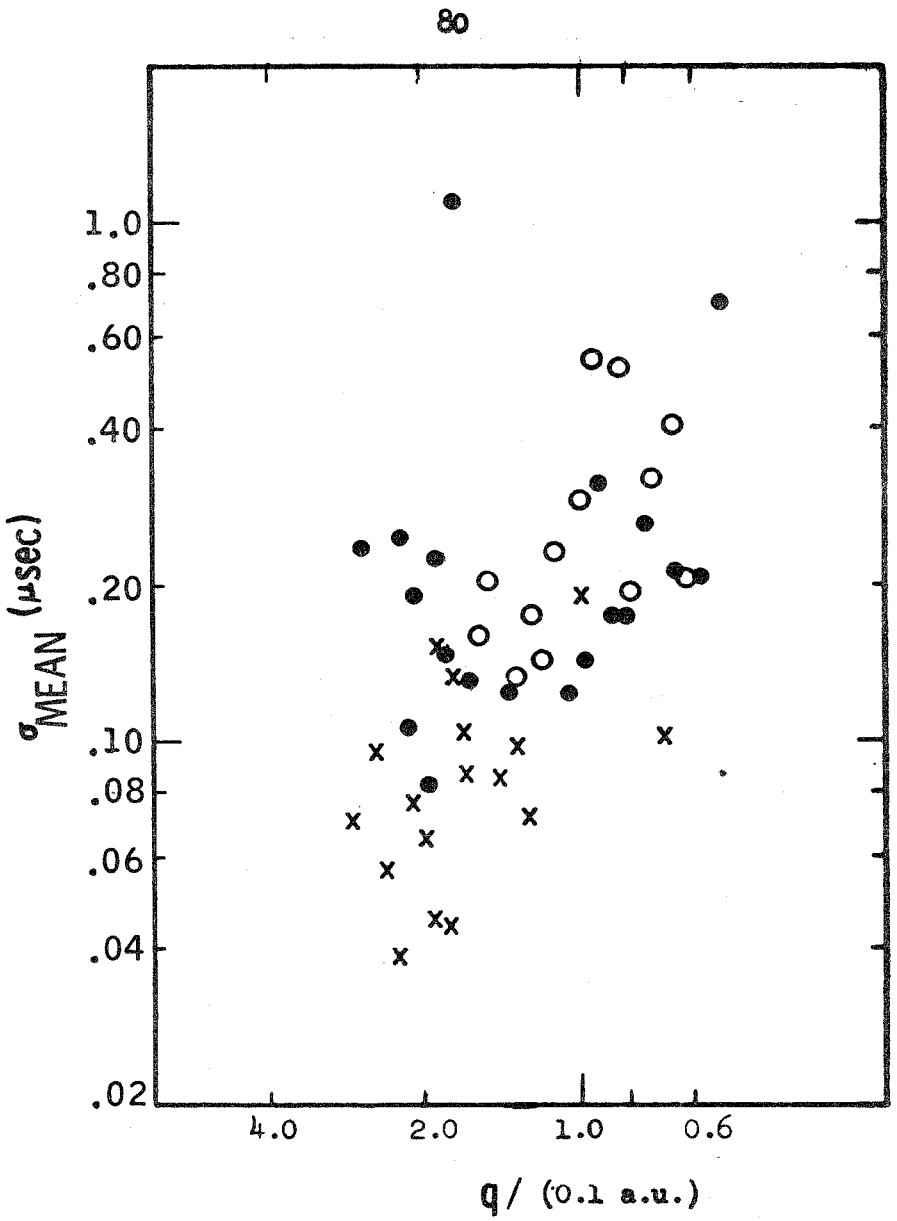

Figure 5.1. The standard deviation of the DRVID data records about their individual average values plotted against the distance of closest approach. Note the large scatter. x,MM69. 0,MM71 preconjunction. ●,MM71 postconjunction. The standard deviation values may be converted to one way columnar content (cm^{-2}) by multiplying by 8.99×10^{14}.

the data noise. Second, there are "humps" in which the columnar content rate reverses its sign. The columnar content rate dominates the data noise. Figure 5.2 is a particularly striking example of this form. One has the impression of two clouds of high density plasma crossing the ray path. If the time scale, $\sim 10^4$ sec, is multiplied by the solar wind velocity normal to the ray path, ~ 300 km sec^{-1}, the scale size is $\sim 3 \times 10^6$ km. Many other data records have structures of a similar scale.

A few million kilometers is often mentioned as a typical size for the most important density fluctuations in the solar wind. The DRVID data records support this contention. In a qualitative analysis the DRVID data are sensitive to changes taking more than about 1/2 hour and less than about 10 hours. However, all important columnar content changes appear to take place on a time scale greater than one hour and usually less than 5 hours. These times correspond to scale sizes of greater than 1 million, but less than 6 million kilometers, if the velocity normal to the ray path is taken to be 300 km sec^{-1}.

If one assumes that the humps are caused by a single, dense, roughly spherical cloud crossing the ray path, the local density change can be inferred. The thickness of the cloud is $\sim L$, where L is estimated as above, and $\Delta n = \Delta I/L$. For the data of Figure 5.2 one gets $\Delta n \cong 2 \times 10^3$, which represents about a 200% change in the local electron density (assumed to vary as r^{-2}) if the region crosses the ray path at its point of closest approach to the sun. Of the 50 data records used in this study, 12 show columnar content changes equalling or exceeding that in Figure 5.2.

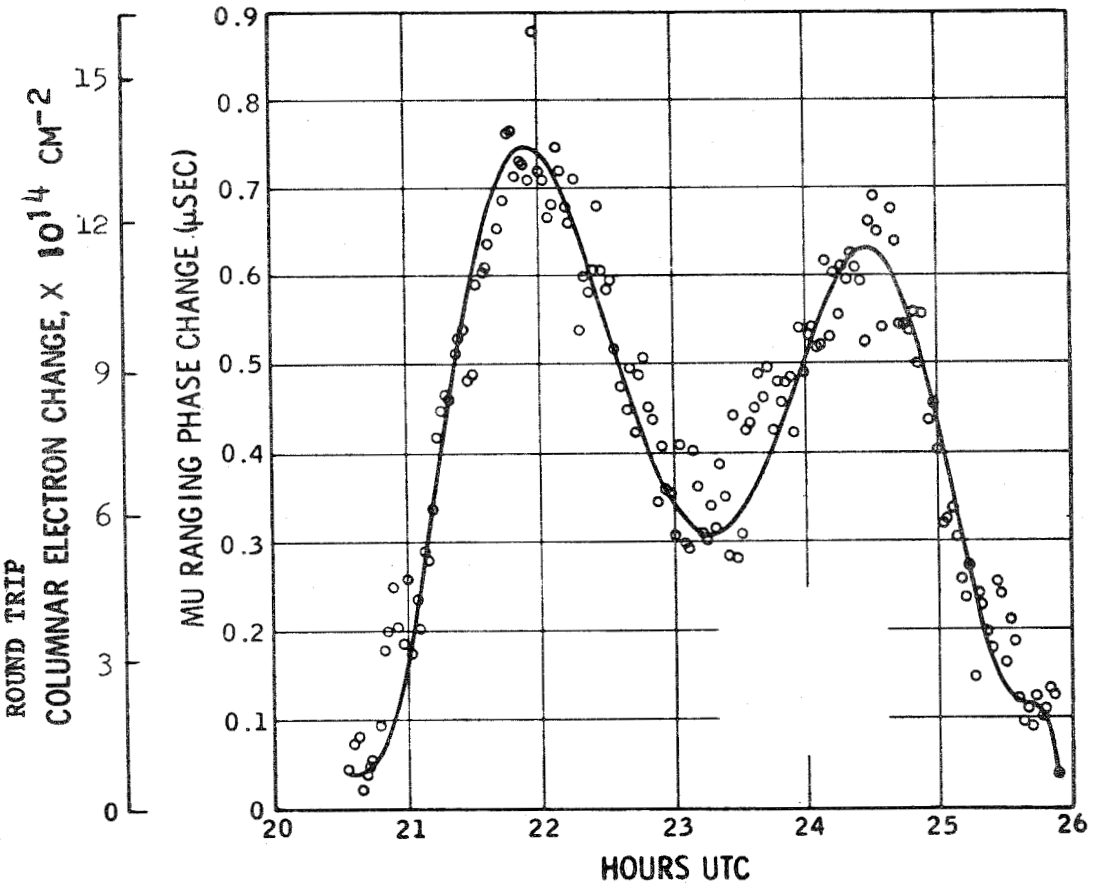

Figure 5.2. An example of a DRVID data record showing a large columnar content change. The columnar content change can be viewed as two clouds crossing the line of sight. The data were obtained while tracking Mariner 7 on 1970 May 29. The sun-earth-probe angle was 6°, and the distance to the spacecraft was 2.5 a.u.

Columnar content variations like that in Fig. 5.2 represent about a 20% change in the total columnar content. The fact that the total columnar content varies only about 20% when local density changes exceed 100% gives indirect evidence of the scale size of the solar-wind turbulence. If the ray path is viewed as a number of cells whose densities vary randomly by a factor of about 2, the number of cells required to keep the variation of the total columnar content to 20% is given by $\Delta I/I \sim 1/\sqrt{N_c}$, or $N_c \cong 25$. For ray paths which pass fairly near the sun, the part of the path nearest the sun makes the dominant contribution to the columnar content. Thus, the scale size of the turbulence, viewed simply as a number of equally sized clouds, is $\sim$ 0.5 a.u./25 = 3×10^6 km.

B. THE AVERAGE DRVID SPECTRUM

The program described in the third section of Chapter III was used to average the data from the MM69 and MM71 missions into the spectra shown in Figures 5.3 and 5.4. Because the data records were shorter for the MM69 mission the spectral resolution is less, and no attempt was made to combine the MM69 and MM71 spectra. The spectra shown are "one-sided" spectra produced by the formulae in Bendat and Piersol (1966) and are twice the value of the mathematical spectra of Chapter IV.

Data characterizing spectra discussed in this section are in Table 5.1. The columns give

(1) The data averaged, designated by line number from Table 2.1;

(2) The number of individual spectra averaged;

(3) The parameters S, D, $(\beta - 1)$ of the model spectrum fit to the data,

$$P_F(\nu) = S + D\nu^{-(\beta - 1)}; \qquad (5.1)$$

(4) The value of the averaged spectrum at $\nu_3 = 3 \times 10^{-4}$ Hz, $P_A(\nu_3)$;

(5) The value of the model spectrum at $\nu_3 = 3 \times 10^{-4}$ Hz, $P_F(\nu_3)$; and

(6) The average value of q in units of 0.1 a.u.

The amplitudes of the spectra were measured at 3×10^{-4} Hz, in spite of the theoretical minima, because the spectra suffered the least corruption from noise and the limited length of the data records at that frequency. At higher frequencies the inaccuracies in the subtraction of the noise level become important, while at lower frequencies the amplitudes cannot be reliably estimated from data records as short as those used.

(1) Data Sets		(2) N	(3) S	(3) D	(3) β-1	(4) $P_A(\nu_3)$	(5) $P_F(\nu_3)$	(6) $\underline{q}$
1-17	MM69	17	1.0E29	4.0E20	2.85	4.8E30	4.4E30	1.85
18-50	MM71	33	2.0E29	4.8E20	2.95	7.8E30	1.2E31	1.32
1-17 odd	MM69	9	1.5E29	8.3E20	2.70	3.1E31	2.5E30	1.86
1-17 even	MM69	8	7.0E28	1.5E20	3.00	6.7E30	5.8E30	1.85
18-50 Alt 1	MM71	16	3.5E29	4.0E20	3.00	6.5E30	1.5E31	1.30
18-50 Alt 2	MM71	17	3.5E29	7.5E20	2.90	9.4E30	1.4E31	1.34

Table 5.1. The overall average spectra of the MM69 and MM71 DRVID data are shown on the top two lines. The errors in these spectra are estimated by dividing each mission's data into two groups by taking every other data set, and then averaging these groupings. This procedure estimates both the quality of the original data and the reliability of the fitting process used to get the model parameters in column 3. The columns are more fully described in the text.

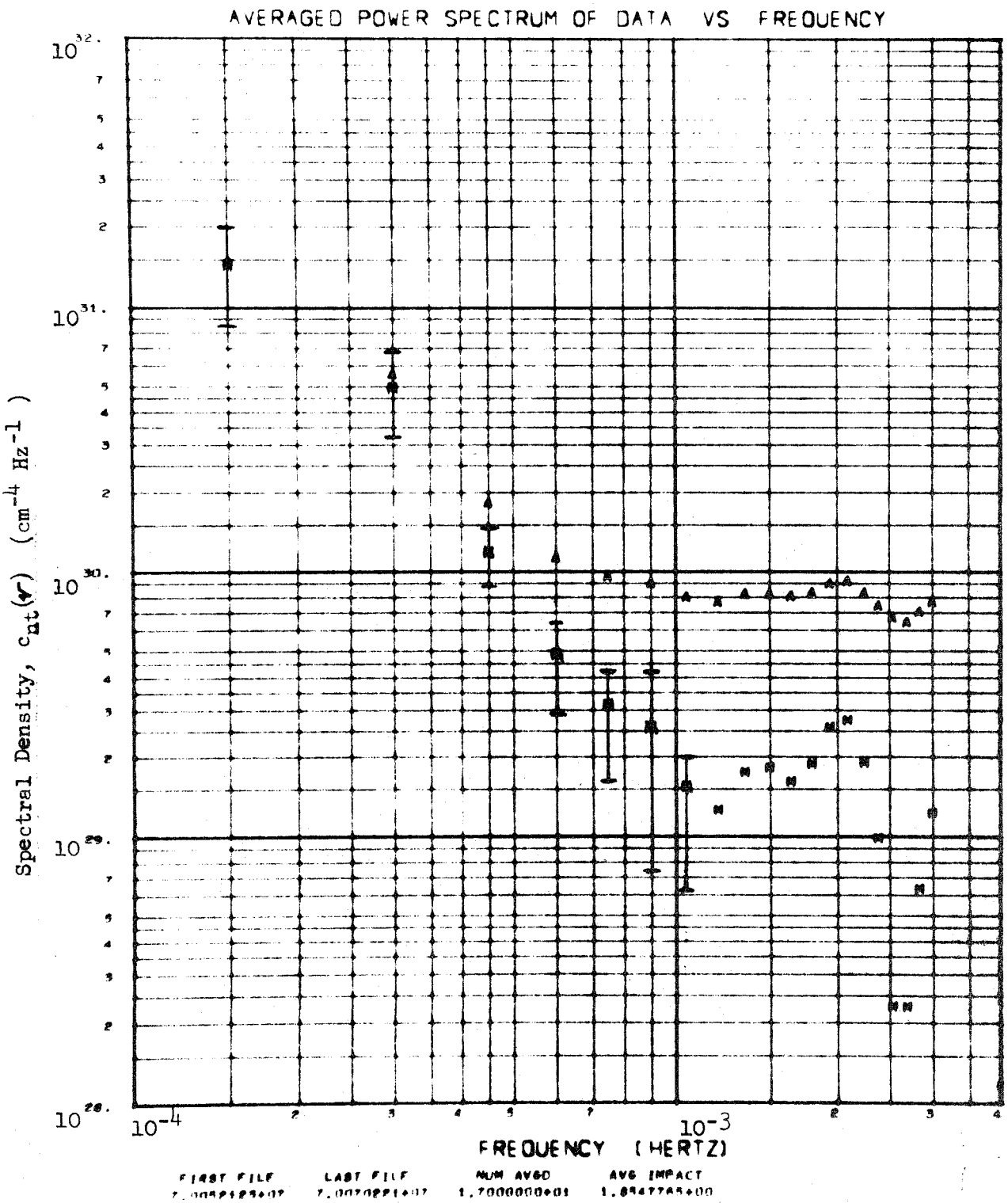

Figure 5.3. Overall average spectrum of MM69 data. Error bars show variations found when alternate data sets are averaged (See Table 5.1). The M's give the spectral values after the minimum of the average values (A's) is subtracted from all points. "AVG IMPACT"is the average distance of closest approach in tenths of a.u.

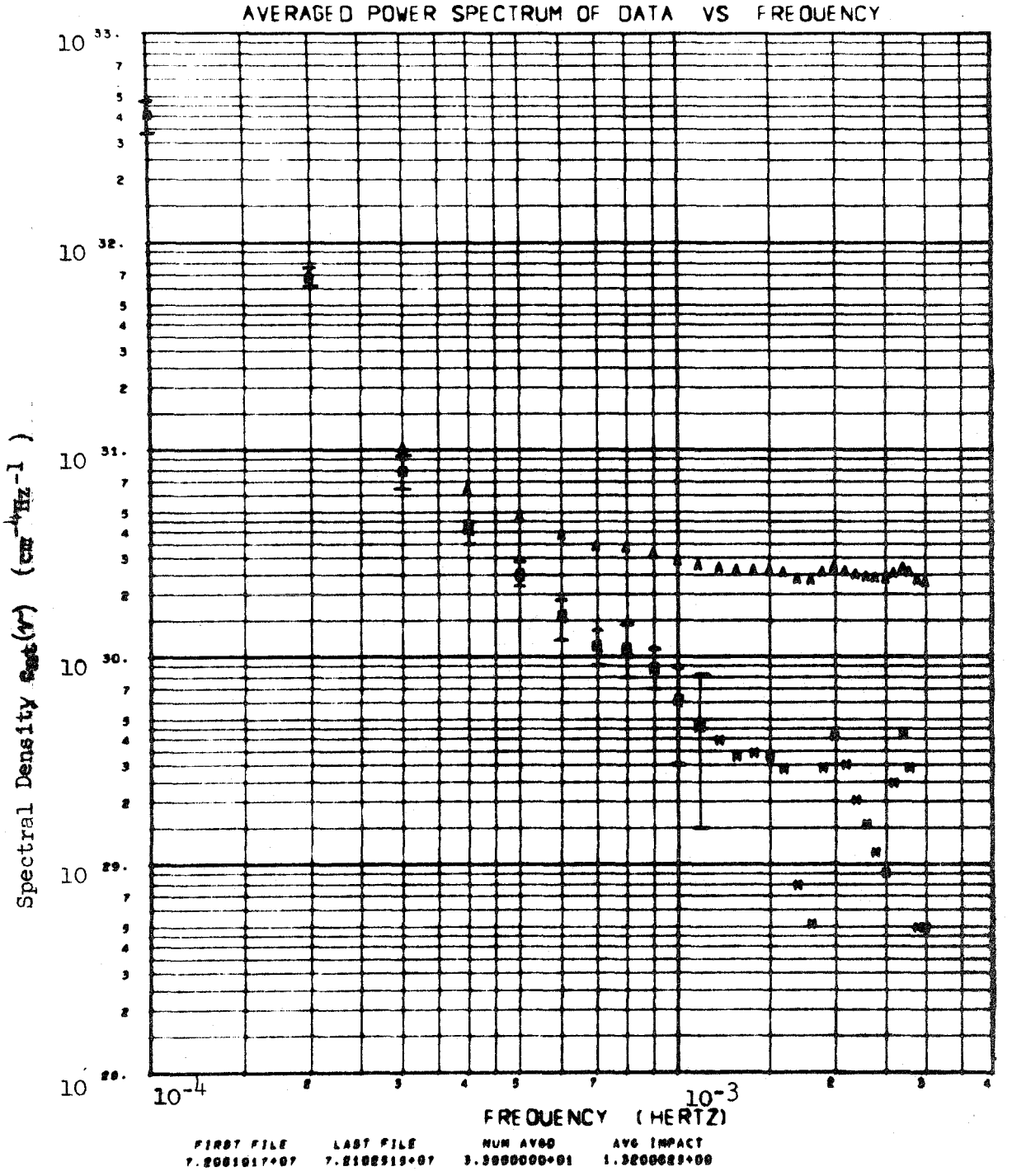

Figure 5.4. Overall average spectrum of MM71 data. Averaging more data gives smaller error bars and a better estimate of the noise than for the MM69 data. Even with the noise subtraction the spectrum flattens somewhat between 7 and 9×10^{-4} Hz. Other comments of Figure 5.2. also apply to this figure.

The parameters for the overall average spectra are on the top two lines of Table 5.1. The parameter of most interest is the spectral index. Its value is 2.85 for the MM69 data, 2.95 for the MM71 data. The error in these slopes, based on the possible fits to the spectra, is approximately $\pm$ 0.2. The error may also be estimated by forming average spectra with alternate data sets from Table 2.1 and comparing the results to Figures 5.3 and 5.4. The next four lines of Table 5.1 give the parameters for these spectra. Again the error in the slopes is about $\pm$ 0.2

Figures 5.3 and 5.4 show the $\sqrt{N}$ improvement in signal to noise ratio expected after averaging. In Figure 5.4 the noise level after subtraction is a factor of 6 (N = 33) less than before. Since the spectrum has a slope of about 3, this gives an extension of the frequency range by a factor of 2 from $\sim 4 \times 10^{-4}$ Hz to $\sim 7 \times 10^{-4}$ Hz. The spectrum in the region 8×10^{-4} to 1.3×10^{-3} Hz has its slope reduced slightly by the noise.

For the MM69 data (Figure 5.3) the amplitude of the lowest frequency point is reduced because of the shortness of the original data records. The data were only sufficient to provide a reliable spectrum above $\sim 3 \times 10^{-4}$ Hz. However, to obtain increased resolution at higher frequencies, the point at 1.5×10^{-4} Hz was computed. The signal to noise ratio was improved by about a factor of 4 by the noise removal.

The average spectrum of the MM71 data shows little or no effect which could be attributed to a long wavelength limit to the solar wind turbulence. The numerical integrations of Eq. (4.16) then suggest that $\ell_o \gtrsim 1.2 \times 10^7$ km. In this case the use of Eq. (4.19) which ignores the long wavelength cutoff is completely justified.

A line of slope 2.9 provides a good fit to both averaged spectra. It implies a comoving spectral index $\beta = 3.9 \pm 0.2$. IW report a spectral index for proton density fluctuations which gives $\beta = 3.3 \pm 0.3$. However, $\beta = 3.5$ provides a good fit to their data and values up to $\beta = 3.8$ are possible. Because of the small ($\lesssim 10^3$ cm) Debye length in the solar wind, one would expect the electrons and protons to have the same turbulence spectrum. Thus, over a considerable range of heliocentric distances and more than one-half a solar cycle the spectral index of the solar wind turbulence appears to vary hardly at all.

The averaged DRVID spectra ($c_{nt}(\nu)$) can be compared to the spectrum of IW ($F_{nt}(\nu)$) by using Eq. (4.28), where a factor of 2 has been introduced to account for the one-sided spectrum output by the data processing programs.

$$c_{nt}(\nu) \cong \left[\frac{F_{nt}(\nu)}{\nu}\right] 3.18 \times 10^{24+2\gamma} \frac{\Gamma\left(\frac{\beta-1}{2}\right)}{\Gamma\left(\frac{\beta-2}{2}\right)} \left(\frac{R_o}{\text{a.u.}}\right)$$
$$\left(\frac{R_o/\text{ a.u.}}{q/0.1\text{ a.u.}}\right)^{3+2\gamma} \left(\frac{v_o}{400\text{ km s}^{-1}}\right) \left\{\frac{1 + e^{-d} \cos d\mu_2}{2}\right\} .$$

Since the spectral indices are very similar the comparison gives the index γ which measures the rate of fall-off of the density fluctuations between the point of the ray path's closest approach to the sun and 1 a.u. where the proton spectrum was measured. Comparisons were made at 3×10^{-4} Hz and 6×10^{-4} Hz for both the MM69 and the MM71 data. The effect of the theoretical minima at 3×10^{-4} Hz was ignored; the term in braces was set to 1 at 3×10^{-4} Hz and to 1/2 at 6×10^{-4} Hz. Table 5.2 gives the results of the comparisons and their errors based on the range of the alternate spectra. The average value of γ is $\bar{\gamma} = 0.38 \pm 0.11$. The quoted error is the standard deviation of the values from $\bar{\gamma}$. The small value of γ for the MM71 data at 3×10^{-4} Hz may result from ignoring the predicted minima there; using $P_F(\nu_3) = 1.2 \times 10^{31}$ gives $\gamma = 0.28$.

The comparisons between the DRVID spectra and the spectrum of IW show that, on the average, the amplitude of solar-wind density fluctuations falls off considerably faster than r^{-2} between 0.15 and 1 a.u. The determination of γ is based on the assumption that the solar-wind density fluctuations have a uniform power-law dependence on heliocentric distance between the point of closest approach to the sun of the Mariner line-of-sight and 1 a.u. If this assumption is not correct and there is a region near the sun where the density fluctuations fall off more slowly than r^{-2} (see the next section), the effective value of γ outside this region may be reduced from the values given above. That is, from the outer edge of the region of enhanced turbulence to 1 a.u. the fluctuations may decline as r^{-2}, but in comparing the interior of the region to 1 a.u. one finds $\Delta n(r) \propto r^{-2.38}$.

Table 5.2

Summary of the comparison of DRVID spectral amplitudes to the spectrum of Intriligator and Wolfe (1970) to find the large-scale radial dependence of the solar-wind turbulence assumed to behave as $\Delta n(r) \propto r^{-(2+\gamma)}$. $R_0 = 0.95$ a.u.

DRVID Data	Frequency (hz)	Spectral Value (cm^{-4} Hz^{-1})	Average q (0.1 a.u.)	Intriligator and Wolfe Value (cm^{-6} Hz^{-1})	γ
MM69	3×10^{-4}	4.8×10^{30}	1.85	1.1×10^{3}	0.39 ± 0.12
	6×10^{-4}	4.9×10^{29}	1.85	3.6×10^{2}	0.45 ± 0.10
MM71	3×10^{-4}	7.8×10^{30}	1.32	1.1×10^{3}	0.18 ± 0.12
	6×10^{-4}	1.6×10^{30}	1.32	3.6×10^{2}	0.42 ± 0.04

Average $\gamma = 0.38 \pm 0.11$

The comparisons also ignore any short-or long-term time variations in the amplitude of the turbulence. The short-term effects should not be too important because of the long spans of data averaged. The data of IW cover three weeks. The DRVID spectra each cover at least six weeks and agree well over a separation of two years. The possibility of long-term variations cannot be ruled out. The DRVID data were obtained near the maximum of the current sunspot cycle, while the data of IW were obtained (1965 December, 1966 January) near the minimum. Data presented in the next section shows that short-term variations in the amplitude of the turbulence spectra correlate with sunspot activity. The data in Table 5.2 show that the MM69 spectrum taken nearer the sunspot maximum give larger values of γ than the MM71 spectrum. If these correlations between sunspot number and spectral amplitude hold throughout the solar cycle, the value of γ corrected for this effect may not differ significantly from zero. Thus, there is either strong overall radial variation or strong long-term time variation in the solar-wind turbulence.

C. RADIAL VARIATION OF THE DRVID SPECTRA NEAR THE SUN

The measurement of the radial dependence of the solar-wind density fluctuations near the sun is extremely important for theories of solar wind heating. DRVID spectra are a useful probe of the solar wind near the sun. To make clear any systematic changes of the spectra with q by smoothing out the large day to day variations in the amplitudes, several spectra with similar values of q were averaged together. The data were grouped so that approximately one-quarter of the spectra were in each averaged spectrum. During the MM71 mission data were obtained before and after the spacecraft's superior conjunction so the data were grouped by both time period and q.

The results of averaging the grouped spectra are given in Table 5.3; its format is the same as Table 5.1. The amplitudes of the averaged spectra at 3×10^{-4} Hz are plotted against q in Figure 5.5a. The overall averaged amplitudes are also shown with their errors (based on alternate data sets) to indicate the range of variation expected. Figure 5.5a shows that generally the MM69 spectra fit in rather well with the MM71 data. However, the MM69 data may fall off somewhat more rapidly with q. Figure 5.5b shows that the MM71 post-conjunction amplitudes are all substantially less than the preconjunction amplitudes, but the radial dependence is very similar.

Table 5.3

Groupings of DRVID data used to investigate variation of the spectra near the sun.

(1)	(2)	(3)			(4)	(5)	(6)
Data Sets	N	S	D	β	$P_A(3\times10^{-4})$	$P_F(3\times10^{-4})$	$0.1\ a_{a.u.}^{q}$
1-4	4	7.0E28	9.4E18	3.40	1.1E31	9.0E30	1.20
5-9	3	2.0E29	5.9E21	2.55	5.9E30	5.9E30	1.81
10-13	4	2.0E29	1.3E19	3.20	2.0E30	2.4E30	2.00
14-17	4	1.7E29	1.3E23	1.80	2.8E29	2.6E29	2.42
28-34	7	4.0E29	5.0E20	3.00	1.6E31	1.8E31	0.68
24-27, 35-39	9	3.5E29	6.3E20	2.95	1.1E31	1.5E31	0.95
18-23, 40-42	9	2.0E29	1.2E29	2.45	3.8E30	6.0E30	1.45
43-50	8	5.0E29	1.0E20	3.00	2.0E30	3.5E30	2.15
28-20	3	1.5E30	6.3E22	2.45	2.4E31	2.6E31	0.71
31-34	4	1.5E30	1.0E20	3.20	1.2E31	1.9E31	0.66
24-27	4	5.0E29	2.0E31	2.90	3.0E31	3.0E31	0.94
35-38	5	3.0E29	1.8E20	2.97	4.3E30	5.8E30	0.96
18-23	6	4.0E29	3.3E21	2.60	4.7E30	5.1E30	1.37
40-42	3	7.0E29	2.7E22	2.30	2.2E30	4.3E30	1.59

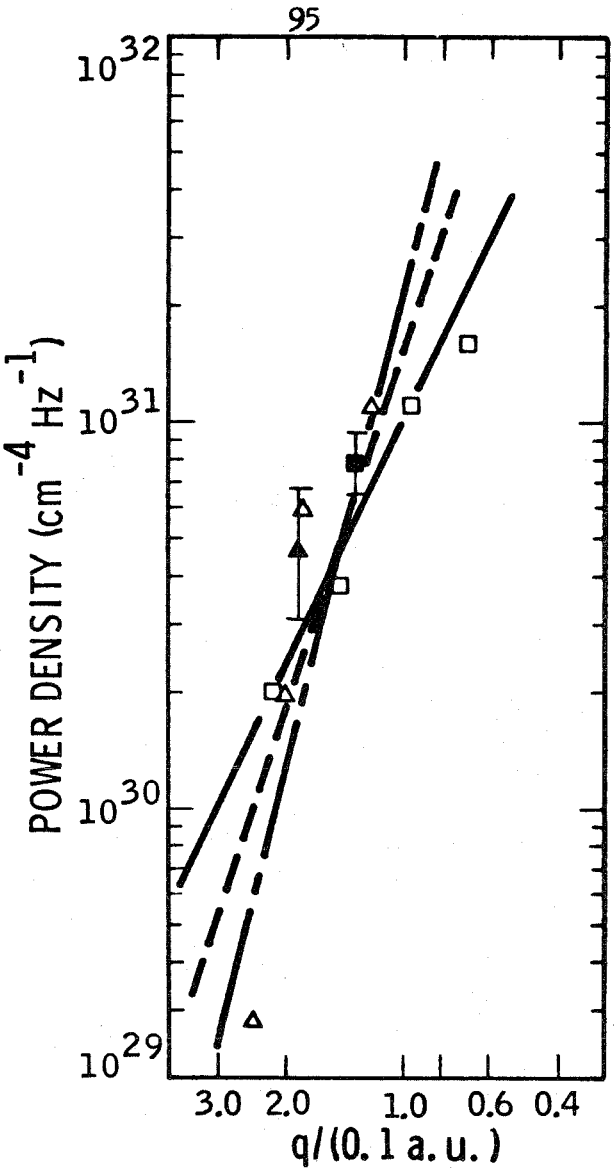

Figure 5.5a. Averaged spectral amplitudes plotted against distance of closest approach. The data were divided into four groups based on the distance of closest approach: △, MM69; □, MM71. The overall average amplitudes, with error bars representing the variations between alternate spectra (Table 5.1), are given with the filled symbols. The lines have slopes: solid, 2.0; dashed, 3.0; dash-dot, 4.0. These slopes correspond to $\Delta n(r) \propto r^{-\theta}$ with θ= 1.5, 2.0, 2.5, respectively.

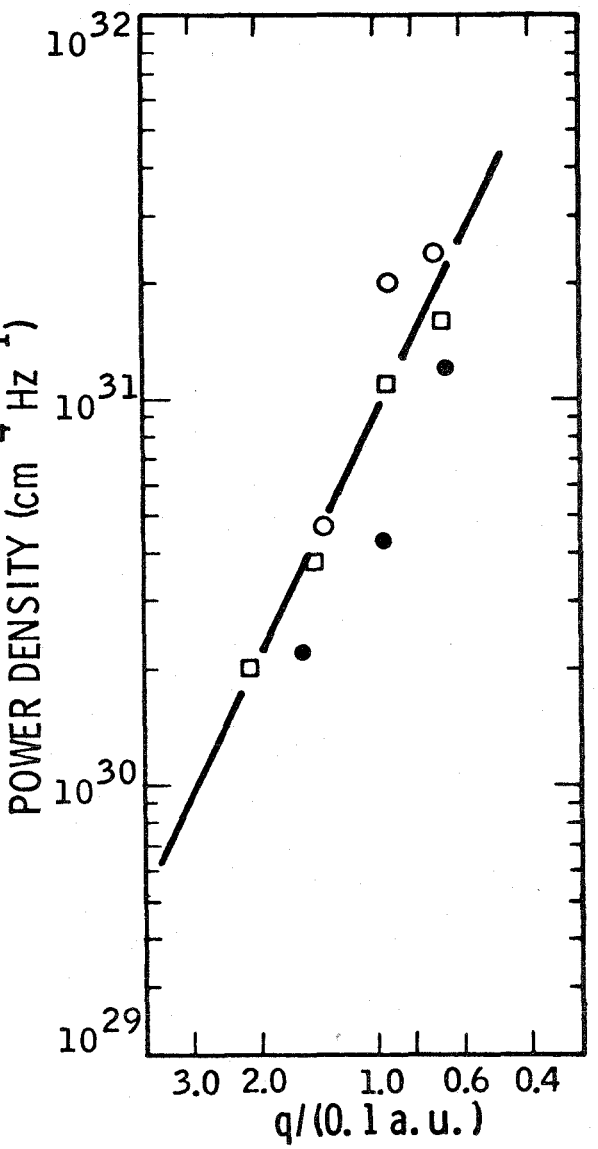

Figure 5.5b. MM71 averaged spectral amplitudes plotted against distance of closest approach. The data were first divided into four groups based only on distance of closest approach (□). The data within these groups were separated into preconjunction (0) and post-conjunction (●) sets. The group with the largest q contains no preconjunction data. Note that the slopes are similar although the actual amplitude changed. The line has slope 2.0 implying that $\Delta n(r) \propto r^{-1.5}$.

The data of Figure 5.5a show that while the MM69 spectra fit in fairly well with those of MM71, they may fall off somewhat more rapidly with q. Because the range in q is only a factor 2 and the point at q = 0.24 a.u. has a low signal to noise ratio, it is difficult to reliably estimate this fall off. However, the amplitudes roughly decrease as $q^{-3.0}$ to $q^{-4.0}$. This implies that (see Eq. 4.19) Δn decreases as $r^{-2.0}$ to $r^{-2.5}$ in the region $0.12 \leq r \leq 0.24$ a.u. This fall-off may be compared to the observations of Counselman and Rankin (1972) (hereafter called CR) who found that the electron density in the range $5 \leq r \leq 20$ $R_\odot$ during 1969 and 1970 June decreased as $r^{-2.9\pm0.2}$. Their measurements were made near the sun's south pole while the DRVID observations were taken near the north pole, but they state that the corona had a symmetric appearance during this period. The MM69 Relativity Experiment (Anderson et al., 1972), which used range data associated with the MM69 DRVID measurements, found that for a large range of solar distances ($0.03 \leq r \leq 0.30$ a.u.) the solar-wind density declined as $r^{-2.0\pm0.25}$. Thus, there is considerable scatter in the reported exponents, although some of the apparent disagreement may be due to the different radial regimes sampled. In the radial regime $r \lesssim 10$ $R_\odot$ the density is known to have a significant component which has a radial dependence r^{-6} (Anderson et al., 1972) and thus increases rapidly near the sun. Much of the data of CR is in this region so their result may not apply to the large-scale variation of the solar-wind density. Anderson et al. (1972) have little data inside r = 10 $R_\odot$.

The amplitudes of the MM71 grouped spectra are plotted against q in Figure 5.5b. The data are also separated into pre- and post-conjunction groups. The line drawn through the data has slope -2.0. It is a good fit to the data, and the variation in the slope is only $\pm$ 0.2. These observations imply that $\Delta n(r)$ falls off as $r^{-1.5\pm0.2}$ for $0.07 \leq r \leq 0.22$ a.u. This decline is much less than that suggested for the MM69 data. The MM71 Relativity Experiment (Anderson and Lau, 1973) again found that the large-scale variation of the solar-wind density is $r^{-2.0\pm0.1}$. CR report preliminary results of their experiment conducted in 1971 June. They find that the density declined as $r^{-1.4\pm0.1}$ for $5\ R_\odot \leq r \leq 20\ R_\odot$, if the corona is assumed to be spherically symmetric. However, they point out that as solar activity declines the corona develops a strong enhancement near the equator, thus distorting observations at the poles. They obtain a good fit to their observations if the density varies from equator to pole as $\cos^2 \lambda$, where λ is heliographic latitude, and the density decreases with radius as $r^{-2.4\pm0.4}$.

Solar activity in 1971 June when CR made their observations was similar to that in late-1972 when the MM71 DRVID data were obtained. In Figure 5.6 the amplitudes of the MM71 grouped spectra multiplied by $q^{3.5}$ are plotted against the latitude of the point of closest approach. The $q^{3.5}$ factor is to account for the steep radial fall-off found in the MM69 data and would give a radial density dependence of $\Delta n \propto r^{-2.2}$ similar to the second value of CR. The scaled data show a very strong latitude

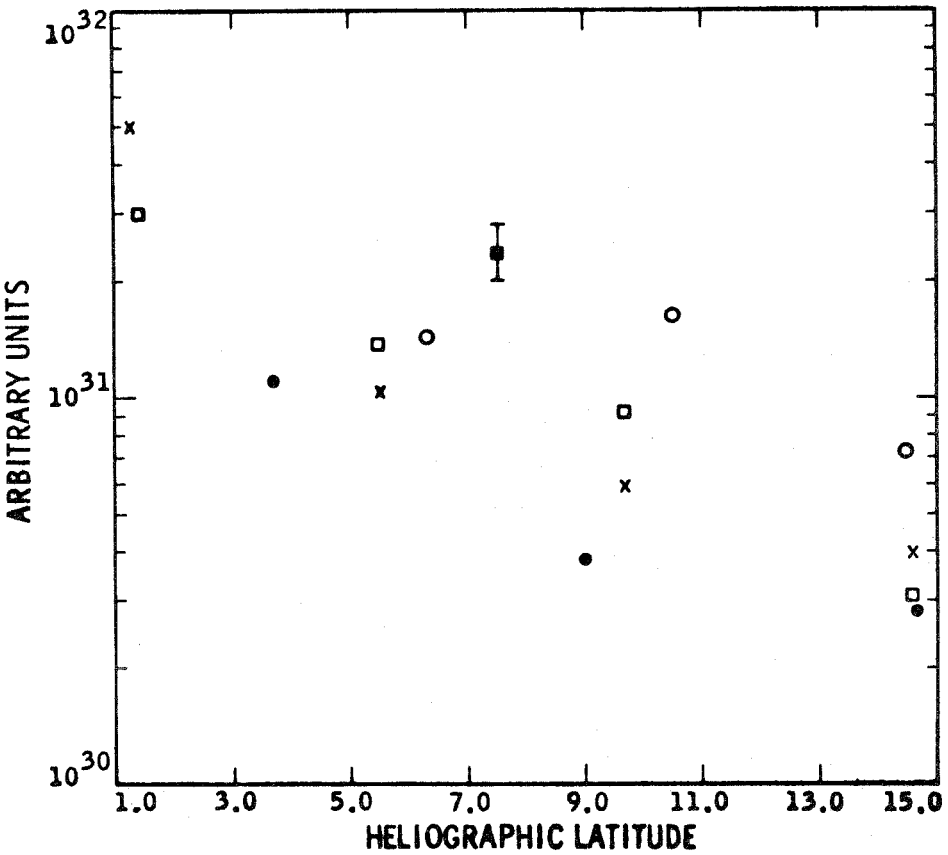

Figure 5.6. Scaled spectral amplitudes of MM71 data plotted against heliographic latitude of the point of closest approach. The spectral amplitudes have been multiplied by $q^{3.5}$ (q in units of 0.1 a.u.), the radial variation that would obtain if $n(r)\ r^{-2.25}$-- approximately the result for the MM69 data. The figure tests the hypothesis that the slow radial fall-off of the MM71 spectra is caused by a latitude-dependent effect. The strong latitude function required to match the scaled data suggests that the slow fall-off is not due to a latitudinal variation of the turbulence. ■ , MM71 overall average. □, MM71 data grouped into quarters by q. O, MM71, preconjunction data from each quarter. ●, MM71, postconjunction data from each quarter. X, 1/sin(latitude), scaled to fit the □'s.

dependence--approximately $1/\sin\lambda$. A $\cos^2\lambda$ dependence cannot account for the data in Figure 5.6. The radial fall-off is less steep in the MM71 data than in the MM69 data. However, a determination of the latitude variation is very difficult because of the strong correlation between the distance of closest approach and the latitude of closest approach.

We may summarize these observations as follows: First, the large-scale ($0.03 \leq r \leq 0.30$ a.u.) decrease of the solar-wind density is $r^{-2.0\pm0.2}$ (Anderson et al., 1972. Anderson and Lau, 1973). This result seems to be independent of the solar cycle, and its determination is not significantly influenced by density variations with latitude or in the inner corona ($r \lesssim 10\ R_\odot$). Second, the decrease of both the density and fluctuations with radius may depend on the solar cycle. It appears that near solar maximum the decline is more rapid ($\Delta n \sim r^{-2.25}$, $n \sim r^{-2.9}$) than later in the cycle ($\Delta n \cong n \sim r^{-1.5}$). However, as solar activity declines heliographic latitude dependence, which is difficult to separate from the radial dependence with the radio techniques employed, may come into play and account for some of the apparent lessening of the radial fall-off. Third, in the region near the sun ($0.07 \leq r \leq 0.20$ a.u.) the density fluctuations decline more slowly than they do on the average (Section B) between ~ 0.15 a.u. and 1 a.u. The implications of this result will be discussed in Chapter VII.

Other radial variations of the DRVID spectra were also investigated. The spectral indices of the grouped spectra were plotted against q. The data show no variation with q. The fact that the spectral index is independent of q is interesting in itself. It is also important because it shows that the model spectra fit to the data were not influenced by the noise in the high frequency regime.

D. TEMPORAL VARIATION OF THE DRVID SPECTRA

The data presented in Figure 5.5a show that the amplitudes of the MM69 and MM71 spectra agree rather well. This observation suggests that there was little long term (~ 2 year) change in the solar-wind turbulence between mid-1970 and late 1972. Such modulation might be expected from the 11-year solar cycle. Judged by Zurich sunspot number (Solar Geophysical Data) the maximum of the current cycle was quite broad and extended from 1968 July to 1970 July. (The predicted peak was 1968 October.) After some decline in solar activity a secondary maxima (~ 75% of the primary) occurred around 1972 March. Thus, while the solar cycle should have declined nearly half way from its maximum to its minimum between the MM69 and MM71 observations, such a change did not occur in this cycle, and little meaningful judgment about long term modulation can be drawn from these data.

The MM71 data presented in Figure 5.5b show that significant variations in the amplitude of the turbulence occur with a time scale of a few weeks. Figure 5.7 shows the MM71 averaged spectral amplitudes as a function of date. No changes in the data acquisition system were made between the pre- and post-conjunction groups of data. An investigation was made to see if these short-term amplitude variations could be correlated with solar activity indices or surface features.

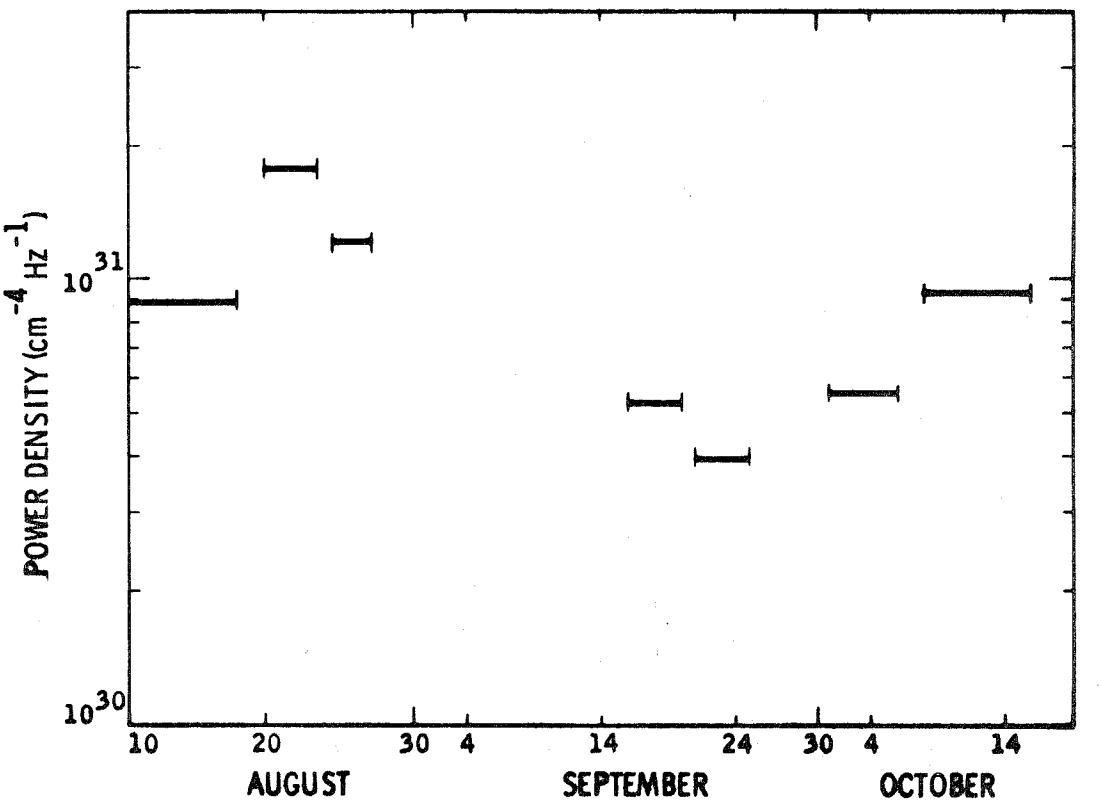

Figure 5.7. MM71 spectral amplitudes plotted against date. The data have been multiplied by q^2 to remove the radial variation shown in Figure 5.5b. The data groupings are the same as those in Figure 5.5b (See bottom part of Table 5.3.). The data show definite temporal structure, but the figure also shows that when pre- and post- conjunction data with the same values of q are combined, there will be essentially no time variation.

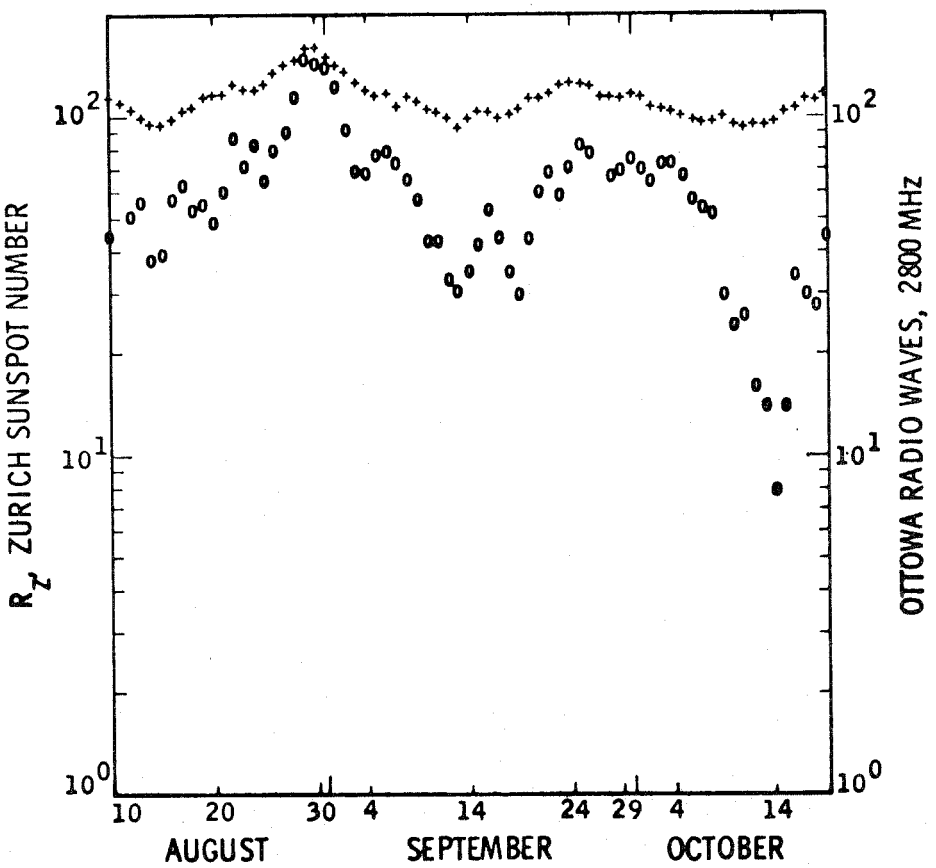

Figure 5.8. Daily solar indices (from Solar Geophysical Data, Prompt Reports) plotted against date. +, Radio flux at 2800 MHz, corrected for bursts. 0, Zurich sunspot number. These data correlate with the spectral amplitudes in Figure 5.7 if the proper shift is made to account for the longitude of the point of closest approach.

The Zurich sunspot number and the solar radio flux at 2.8 GHz (Ottowa) were obtained from Solar-Geophysical Data (Prompt Reports) and plotted against date (Figure 5.8). However, these indices are taken from the earth, while the most important region for the DRVID data is where the ray path goes near the sun. The point is approximately 90^{o} in heliographic longitude from the subearth point or about 7 days of solar rotation. If the two indices are displaced in time 6 days backwards before conjunction and 10 days forward after conjunction, a moderate correlation between the indices and the spectral amplitudes is found. While 10 days is larger than the 7 days expected it is in the correct range: The spectral amplitudes appear to be roughly proportional to sunspot number. If the indices are displaced in the opposite direction from that required by solar rotation no correlation can be found. A simple superposition of the indices on the spectral amplitudes also gives no correlation. Thus, there is only the correlation of the spectral amplitudes with large scale indices of solar activity that one might have expected.

The averaged spectral amplitudes were plotted as a function of Carrington longitude, and the locations of McMath plage regions were superimposed. No relationship between either number or the intensity of the regions and the spectral amplitudes was found. The hourly x-ray flux at 0 and 1200 UT reported by Explorer 44 (Solar Geophysical Data) was plotted against date. No

significant correlation between it and the spectral amplitudes, at any relative displacement, could be found. Thus, there seems to be no correlation of the spectral amplitudes with localized features on the sun's surface. The possible relationship between sunspots and solar wind heating is discussed at the end of the first section of Chapter VII.

E. THE EXISTENCE OF SPECTRAL MINIMA NEAR 3×10^{-4} HZ

The MM71 spectra have been examined for the minima predicted to occur (Eq. (4.19)) at odd multiples of 3×10^{-4} Hz. The MM69 spectra do not have sufficient resolution to permit an investigation. The evidence for the minima is meager. The data in Table 5.3 show that the model spectrum is always greater than the true spectrum at 3×10^{-4} Hz. A similar comparison made at 6×10^{-4} Hz shows no such bias. Thus, there is some evidence that on the average the spectrum amplitude is depressed at 3×10^{-4} Hz.

Figure 5.9 provides additional support for the view that the minima have been observed. The frequency interval for the minima is slightly larger than 3×10^{-4} Hz, $\sim 3.3 \times 10^{-4}$ Hz. Several other spectra show similar evidence of the minima. They show up most clearly in MM71 data from early August (lines 18-23) and mid-September (lines 40-42).

On the other hand, Figure 5.4 shows that the minima do not exist in the overall average spectrum, except for a slight depression in the spectrum at 3×10^{-4} Hz.

It was shown in Chapter IV that decreasing the radial dependence of the velocity and density near the sun tended to remove the minima in the predicted spectra. Furthermore, there were effects not taken into account which would also decrease the depth of the minima. It is not surprising then to find only limited evidence for them, and for that evidence to be observed on ray paths fairly far from the sun on days when the solar wind was rather quiet.

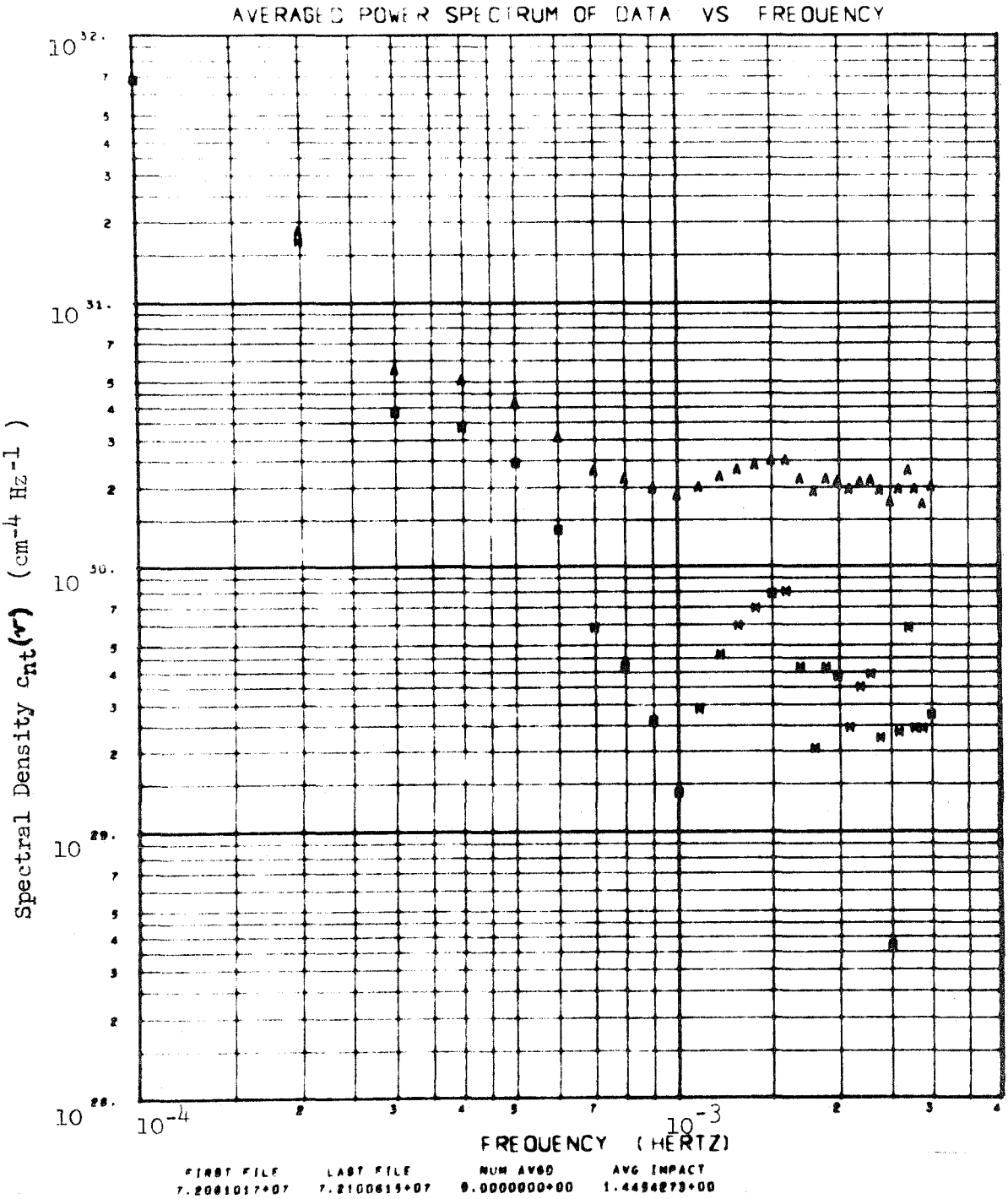

Figure 5.9. Averaged spectrum of MM71 data (pre- and post-conjunction) with distances of closest approach in the interval 0.117 to 0.171 a.u. The spectrum shows a definite depression at 3×10^{-4} Hz, and perhaps one at 1×10^{-3} Hz. This spectrum is the best observational evidence of the spectral minima predicted in Chapter IV.

F. SUMMARY OF DRVID SPECTRAL OBSERVATIONS

The power spectra of the DRVID data have provided interesting and useful observations of the solar-wind turbulence. The principal observations are

(1) The scale size most important for solar-wind density fluctuations is $1 \times 10^6 \lesssim L \lesssim 6 \times 10^6$ km, and $L \cong 1.5\text{-}3.0 \times 10^6$ km.

(2) Local changes in the electron density of at least 100% occur near the sun.

(3) The solar-wind turbulence may be represented by a power-law for frequencies $1 \times 10^{-4} < \nu < 1 \times 10^{-3}$ Hz. The power-law index ($P \propto \nu^{-\beta}$) in a frame moving with the solar wind is $\beta = 3.9 \pm 0.2$.

(4) By comparing spacecraft observations near 1 a.u. to the DRVID spectra it is found that the solar-wind density fluctuations decrease as $\Delta n(r) \propto r^{-2.38 \pm 0.11}$ between $r \cong 0.15$ and 1 a.u. assuming no time variations. If the fluctuation amplitudes are approximately proportional to sunspot number $\Delta n(r) \propto r^{-2}$ fits the observations.

(5) There is little change in the overall spectrum of the solar-wind turbulence between mid-1970 and late-1972.

(6) For the MM71 data the variations in spectral amplitude are correlated with changes in overall solar activity as measured by Zurich sunspot number and 2.8 GHz radio flux.

(7) The variation of the solar-wind density fluctuations with radius near the sun ($0.07 \leq r \leq 0.22$ a.u.) is complex. The radial fall-off appears to be faster ($\sim r^{-2.0}$ to $r^{-2.5}$) for the MM69 data than for the MM71 data ($\propto r^{-1.5\pm0.2}$). The latter determination may be affected by variations of the fluctuations with latitude (Counselman and Rankin, 1972). The indices found are in agreement with those of Counselman and Rankin (1972) for the respective periods, so the density and the density fluctuations have the same radial dependence at these times.

(8) There is only marginal evidence for the minima in the spectra predicted in Chapter IV.

VI: THE ATTEMPT TO LOCATE DENSITY ENHANCEMENTS ALONG THE RAY PATH AND RELATE THEM TO FEATURES ON THE SUN'S SURFACE

Because DRVID data are obtained by a round trip measurement, it is possible to detect where density enhancements cross the ray path. The technique, which uses the autocorrelation function of the data, is outlined here. After density enhancements are located, an attempt is made to relate them to features on the sun's surface. Such a relation would provide additional information about the sources of solar-wind turbulence.

Recently, interest in the relation of surface features to the solar wind has been revived by the prediction (Pneuman, 1973) and observation (Krieger et al., 1973) that coronal "holes" (regions of low x-ray emission and open magnetic field structure) are the source of high speed solar wind streams. Krieger et al. (1973) found that mapping along ideal Archimedian spirals (i. e., radial velocity from rotating sun) with the observed solar-wind velocities was quite successful. This is in contrast to the earlier results of Neugebauer and Snyder (1966), who tried to map high velocity streams to calcium plage regions, and Pathak (1971), who tried to map streams to regions of enhanced $\lambda 5303$ emission. Both found that higher than observed radial velocities were needed for the mapping to be successful. Other attempts to relate solar-wind velocity variations to solar features have been made by Couturier and Leblanc (1970), Bohlin (1970), and Rosen (1969).

Here, we attempt to relate density enhancements to McMath calcium plage regions. Neugebauer and Synder (1966) observed that density enhancements often occur at the leading edge (in the sense of solar rotation) of high velocity streams. This observation and their finding that higher than observed velocities are needed suggest that for the mapping to be a success either much higher than average wind velocities will be needed or the mapping will reach regions ahead of those considered for velocity streams. (The mapping is explained in the second section of this chapter.)

The first section of this chapter describes the autocorrelation technique for locating density enhancements which cross the ray path. The spatial resolution of the technique is discussed for the discretely sampled DRVID data. The statistical limitations to the method are pointed out. Based on these limitations criteria for selecting the autocorrelation peaks that represent density enhancements are developed. It is found that the stream detection is limited by the shortness of the available data records which gives low statistical reliability to the points selected as representing streams.

The mapping from the ray path to the sun's surface is outlined in the second section. The mapping is limited by the relatively long time ($\sim$ 100 sec) between DRVID data samples which limits the resolution of the autocorrelation function. The mapping accuracy is also hampered by the lack of measured solar-wind velocities along the ray path.

The solar data used to compare to the mapped autocorrelation peaks are discussed in the third section. The data used for detailed analysis were the locations McMath calcium plage regions. The criteria for deciding if a McMath region was present at a specified time and longitude are given. These data were used because of their accuracy, frequency of measurement, and association with other types of solar activity. Krieger et al. (1973) suggest that calcium emission is somewhat weaker in corona holes. This would agree with their inferences of a reduced magnetic field there (Zirin, 1966). It also would imply a lack of McMath regions in coronal holes. Then, one might hope that the density enhancements ahead of high velocity streams would map, with normal solar-wind velocities, to McMath regions preceding coronal holes.

Finally, the results of the density enhancement detection and mapping are presented for both the MM69 and MM71 data. It is found that there is no preferred longitude on the sun's surface. If there were a long lasting region ejecting material such a longitude should have been found. In the MM69 data the coincidences of longitudes, when both Mariner 6 and Mariner 7 were tracked on the same day, are not above the level of chance. The matching ($\pm 3^{\circ}$) of McMath regions on the sun's surface with supposed density enhancements crossing the ray path is also not above the level of chance on the whole. However, if only the rigorously statistically significant correlation peaks are used, the mapping of the MM69 data meets with marginal success. The success of the mapping is summarized in Table 6.1.

A. LOCATING DENSITY ENHANCEMENTS WITH THE AUTOCORRELATION FUNCTION

The technique of locating density enhancements crossing the ray path with the autocorrelation function was originally proposed by Thiede and Lusignan (1970). MacDoran et al. (1971) independently rediscovered the method. The key requirement of the technique is that the columnar content measurement be made in a round trip manner. In Eq. (4.7), which reads

$$c_{nt}(\tau) = \int_0^L b(\underset{\sim}{r})\, ds \int_{-s}^{L-s} d\ell\; G_{nr}\left[\underset{\sim}{R} - \underset{\sim}{v}(\tau + \frac{\ell}{c})\right]$$

$$+ G_{nr}\left[\underset{\sim}{R} - \underset{\sim}{v}(\tau + (\frac{\ell + 2(s-L)}{c})\right] +$$

$$G_{nr}\left[R - \underset{\sim}{v}(\tau - \frac{\ell + 2(s-L)}{c})\right] + G_{nr}\left[\underset{\sim}{R} - \underset{\sim}{v}(\tau - \frac{\ell}{c})\right]$$

the second and third terms, the cross-correlation of the signal propagating to the spacecraft with that returning, contain the information about the location of density enhancements (Thiede and Lusignan, 1970).

The correlation function $G_{nr}(x)$ has its maximum value when $x = 0$. Since the ℓ-dependence of the argument is integrated out in Eq. (4.7), the cross-correlation term attains its maximum at lags τ given by

$$\tau = 2(L - s)/c.$$

Thus if the density function $b(\underset{\sim}{r})$ has an enhancement at some point s_0 along the ray path, the autocorrelation function of the DRVID data will show a peak of a lag $\tau_0 = 2(L - s_0)/c$. Figure 6.1 taken from MacDoran et al. (1971), is a schematic of the technique and makes clear the result. Note that density disturbances near the spacecraft show up near $\tau = 0$, those near the earth, at $\tau \sim 2L/c$ (the round trip light time to the spacecraft). The amplitude of the DRVID autocorrelation peak at τ_0 will be proportional to the square of the density enhancement at s_0 (Thiede and Lusignan, 1970).

An important consideration in the use of the autocorrelation technique to find streams in the solar wind is its resolution. This is particularly important because the DRVID data are discretely sampled. If sufficient resolution is available, the width of the density enhancement can be determined, as well as its location and density.

The autocorrelation functions used to search for the streams were obtained from DRVID data records with a low-order polynomial, fit by least-squares to the data, subtracted from each point. The fit removed the natural time scale of the solar wind, $\sim 3 \times 10^6$ km/300 km $sec^{-1} = 10^4$ sec, and left the data sampling time of $\sim$ 100 sec.

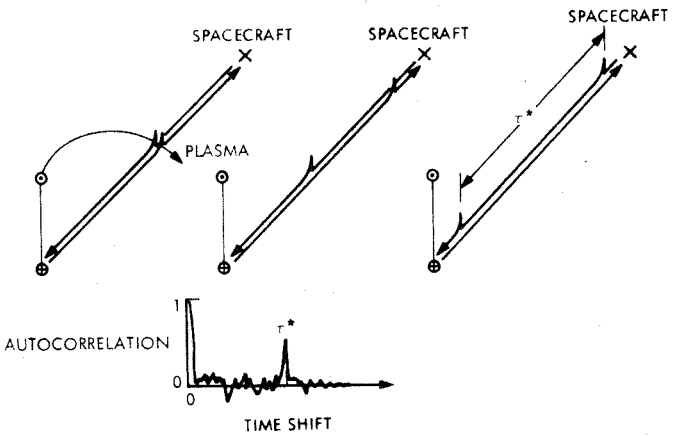

Figure 6.1. Schematic diagram of autocorrelation technique for detecting density enhancements. The autocorrelation lag τ^* is twice the light travel time from the stream to the spacecraft. The diagram makes clear why a round trip signal path is needed for the detection technique.

Such "high pass filtering" was recommended by Thiede and Lusignan (1970) to improve the resolution of observations. However, a localized solar wind disturbance can be expected to be less than $\sim$ 100 sec x c = 3 x 10^7 km, the resolution size of the data. Thus, DRVID data will not provide information on the width of the disturbance.

Another connotation of resolution is the minimum separation of two streams needed to distinguish them. Clearly, the required distance is approximately one correlation lag $\sim$ 3 x 10^7 km. For a ray path of 2.6 a.u. there are about 12 "resolution cells" in which density enhancements may be found. It is also possible for streams to fall between correlation lags and be missed if they are much less than 3 x 10^7 km in width.

The autocorrelation functions of all DRVID records which were unbroken (i. e., no reacquisitions) for periods long compared to the round trip light time (RTLT) to the spacecraft ($2L/c \cong 45$ min.) were searched for peaks. It is clear from the expression for τ_0 that the data record must be long enough to give reliable estimates of the autocorrelation functions at lags near the RTLT. Thus, records shorter than about 3 times the RTLT are unsuitable for this analysis. Seventeen records suitable for autocorrelation analysis were obtained in both the MM69 and MM71 missions.

The autocorrelation peaks were initially selected merely on the basis that the point "stood out". Such a point is either exceptionally high or its neighbors are exceptionally low. Both criteria were used. Because of the physical situation expected—a dense stream surrounded by average or below average density plasma—particular attention was paid to the second condition. A depression around the peaks is also expected because of the high pass filtering.

Since the autocorrelation peaks were initially selected without careful regard for their statistical significance, many of the points selected were not true indications of density enhancements. The statistical significance of the autocorrelation peaks may be judged in the following way: The variance of the autocorrelation function $C(\tau)$ for discretely sampled records of N points which are correlated to a maximum lag of m points "is conservatively given by" (Bendat and Piersol, 1966)

$$\text{Var}\left[C(\tau)\right] \approx \frac{m}{2N}\left[C^2(0) + C^2(\tau)\right]. \tag{6.1}$$

Eq. (6.1) may be simplified for the case of a normalized autocorrelation function ($C(0) = 1$) and high pass filtered data ($C^2(\tau) \ll 1$) to

$$\text{Var}\left[C(\tau)\right] \leq m/2N \quad . \tag{6.2}$$

Clearly, this overestimates the variance of the points near zero lag, but it will be used below as an upper bound. If one now assumes that the values of $C(\tau)$ are from a zero-mean Gaussian random function whose variance is given by Eq. (6.2), the probability of $C(\tau)$ exceeding any value C_1 is

$$P(C(\tau) > C_1) = \frac{2N}{\sqrt{2\pi\, m}} \int_{C_1}^{\infty} \exp\left[-4N^2 x^2/m\right] dx \quad . \tag{6.3}$$

C_1 is selected so that in the number of lags required to reach a RTLT one expects (i. e., $P(C_1) * m$) less than one-half a point exceeding C_1. The DRVID data sampled every two minutes then require $C_1 \cong 2.0(m/2N)$, while the one minute data require $C_1 \cong 2.3(m/2N)$.

Table 6.1 summarizes information about the number of autocorrelation peaks selected, the statistical significance of the peaks selected, and the success in mapping from them to McMath plage regions. The table shows that many more lags were available in the MM71 data. This is because much of that data was obtained with a one minute sample time. However, there are fewer suspected peaks and far fewer significant peaks in the MM71 data.

The MM71 DRVID data do not contain useful autocorrelation information largely because of the way in which the data were acquired. The flexibility of the Mu system during the MM71 mission, which made possible greatly improved observations of the solar-wind turbulence spectrum, worked against obtaining long unbroken (i. e., no reacquisitions) DRVID records. Since the turbulence spectrum could be obtained from data containing reacquisitions and the relativity experimenters, who had highest priority, desired many reacquisitions, the long records needed for the stream detection were assigned the lowest priority.

B. MAPPING FROM THE RAY PATH TO THE SUN'S SURFACE

The mapping from the ray path to the sun's surface was described in the last section of Chapter III. The point corresponding to each correlation lag was mapped to a Carrington longitude on the sun. The mapping was done along ideal Archimedian spirals with solar-wind velocities of 400 and 700 km s^{-1}. Figure 6.2 shows the effect of varying the velocity. The lower velocity spirals are more tightly wound.

One of the outputs of the mapping program is shown in Figure 6.3. The plot gives the Carrington longitude corresponding to points along the ray path. The two curves result from the two mapping velocities (4 = 400 km sec^{-1}, 7 = 700 km sec^{-1}). Two things should be noted from the figure: In the region where the ray path goes near the sun ($\tau \sim$ 1000 to 1700 sec) the mapping from a given point is insensitive to velocity. Near the sun the longitude changes rapidly with position along the ray path. Thus, in this region small errors in the estimation of the point where the stream intersects the ray path cause large errors in the inferred longitude, even though the result is insensitive to the solar-wind velocity. Figure 6.3 shows that erros of $\pm$ 10° in longitude could be made due to the finite resolution of the autocorrelation function. Conversely, far from the sun, where it is important to know the wind velocity accurately, the longitude changes slowly with position along the ray path. In fact, the ray path to longitude mapping is not unique far from the sun.

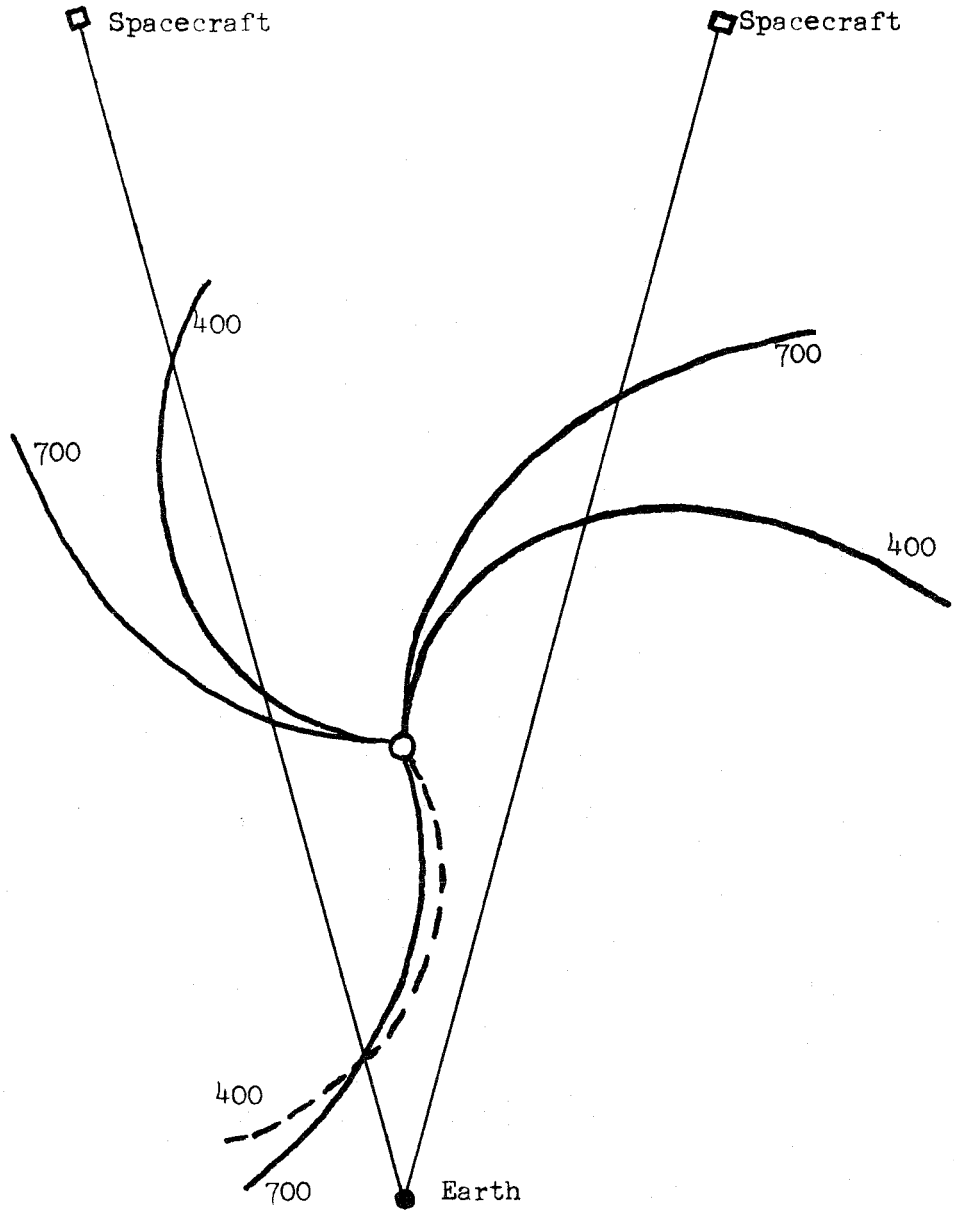

Figure 6.2. Examples of Archemedian spirals corresponding to solar-wind velocities of 400 and 700 km sec^{-1}. On the right two streams leave the sun at the same longitude. On the lower left two streams intersect the ray path at the same point, 0.7 a.u. from the sun; the feet of the spirals are then separated by 18.6^{o} in longitude. On the upper left a double intersection of the slower stream with the ray path is shown.

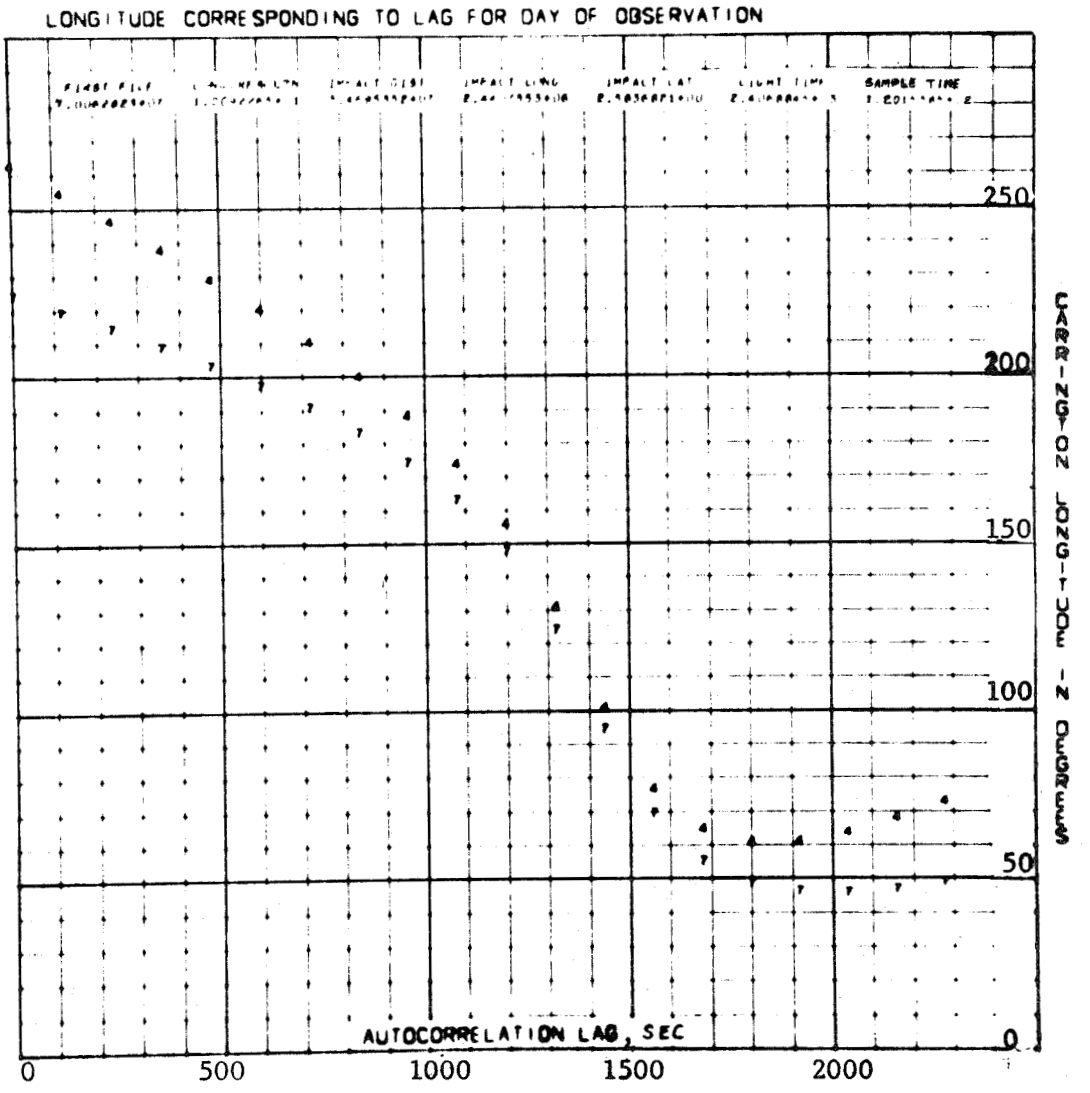

Figure 6.3. Computer generated plot of mapping from points along the ray path to Carrington longitudes on the sun's surface. Points along the ray path are specified by their corresponding autocorrelation lag so that lags near 0 are nearest to the spacecraft. The 4's give the longitudes reached with an assumed solar-wind velocity of 400 km sec^{-1}, the 7's, 700 km sec^{-1}. The longitude resolution at the point of closest approach is 10^{o}. For this geometry (the spacecraft on the west side of the sun) the mapping is double valued for points near the earth.

The low-velocity spirals are wound tightly enough to intersect the line of sight in two places. A stream detected near the Earth or the spacecraft (depending on which side of the sun the line of sight passes) should also show up near the sun.

The accuracy of the mapping is somewhat limited by the absence of velocity data at points along the ray path. However, in the important region near the sun the mapping is not too sensitive to the velocity. Some velocity data are available from the Pioneer spacecraft. The data show that most of the time during both the MM69 and MM71 missions the solar-wind velocity was about 400 ± 50 km sec^{-1}. At very quiet times the velocity declined to $\sim$ 300 km sec^{-1}. During each mission the velocity exceeded 700 km sec^{-1} only once, but often exceeded 500 km sec^{-1}. Thus, the velocities chosen for the mapping represent the typical and extreme behavior of the solar wind.

C. SOLAR SURFACE DATA

What information should be used to characterize solar activity at each Carrington longitude? The data should be taken as often as possible, associated with other solar features, of high resolution and positional accuracy, and available in computer readable form, if possible. The data which best fit this description and which are used here are the locations of McMath calcium plage regions. Daily values of the position in heliographic longitude and latitude, the area (estimated in millionths of the sun's surface), and the intensity

(subjective estimate) are reported in Solar Geophysical Data (Prompt Reports) along with information about the sunspots located in each region. This information is also available on punched cards or magnetic tape from the World Data Center A for Solar-Terrestrial Physics. Boulder, Colorado. I obtained a magnetic tape of the data covering the time spans of the DRVID data.

Calcium plages are regions of enhanced emission in the K line (λ3934) of Ca II. The emission regions overlie sunspots. The structure seen in Ca II emission is quite similar to that observed in Hα light. It has been shown by Babcock that the plages correspond to areas of enhanced magnetic field (Zirin, 1966).

Examination of the x-ray and radio data reported in Solar Geophysical Data (Prompt Reports) shows that activity in these wave lengths is usually coincident with the McMath plages. The resolution of the plage data is equal to or better than that of these data. The plages are extended in longitude by about 10 to 30 degrees; the datum reported for each day is the longitude of the center of the region which can be determined to about $\pm$ 1°. The sunspot data accompanying the plage reports is accurate to 1 degree or less since the spots are very small features. The x-ray data have the possibility of small scale resolution, but the data available for the MM69 and MM71 missions only report features of the same size as the plage regions.

The plage data obtained on magnetic tape were sorted and output by region number. For each day of observation the Carrington longitude, latitude, area, and intensity were printed. The date and mapped Carrington longitude of each suspected autocorrelation peak were compared to these tables for both velocities used. Plage regions within $\pm 3^{\circ}$ and $\pm 8^{\circ}$ of the mapped longitudes were recorded regardless of latitude. If a plage region was growing (east limb) or declining (west limb) and the mapped longitude was not visible at the supposed time of ejection, a reasonable estimate of whether the region was active at the appropriate time was made. The estimate was assisted by checking the preceding or following solar rotations for activity at that longitude.

D. RESULTS OF THE MAPPING OF AUTOCORRELATION PEAKS

The Carrington longitudes corresponding to the suspected autocorrelation peaks were investigated in three ways. First, the longitudes were grouped into bins to see if any area had long-lived or strong activity. No such region was found. Second, longitudes from data records obtained one day or less apart were checked for coincidences of longitudes (within $\pm 3^{\circ}$). This test eliminates time variations as an important factor. No significant repetition of longitudes was found. Finally, the mapped longitudes were compared to the longitudes of McMath calcium plage regions. The results of this comparison are summarized in the lower part of

Table 6.1. The mapping was not generally successful. However, the mapping of the statistically significant peaks from the MM69 data did meet with some marginal success.

The longitudes mapped from the suspected autocorrelations were tested for clustering. The MM69 data span only 1 1/3 solar rotations, so for a longitude to show up it must have been quite active. The MM71 data cover 3 solar rotations so that either an active or a persistent area would be noticed. The longitudes were put into bins of 5° and 10°, and the counts compared to a Poisson distribution. The counts did not deviate from the Poisson distribution for either bin size or mapping velocity for the MM69 or the MM71 data. This indicates that the data fall randomly on the sun and no region is particularly active or long-lived. There are too few statistically significant correlations to perform this sort of analysis on those data.

Since no longitude showed long-term activity, a check for short-term activity was made. When data were taken one day or less apart, all the longitudes of the two data sets corresponding to suspected autocorrelation peaks were compared to see if a longitude repeated itself (to within $\pm 3^{\circ}$). The MM69 data were particularly useful because the ray paths to Mariners 6 and 7 were very similar, and on four occasions they were both tracked on the same day. The repetition of longitudes was not above the level of chance for any of the data investigated. Thus, the autocorrelation technique shows no signs

of long-term or short-term density enhancements in the solar wind. These two observations are contrary to a large body of observations of the sun's surface and the solar wind. It is well established that these are both very active and very persistent features on the sun and in the solar wind.

The mapped longitudes were compared to the longitudes of McMath calcium plage regions. A set of longitudes and dates selected from a table of random digits was also compared to the MM71 plage data in the same way. The results are given in Table 6.1. The table gives the number and percent of autocorrelation peaks for which the mapped longitudes fall within $\pm 3^{\circ}$ or $\pm 8^{\circ}$ of one or more McMath regions. The results are given for both mapping velocities, and for the suspected and statistically significant peaks. The last entry is for the randomly selected control data matched to the MM71 plage data. In all cases but one (MM69, $\pm 3^{\circ}$, v = 400 km sec^{-1}) the percentage of success is higher for the actual data then for the control data. However, the differences are small compared to the expected errors in the counts $\sim \sqrt{N}$. (The "quantization error" due to the discrete nature of the data is 2.3%.) The results show no velocity preference.

The statistically significant peaks in the MM69 data fare somewhat better than the mass of data. If the results for the suspected peaks are taken as a background or chance level, then it appears that one or two real matches have been made. The mapping with v = 700 km sec^{-1} is the more successful one.

Table 6.1: Summary of Stream Detection and Mapping

	MM69	MM71
Total number of data records examined	17	17
Total number of autocorrelation lags examined	361	633
Number of suspected autocorrelation peaks (Percent of total lags)	43 (11.9%)	43 (6.8%)
Number of statistically significant autocorrelation peaks (Percent of total lags)	10 (2.77%)	3 (0.47%)
Number (percent) of suspected peaks mapped to McMath regions,		
within $\pm 3^{\circ}$ v = 400	14 (32.6%)	19 (44.2%)
v = 700	21 (48.8%)	17 (39.5%)
within $\pm 8^{\circ}$ v = 400	32 (74.4%)	29 (67.4%)
v = 700	30 (69.8%)	29 (67.4%)
Number (percent) of statistically significant peaks mapped to McMath regions,		
within $\pm 3^{\circ}$ v = 400	4 (40%)	0
v = 700	6 (60%)	0
within $\pm 8^{\circ}$ v = 400	7 (70%)	0
v = 700	10 (100 %)	0
Number (percent) of 68 randomly selected longitude/time pairs matching McMath regions,		
within $\pm 3^{\circ}$	-	26 (38.8%)
within $\pm 8^{\circ}$	-	42 (61.8%)

The statistically significant peaks in the MM71 data have no success at all in the mapping. All the statistically significant peaks taken together do no better than suspected peaks. In evaluating the success with the MM69 data two things must be considered. First, the number of points being dealt with is small so the error in the percent of successes is likely to be large. Second, the reliability of the "statistically significant" points can be questioned. These points were selected on the basis that they exceeded a value which less than 1/2 point per data record would exceed. In examining 17 records one would expect to find $\sim$ 8 points meeting this criterion. Finding 10 points is then not too surprising (Finding only 3 points for the MM71 data is a little surprising.), and the points may not be statistically significant at all.

The attempt to detect solar-wind density streams and relate them to features on the sun's surface was not a success. Even when the few statistically reliable (on an individual record basis) autocorrelation peaks are used, the success in mapping to McMath plage regions is not clear. A similar lack of success in mapping high velocity streams to plage regions was noted by Neugebauer and Snyder (1966). Krieger et al. (1973) suggest that the fault is not in mapping along ideal spirals, but that the features mapped to have been incorrect. Unfortunately, detailed x-ray data such as they used is not available for the mappings done here.

The DRVID data are of dubious quality for stream detection in the first place. For good stream detection records about 10 hours long with data sampled at least once per minute are needed. Doppler residuals (observed doppler frequency with all modelable contributions removed) satisfy these criteria, but it is very difficult to high pass filter long records of these data to make the autocorrelation peaks stand out. It would be useful on a future mission to obtain DRVID data suitable for the detection of density enhancements. Then, a more meaningful investigation of the relationship of the solar-wind density to features on the sun's surface could be made.

VII: IMPLICATIONS OF DRVID OBSERVATIONS FOR CURRENT PROBLEMS IN UNDERSTANDING THE SOLAR WIND

The DRVID observations presented in Chapter V are important additions to our knowledge of the solar wind. The data are particularly valuable because they probe the solar wind near the sun. The spectral data have a straightforward interpretation and good time resolution. The difficulties in observing the solar wind near the sun were pointed out in Chapter I.

Knowledge about the solar wind close to the sun is very important for resolving two of the outstanding problems about the solar wind--its heating and acceleration, and its overall turbulence spectrum. In this chapter these problems are outlined. The contributions that the DRVID observations make to their solutions are summarized. At the end of the chapter the importance of further systematic observations is stressed.

A. TURBULENCE AND THE HEATING OF THE SOLAR WIND

One of the most important problems to be solved to complete our understanding of the solar wind is the mechanism for heating the solar-wind protons and accelerating the bulk flow to the observed velocities. An additional related problem is reducing the electron heat conductivity so that the predicted heat flux agrees with observations.

The solar wind flow can be well described "by an appropriately chosen fluid theory" (Barnes, 1973). While many properties of the solar wind may be investigated with a one-fluid model (Parker, 1963) a more complete description should be provided by the two-fluid model (Sturrock and Hartle, 1966; Hartle and Sturrock, 1968). In the two-fluid model the electrons and protons are allowed to have different temperatures, but an energy exchange mechanism exists so the two species may approach equilibrium. In other respects the two-fluid model is the same as the one-fluid model when an energy equation is included.

When the equations of the two-fluid model are solved with reasonable, although admittedly somewhat uncertain, boundary conditions near the sun, the results do not agree with spacecraft observations near 1 a.u. Barnes (1973) points out that such agreement may not be a valid test of the theory; but it is an embarassment and the only experimental check available. The two-fluid model's predicted velocity ($\sim$ 250 km s^{-1}) and proton temperature ($\sim 4 \times 10^3$ K) are much too low, and the density ($\sim$ 10 cm^{-3}) and electron temperature ($\sim 3 \times 10^5$ K) are somewhat too high. However, the model does predict (Hartle and Barnes, 1970) the $v \propto T_p^{1/2}$ relationship observed in the solar wind by Burlaga and Ogilvie (1973). Furthermore, Hundhausen (1969) has pointed out that the total energy flux in the model is correct, but it is not correctly divided between bulk motion and conduction (by

the electrons). One-fluid models predict too much energy flux altogether, since the electrons are very hot, and the conduction energy flux is proportional to $T_e^{7/2}$.

Two solutions to the two-fluid dilemma have been proposed. The one most stressed in the literature is non-thermal heating of the protons by wave damping. The other solution is the inhibition of electron heat conduction by various mechanisms. In all cases the crucial region for these effects is $5\ R_\odot \lesssim r \lesssim 40\ R_\odot$.

Non-thermal heating of the protons has been investigated by Hollweg (1973), Barnes et al. (1971), and Hartle and Barnes (1970), and reviewed recently by Barnes (1973). The exact heating mechanisms chosen by the authors are different, but the results are the same: The input of about 10^{26}-10^{27} ergs s^{-1} of wave energy at the base of the corona (an order of magnitude less than the power required to maintain the corona's temperature [Barnes, 1973]), with heating extending from about 2 $R_\odot$ to 25 $R_\odot$, causes an increase in v and T_p, and a decrease in n and T_e predicted at 1 a.u. The values approach those observed near the earth. In spite of the addition of energy the total energy flux is still near the observed value. The wave heating preserves the prediction of the v - T_p relationship observed in the solar wind for $v \lesssim 450$ km s^{-1} (Hollweg, 1973; Barnes, et al., 1971).

The reduction of the electron heat conductivity from its usual value in a plasma can be accomplished by the same waves which heat the protons. Hollweg and Jokipii (1972) have shown that the electron thermal conductivity along the average magnetic field is reduced by about a factor of 2 by the observed turbulent magnetic field. Furthermore, Cuperman and Metzler (1973) have shown that the reduced heat conductivities must obtain near the sun ($r \lesssim 40\ R_\odot$) in order to reduce the electron temperature and heat flux at 1 a.u. Thus, the existence of turbulence in the solar wind in the region $5\ R_\odot \lesssim r \lesssim 40\ R_\odot$ is crucial to the agreement of theoretical models with observations.

What information do we have about the solar-wind turbulence, especially near the sun, and its relationship to the other properties of the solar wind? Most of the information comes from spacecraft which orbit the sun near 1 a.u. Information near the sun is obtained from the interplanetary scintillation (IPS) of radio sources, but the interpretation of these observations is still unclear (see next section). The DRVID observations in the important region from $14\ R_\odot$ to $45\ R_\odot$ provide valuable new information.

An important study of the solar-wind turbulence was done by Belcher and Davis (1971) with data from Mariner 5 (1967, Venus). They found that 30 to 50 percent of the time the turbulence was dominated by outward-propagating Alfven waves. The waves were particularly prevalent and had large amplitudes in high speed

streams. The magnetic field components had a power spectrum ($1.6 \times 10^{-4} \lesssim \nu \lesssim 2 \times 10^{-2}$ Hz) of index β 3.5-4.2, the spectrum being flatter (β smaller) when the plasma was hotter. Belcher and Davis (1971) suggested that these waves were remnants of the turbulence near the sun responsible for heating the solar wind.

The DRVID data show that the slope of the density spectrum ($1 \times 10^{-4} \lesssim \nu \lesssim 1 \times 10^{-3}$) is the same as that of the magnetic field components. The data also show that the slope of the spectrum is the same near the sun and at 1 a.u. These results suggest that the waves which heat the solar wind conform to a power-law spectrum of index $\beta \cong 4$.

If the shape of the spectrum is constant with heliocentric distance, the spectral amplitude and its radial dependence become the important measurable quantities for checking theories of solar wind heating. The DRVID observations reported previously provide information about these quantities. By comparing the spacecraft observations of Intriligator and Wolfe (1970) to the DRVID spectra it was found that the average decrease of the density fluctuations with heliocentric distance is $\Delta n(r) \propto r^{-2.38 \pm 0.11}$ between $r \cong 0.15$ a.u. and $r = 1$ a.u., if time variations are ignored. If

the overall fluctuation amplitudes are approximately proportional to sunspot number (as was the case for three months spanned by the MM71 DRVID data), the radial decline is only $\Delta n(r) \propto r^{-2}$. The first result is considerably steeper than the $n(r) \propto r^{-2.0\pm0.2}$ decrease in the steady state density found by Anderson et al. (1972) from MM69 data and by Anderson and Lau (1973) from MM71 data. Support for the sharp decline of the density fluctuations with radius is provided by the IPS observations of Little (1971). He found that the amplitude of the small scale ($L \sim 100$ km) fluctuations declined as $\Delta n(r) \propto r^{-2.6\pm0.2}$ for $0.05 \lesssim r \lesssim 0.8$ a. u. during late 1968 and early 1969.

The DRVID data give a different picture in the region near the sun ($14 \lesssim r \lesssim 45\ R_\odot$; $0.065 \leq r \lesssim 0.22$ a.u.). There the density fluctuations fall off as $r^{-1.5\pm0.2}$ (MM71) or $\sim r^{-2.2}$ (MM69), more slowly than the decline between 0.15 and 1 a.u. (The MM69 data alone give $\Delta n(r) \propto r^{-2.42\pm0.15}$ between 0.15 and 1 a.u.) These observations imply that either there are large temporal variations in the solar-wind density fluctuations, correlated with sunspot number, or there is a region of enhanced turbulence around the sun extending to $r \sim 45\ R_\odot$ (0.2 a. u.). This region is somewhat larger than that required by the turbulent heating mechanisms, but it is of the correct order of magnitude. Furthermore, the longer wavelength waves to which the DRVID measurements are sensitive are able to propagate farther than the waves thought to do the heating ($\nu \sim 3 \times 10^{-3}$ Hz, $L \sim 10^5$ km) because the

damping mechanism is proportional to the wave frequency (Hollweg, 1973). Thus, DRVID observations will show a region of enhanced turbulence larger than that important for the heating.

A region of enhanced turbulence fits in well with the observations of Ekers and Little (1971). Using IPS techniques they observed the acceleration of the solar wind and large random (i. e., nonradial) velocities out to $r \cong 40\ R_{\odot}$. The power required to provide the accelerations and random velocities may be estimated from their data, if it is assumed that the flux is uniform through a sphere of radius $5\ R_{\odot}$. The power is given by

$$P_V \cong \frac{1}{2} \rho (\delta v)^2 v\ 4\pi r^2 .$$

One finds that $\sim 10^{26}$ ergs s^{-1} are required to accelerate the solar wind, a value in agreement with the kinetic energy flux at 1 a.u. (This result is not surprising since the observed $\delta v \sim 300$ km s^{-1} is approximately equal to the wind velocity at 1 a.u.) The power in the random velocities is slightly more difficult to estimate. If the velocities refer only to the small scale fluctuations, as asserted by Ekers and Little (1971), the power is only $\sim 10^{24}$ ergs s^{-1}. On the other hand, if the velocities represent different "streaming velocities" (i. e., large scale turbulence), a possibility rejected by Little and Ekers, the power is $\sim 10^{26}$ ergs s^{-1}--the same as the power needed to provide the accelerations.

Fortunately, the energy source invoked by theorists is consistent with all the observations discussed here. The heating of the solar wind is usually attributed to magnetoacoustic waves (Barnes, 1969) with periods of about 5 minutes (Brandt, 1970; Barnes, 1973). However, Hollweg (1973) uses Alfven waves and a nonlinear damping mechanism for longer period (~ 1-2 hours) waves to supply energy to the solar wind. As was noted above the waves must conform to a spectrum with a power-law index of about 4. Thus, if the heating is done by waves of about 5 minute period ($L \sim 10^5$ km), their amplitudes will be significantly reduced from the amplitudes of the 10^6 km and larger structures which appear to dominate the solar-wind turbulence.

A simple order of magnitude calculation shows that these higher frequency waves probably have the required 10^{26}-10^{27} ergs s^{-1} in the region near the sun. If we consider Alfven waves, the energy flux through a sphere of radius r at frequency ν is given by

$$P_A(\nu, r) = \delta B^2(\nu, r)\, v_A(r)\, r^2,$$

where δB^2 is the field fluctuation and v_A is the Alfven speed, $v_A = B/\sqrt{4\pi\rho}$. B is the average magnetic field and ρ is the mass density; both scale as r^{-2} from the sun. Let us fix the radius at 5 $R_\odot$. Since $\delta B^2(\nu, r)$ is measured by spacecraft near 1 a.u. (see, for example, Blake and Belcher, 1973), the key question is the scaling of δB with r.

Blake and Belcher (1973) found that for $0.7 \lesssim r \lesssim 1.4$ a.u. the power in the magnetic field fluctuations (i. e., δB^2) falls off only as r^{-1}. Hollweg (1973) predicts such a radial variation of δB^2 for undamped Alfven waves. If this holds all the way from 1 a.u. to 5 $R_\odot$, there is not enough wave energy to heat and accelerate the solar wind (or maintain the corona's high temperature) at frequencies $\nu > 10^{-4}$ Hz. One solution to this problem is to heat the solar wind with longer wavelength waves ($\nu < 10^{-4}$), which have $P_A \sim 10^{26}$ ergs s^{-1}, as suggested by Hollweg (1973).

A second solution to the heating problem is a region of enhanced turbulence near the sun: Suppose that from 1 a.u. to 0.2 a.u. δB^2 is proportional to r^{-1} as observed by Blake and Belcher (1973), but that between 0.2 a.u. (43 $R_\odot$) and 5 $R_\odot$ (0.023 a.u.) δB^2 is proportional to r^{-5}. Then the wave power through the sphere at 5 $R_\odot$ is about 10^{28} ergs sec^{-1} at $\nu = 3 \times 10^{-3}$ Hz. It should be noted that roughly the same value for the wave power is obtained if $\delta B \propto B \propto r^{-2}$ all the way from 1 a.u. to 5 $R_\odot$.

As already noted above the radial variations of the solar-wind density spectra reported here suggest a region of enhanced turbulence, i.e., slower than expected decline in the amplitude of density fluctuations with distance, near the sun. Estimates of the wave power show that a situation in which the density fluctuations are driven by

magnetohydrodynamic waves near the sun is energetically reasonable and also consistent with the observed radial gradient of the magnetic fluctuations near 1 a.u. What is missing from this plausible picture is the detailed connection between the magnetic wave energy and the density fluctuations.

The DRVID observations combined with those of Belcher and Davis (1971) lead to a suggestion contrary to the observation of Krieger et al. (1973) that a coronal hole is the source of a high-velocity stream in the solar wind. Belcher and Davis (1971) observed that Alfven waves were more prevalent and of larger amplitude at the leading edges of high velocity streams. Siscoe and Finley (1972) have shown with a simple model of the solar wind that high velocity streams observed near the earth probably arise from high temperature regions in the corona. The DRVID

spectral amplitudes showed a positive correlation with sunspot activity. Taken together these findings suggest that high velocity streams may originate near areas of sunspot activity. Sunspot regions generally have large magnetic fields, closed field structures, and high temperatures--the opposite of coronal holes.

Pneuman (1973) suggested that high velocity streams might originate from open magnetic structures. The corona would then appear cool at the base of the stream because of the large energy loss by conduction. Krieger et al. (1973) observed the predicted effects. However, if the solar wind is largely driven by waves, and we wish to reduce electron heat conduction near the sun (Cuperman and Metzler, 1973), it might be more plausible for high velocity streams to originate near sunspots. However, the large magnetic fields there could interfere with the damping of magnetoacoustic waves (Barnes, 1969). This leads back to the suggestion by Hollweg (1973) that the solar wind is driven by low-frequency Alfven waves. Such waves may be preferentially produced near regions of sunspot activity.

B. THE SPECTRUM OF THE SOLAR-WIND TURBULENCE

Until now the spectrum of the solar-wind density fluctuations has been investigated largely by two methods--direct spacecraft measurements and the interplanetary scintillation (IPS) (see the review by Jokipii, 1973) of radio sources. The two types of data usually sample different frequency ranges (spacecraft, $\nu \lesssim 10^{-2}$ Hz; IPS, $1 \lesssim \nu \lesssim 10$ Hz) and different radial distances from the sun (spacecraft, $r \cong 1$ a.u.; IPS, $r \lesssim 0.5$ a.u.). The relationship between the spectra measured by these techniques has been the subject of controversy for a number of years. Several authors (Cronyn, 1972; Jokipii and Hollweg, 1972, 1970) have argued that the IPS observations may be interpreted simply as the high frequency extension of the spacecraft-observed power law. Other authors (Rickett,1973; Hewish,1971; Little,1971) claim that the high frequency density spectrum differs from this power law. The DRVID observations provide insight into this problem in two ways. First, they show that large scale (low frequency) density variations are important near the sun. High frequency fluctuations do not dominate density changes there. Second, the DRVID spectra suggest that the low frequency power law is steeper than that of Intriligator and Wolfe (1970) and thus give better agreement between the amplitudes of the IPS and spacecraft spectra.

IPS are restricted by the Fresnel scale to observing fluctuations smaller than $\sim$ 100-200 km ($\nu \gtrsim 1$ Hz). Until recently the interpretation of these data was limited by the assumption of a Gaussian power spectrum for the density fluctuations. With this model

the dominant scale size for density changes was inferred to be 100 km. Such interpretations are no longer made (Jokipii, 1973; Young, 1971). However, it is now asserted by some IPS observers (Rickett, 1973) that the solar-wind power spectrum is enhanced with respect to the spacecraft-observed power-law near 1 Hz. No convincing theoretical reason for the existence of such an enhancement has been advanced.

There are two pieces of evidence in favor of the view that there is an enhancement near 1 Hz. Unti et al. (1972) have presented spacecraft measurements made near the earth which, at least on some occasions, show such an enhancement. The enhancement is small at best, and the effect is not clearly established.

Rickett (1973) has recently reanalyzed much IPS data in terms of a power-law spectrum. He finds that a power-law spectrum of index $\beta = 3.3$, as deduced by Intriligator and Wolfe (1970), does not give the correct dependence on radio wavelength λ for the scintillation index (m) nor does it give the correct amplitude for the density spectrum observed by IPS methods. The scintillation index m is related to the wavenumber power spectrum of the solar wind, $g(\underset{\sim}{k})$, by (Rickett, 1973)

$$m^2 = \int_0^\infty k\, dk \int_0^\infty \lambda^2\, g(k)\, \sin^2\left(\frac{k^2 \lambda z}{4\pi}\right) dz$$

where $k = |\underset{\sim}{k}|$, and λ is the radio wavelength. Rickett finds $m \propto \lambda^{(2+\beta)/4} \equiv \lambda^p$ for $g(k) \propto |k|^{-\beta}$. To fit the $m \propto \lambda^{1.0 \pm 0.15}$ law deduced from the scintillation data requires $\beta \cong 2.0$, implying a flattening in the spectrum near scale sizes of $\sim$ 100 km. In order to fit the amplitude then, the spectrum must drop substantially at some scale size larger than $\sim$ 500 km. Little (1971) independently suggested such a drop.

Rickett's result can be criticized in several ways. Young (1971) using some of the same data as Rickett and other simultaneous data (see below) found a scintillation index-wavelength relationship of $m \propto \lambda^{1.42}$, which gives $\beta = 3.67$. Jokipii and Hollweg (1971) claimed that $m \propto \lambda^{1.25}$ provided a reasonable fit to the data used by Rickett, although Rickett disputes this contention. From these results one is led to question the small error which Rickett attaches to his value of p. The data Rickett uses were not obtained from simultaneous observations at the different radio wavelengths. Since the fluctuations in the solar wind vary substantially with time, a significant error could be introduced into the determination of p if the data are not taken

together. Finally, if the spacecraft data were represented by a somewhat steeper power law, $\beta \cong 3.6$-3.7, the amplitude discrepancy would be removed. Such a value of β is consistent with the observations of Intriligator and Wolfe (1970) ($\beta = 3.3 \pm 0.3$), agrees with the value deduced from IPS by Young (1971), is more consistent than $\beta = 3.3$ with the DRVID observations ($\beta = 3.9 \pm 0.2$), and is suggested by Cronyn (1972) in his comparison of spacecraft and IPS data. Thus, there is a large amount of data, including the DRVID observations, to suggest that $\beta \cong 3.7 \pm 0.3$, ($p = 1.44$) and that there is little or no enhancement near 1 Hz.

The DRVID observations show quite clearly that the most important scale for density changes near the sun is greater than one million kilometers. Structures of this size are found to contain local density changes exceeding 100%. While the DRVID data are not sensitive to changes at frequencies as high as 1 Hz, the DRVID observations do show that 100 km is not the dominant scale for density changes in the solar wind even near the sun. DRVID observations cannot resolve the conflict between the IPS and the spacecraft advocates, but they suggest that the solar wind turbulence may be well represented by a single power-law spectrum of slope $\beta = 3.7 \pm 0.3$ at all heliocentric distances.

C. SUGGESTIONS FOR FUTURE WORK

DRVID observations have been shown to be a useful tool for investigating the solar-wind turbulence particularly near the sun. The observations could be enhanced both by improving the quality of the data and by having available other simultaneous solar wind data. An opportunity for these improved observations will occur (hopefully twice) on the Mariner Venus-Mercury (MVM) mission which will have dual-frequency capability and charged particle experiments as well as DRVID.

The quality of DRVID data could be improved in several ways. Probably the simplest and most important improvement would be longer unbroken data records. Longer records would allow the investigation of lower frequencies with smaller statistical errors. They would also permit a meaningful test of the autocorrelation technique for finding dense streams. If the Mu ranging system were modified so that it continuously sent the high frequency code component, long, unbroken records could be obtained. The usefulness of the data would be improved if they were less noisy. Since this requires more transmitted power (beyond the 400 kW presently in use) or larger antennas, it must be ruled out as a practical matter. The dual frequency data will have less noise than the DRVID data.

The usefulness of DRVID observations could be considerably enhanced if other simultaneous, well-located solar wind data were available. By well-located I mean near enough in time and space so that mapping errors between the observations would be small. Data on the solar-wind velocity and density at some point near the

ray path would allow a better test of the autocorrelation technique for finding streams. The power spectrum of the density could be compared to that of DRVID data to check for the predicted minima in the spectrum. Other solar wind data might clarify the correlation found between the DRVID spectral amplitudes and Zurich sunspot number.

Finally, more observations are needed to check the results found here on the radial fall off of the amplitude of the solar wind turbulence. In particular the slow decline near the sun should be investigated. Counselman and Rankin (1972) have suggested that it is a latitude effect which changes with the solar cycle. Such a variation can be separated from a radial dependence now as the solar cycle continues to decline.

Continued DRVID observations may provide the key to understanding the turbulence near the sun which is thought to play a most important role in the solar wind.

Appendix A

We wish to investigate the integral

$$I(\nu) = \int_{-\mu_1}^{\mu_2} \frac{du\ 1+e^{-i4\pi\nu\mu q/c} e^{+i\varphi}}{1+\mu^2\ 1+\gamma+\beta/2} \tag{A-1}$$

The first term can be looked up in any integral table and needs no discussion. The second term can be expanded in an asymptotic series. For q fairly small ($\lesssim$ 0.25a.u., $\epsilon \lesssim 15^{\circ}$) only the first term is significant. Essentially we assume that the only important effect occurs near the sun ($\mu \tilde{=} 0$) so that the limits of the integral can be pushed to infinity with negligible effect. Thus the second term of (A-1) looks like

$$\begin{aligned} I_2(\nu) &= \int_{-\mu_1}^{\mu_2} \frac{d\mu\ e^{+i\varphi} e^{-i4\pi\nu\mu q/c}}{1+\mu^2\ 1+\gamma+\beta/2} \\ &= \int_{-\infty}^{+\infty} \frac{d\mu\ e^{+i\varphi} e^{-i4\pi\nu\mu q/c}}{1+\mu^2\ 1+\gamma+\beta/2} - \int_{-\infty}^{-\mu_1} \cdots - \int_{\mu_2}^{\infty} \cdots \end{aligned} \tag{A-2}$$

If $\mathrm{Re}(1 + \gamma + \beta/2) > 0$, then from Erdelyi (1954), we find

$$I_2(\nu) = 2\left(\frac{2\pi\nu q}{c}\right)^n \frac{\pi^{1/2} e^{+i\varphi}}{\Gamma(n+1/2)} K_n\left(\frac{4\pi\nu q}{c}\right) - \int_{-\infty}^{\mu_1} \cdots - \int_{\mu_2}^{\infty} \cdots$$

where $n+\frac{1}{2}=1+\gamma+\beta/2$ and $K_n(x)$ is the modified Bessel function of the second type.

If $\gamma+\beta/2$ is an integer, then by a simple contour integration, one gets

$$I_2(\nu) = \frac{2\pi i\, e^{+i\varphi}}{\Gamma(\gamma+\beta/2+1)} \frac{d^{\gamma+\beta/2}}{d\mu^{\gamma+\beta/2}} \left[\frac{e^{-i4\pi\nu\mu q/c}}{(\mu-i)^{1+\gamma+\beta/2}} \right]_{\mu=-i} \int_{-\infty}^{-\mu_1} \cdots \int_{\mu_2}^{\infty} \cdots . \quad (A-4)$$

The first correction terms in our asymptotic series may be evaluated by an integration by parts. The result is

$$I_2(\nu)_{\text{correction}} = \frac{\mu_1}{1+\mu_1^2\ 1+\gamma+\beta/2} - \frac{\mu_2\, e^{+i4\pi\nu q(\mu_2-\mu_1)/c}}{1+\mu_2^2\ 1+\gamma+\beta/2} . \quad (A-5)$$

We see immediately that these terms are a factor $\mu^{-1-2\gamma-\beta}$ less than the first term in the expansion. Roughly, for $\beta \sim 3$, $\gamma \sim 0$, and observations near the sun this factor is $\sim 10^{-3}$, so that the corrections are not important.

REFERENCES

Altschuler, M.D. and Perry, R.M. 1972, Solar Phys., 23,410.

Anderson, J.D., Esposito, P.B., Martin, W.L., and Muhleman, D.O. 1972, Space Research XII, 1623, Akademie-Verlag, Berlin.

Anderson, J.D. and Lau, E.K. 1973, JPL Technical Report 32-1550, Vol. IV, 431.

Barnes,A. 1973, Adv. in Electronics and Electron Phys. (Preprint).

Barnes, A. 1969, Ap.J., 155,311.

Barnes, A., Hartle,R.E., and Bredekamp, J.H. 1971, Ap.J. Lett., 166,L53.

Belcher, J.W. and Davis, L., Jr. 1971, J. Geophys. Res., 76,3534.

Bendat, J.S. and Piersol, A.G. 1966, Measurement and Analysis of Random Data, Wiley and Sons, New York.

Biermann, L. 1951, Zs.f. Astrophys., 29,274.

Biermann, L. 1957, Observatory, 77,109.

Blackman, R.B. and Tukey, J.W. 1959, The Measurement of Power Spectra, Dover, New York.

Blake, D.H. and Belcher, J.W. 1973, Private Communication.

Bohlin, J.D. 1970, Solar Phys., 13,153.

Brandt, J.C. 1970, The Solar Wind, Freeman, San Francisco

Burlaga, L.F. and Ogilvie, K.W. 1973, J. Geophys. Res., 78,2028.

Callahan, P.S. 1974, Ap.J., 187, (In press).

Callahan, P.S. 1973, J. Geophys. Res., 78,4330.

Callahan, P.S., MacDoran, P.F., and Zygielbaum, A.I. 1972, Space Research XII, 1529, Akademie-Verlag, Berlin.

Counselman, C.C. and Rankin, J.M. 1972, Ap.J., 175,843.

Couturier, P. and Leblanc, Y. 1970, Astron. and Astrophys., 7,251.

Cronyn, W. 1972, Ap.J. Lett., 171,L101.

Cronyn, W. 1970, Ap.J., 161,755.

Cuperman, S. and Metzler, N. 1973, Ap.J., 182,961.

Ekers, R.D. and Little, L.T. 1971, Astron. and Astrophys., 10,310.

Erdelyi, A. (ed.) 1954, Tables of Integral Transforms, Vol. I, McGraw Hill, New York.

Hartle, R.E. and Barnes, A. 1970, J. Geophys. Res., 75,6915.

Hartle, R.E. and Sturrock, P.A. 1968, Ap.J., 151,1155.

Hewish, A. 1971, Ap.J., 163,645.

Hollweg, J.V. 1973, Ap.J., 181,547.

Hollweg, J.V. and Jokipii, J.R. 1972, J. Geophys. Res., 77,3311.

Hundhausen, A.J. 1969, J. Geophys. Res., 74,5810.

Intriligator, D. S. and Wolfe, J. H. 1970, Ap.J. Lett, 162, L187

James, J.C. 1970, Solar Phys., 12,143.

Jokipii, J.R. 1973, Ann. Rev. of Astron. and Astrophys., 11,(In press).

Jokipii, J.R. and Coleman, P.J. 1968, J. Geophys. Res., 73,5495.

Jokipii, J.R. and Hollweg, J.V. 1972, in Solar Wind, ed. by Sonnet,et al.

Jokipii, J.R. and Hollweg, J.V. 1970, Ap.J., 160,745.

Jokipii, J.R. and Lee, L.C. 1972, Ap.J., 172,729.

Kreiger, A.S., Timothy, A.F., and Roelof, E.C. 1973, Solar Phys., 29,505.

Little, L.T., Astron. and Astrophys., 10,301.

MacDoran, P.F. 1970, JPL Space Programs Summary 37-62, Vol. II, 28.

MacDoran, P.F. and Martin, W.L. 1970, JPL Space Programs Summary 37-62, Vol. II, 34.

MacDoran, P.F., Callahan, P.S., and Zygielbaum, A.I. 1971, The Deep Space Network Progress Report, JPL Technical Report 32-1526, Vol. I,14.

Martin, W.L. 1971, Private Communication.

Martin, W.L. 1970, JPL Space Programs Summary 37-62, Vol. II, 55.

Martin, W.L. 1969a, JPL Space Programs Summary 37-52, Vol. II, 46.

Martin, W.L. 1969b, JPL Space Programs Summary 37-57, Vol. II, 72.

Muhleman, D.O. and Johnston, I.D. 1966, Phys. Rev. Lett., 17,455.

Neugebauer, M. and Snyder, C.W. 1966, J. Geophys. Res., 71,4469.

Newkirk, G. 1967, Ann. Rev. of Astron. and Astrophys., 5,213.

Parker, E.N. 1963, Interplanetary Dynamical Processes, Interscience, New York.

Pathak, P.N. 1971, Solar Phys., 20,462.

Perry, R.M. and Altschuler, M.D. 1973, Solar Phys., 28,435.

Pneuman, G.W. 1973, Solar Phys., 28,247.

Rickett, B.F. 1973, J. Geophys. Res., 78,1543.

Rosen, J. 1969, Solar Phys., 8,450.

Salpeter, E.E. 1967, Ap.J., 147,433.

Siscoe, G.L. and Finley, L.T. 1972, J. Geophys. Res., 77,35.

Solar Geophysical Data (Prompt Reports), U.S. Dept. of Commerce, Boulder, Colorado.

Sonnet, C.P., Coleman, P.J., Jr., and Wilcox, J.M. 1972, (eds.), Solar Wind, NASA.

Sturrock, P.A. and Hartle, R.E. 1966, Phys. Rev. Lett., 16,628.

Thiede, E.C. and Lusignan, B.V. 1970, IEEE Trans., AP-18, 1.

Unti, T.W.J., Neugebauer, M., and Goldstein, B.E. 1973, Ap.J., 180,591.

Wilcox, J.M. and Ness, N.F. 1965, J. Geophys. Res., 70,5793.

Young, A.T. 1971, Ap.J., 168,543.

Zirin, H. 1966, The Solar Atmosphere, Blaisdell, Waltham, Massachusetts.